

Sheffield Hallam University

Unidirectional solidification studies of ingot mould cast irons

HORNBY, Sara A.

Available from the Sheffield Hallam University Research Archive (SHURA) at:

<http://shura.shu.ac.uk/19826/>

A Sheffield Hallam University thesis

This thesis is protected by copyright which belongs to the author.

The content must not be changed in any way or sold commercially in any format or medium without the formal permission of the author.

When referring to this work, full bibliographic details including the author, title, awarding institution and date of the thesis must be given.

Please visit <http://shura.shu.ac.uk/19826/> and <http://shura.shu.ac.uk/information.html> for further details about copyright and re-use permissions.

BAR CODE

101 381 299 9

ProQuest Number: 10697132

All rights reserved

INFORMATION TO ALL USERS

The quality of this reproduction is dependent upon the quality of the copy submitted.

In the unlikely event that the author did not send a complete manuscript and there are missing pages, these will be noted. Also, if material had to be removed, a note will indicate the deletion.



ProQuest 10697132

Published by ProQuest LLC (2017). Copyright of the Dissertation is held by the Author.

All rights reserved.

This work is protected against unauthorized copying under Title 17, United States Code
Microform Edition © ProQuest LLC.

ProQuest LLC.
789 East Eisenhower Parkway
P.O. Box 1346
Ann Arbor, MI 48106 – 1346

UNIDIRECTIONAL SOLIDIFICATION STUDIES

OF

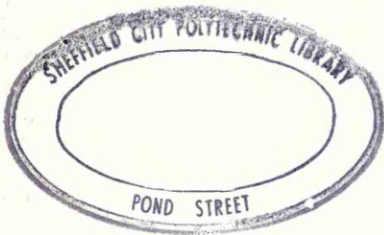
INGOT MOULD CAST IRONS

by

SARA ANN HORNBY, B.Sc., A.I.M. TECH., TECH. C.E.I.

This thesis is submitted in part fulfilment of the requirements for the degree of Doctor of Philosophy in Industrial Metallurgy of the Council of National Academic Awards. The work was carried out at Sheffield City Polytechnic, Department of Metallurgy, in collaboration with Swinden Laboratories, British Steel Corporation.

February 1980



7903633

UNIDIRECTIONAL SOLIDIFICATION STUDIES OF INGOT MOULD CAST IRONS

by

SARA ANN HORNBY

A furnace has been developed in which liquid iron, supplied from an external source, may be held at elevated temperature whilst solidifying in a cylindrical ceramic mould whose base is supported and closed by a water cooled copper chill.

Readings from a series of thermocouples, monitoring temperatures within the iron, have enabled the establishment of a controlled solidification technique, under unidirectional heat flow conditions, with cooling rates varying from $623^{\circ}\text{C}/\text{min}$. (at the chill/metal interface) to $4.35^{\circ}\text{C}/\text{min}$. (near the feeder head). Statistical analysis of cooling rate reproducibility between castings has indicated insignificant variability.

The solidification technique has been used to study the microstructure of an ingot mould cast iron at three sulphur levels (0.02-0.10 mass %) two nitrogen levels (0.005-0.012 mass %) and the interaction of these 6 variations with increasing titanium additions (0.09-0.49 mass %).

Thermodynamic data indicates that the manganese content of the iron (0.8 mass %) should reduce free sulphur to very low values but, even so, the higher sulphur composition (0.1 mass %) showed retardation of graphitic eutectic formation compared with the other two levels.

Titanium's greater affinity for nitrogen rather than sulphur, promoted graphitisation at all sulphur levels in the high nitrogen melts at low titanium concentrations, by virtue of the Ti/N interaction whilst, at low nitrogen, titanium graphitised the 0.10, and possibly 0.05, mass % sulphur melts by virtue of titanium sulphide formation. Increasing titanium promoted the carbide eutectic at contents less than previously suggested by other authors. Titanium also induced complex inclusion clusters as identified by S.E.M. examination.

The castings exhibited Hong's Type I, II and III mottled structures in regions where graphite morphology has been designated streamer 'grey' and cellular respectively. It is suggested that streamer and 'grey' areas result primarily from direct formation from liquid iron as well as decomposition of eutectic cementite.

This thesis is submitted in part fulfilment of the requirements for the degree of Doctor of Philosophy in Industrial Metallurgy of the Council of National Academic Awards. The research described was carried out during the period of June 1975 to June 1978 in the Department of Metallurgy at Sheffield City Polytechnic and financed by a Sheffield Local Education Authority Grant. No part of this dissertation has been submitted for a degree at any other University or College.

During the period of this work the author attended the following lectures which constituted part of the M.Sc in Metallurgical Process Management at Sheffield City Polytechnic:

Module I: Process Metallurgy

Fabrication Metallurgy

Advanced Thermodynamics

Module II: Computing and Numerical Analysis

Accounting

Economics

Module III: Quality Assurance

Powder Metallurgy

Solidification

Heat Treatment and Transformations

Metals and Competitive Materials

High Strength Steels.

Module IV: Case studies in the subject areas of:-

Quality Assurance

Powder Metallurgy

Ingot Mould Performance (Appendix 3 of this
dissertation)

The author wishes to thank her supervisors Mr.G.Butterworth and Dr.F.Wilson for their guidance, and all the technical staff and other Research Personnel who contributed in their own individual ways to her education. More especial thanks to Messrs : D.Latimer, G.Gregory, J.Bradshaw, B.Dodds, S.Jaiswal and Dr.R.Acheson without whom this dissertation would not have been completed.

The author would also like to thank her current employers, B.S.C. Sheffield Division for their financial and practical assistance and Mr.J.V.Anderson of William Lee Malleable for the use of their analytical facilities.

CHAPTER 1	INTRODUCTION	1
CHAPTER 2	LITERATURE REVIEW	
2.1	COMMERCIAL CAST IRONS	2
2.2	THE SOLIDIFICATION MODES OF CAST IRON	6
2.2.1	Grey Cast Iron	6
2.2.2	Indirect Graphite Formation	12
2.2.3	Spheroidal Graphite Cast Iron	13
2.2.4	White Cast Iron	14
2.2.5	Mottled Cast Iron	16
2.3	THE EFFECT OF COOLING RATE ON THE MICROSTRUCTURE OF CAST IRONS	17
2.4	GRAPHITE NUCLEATION	20
2.5	COMPOSITIONAL INFLUENCES ON CAST IRON STRUCTURE	25
2.5.1	Carbide Stabilising and Graphite Stabilising Elements	26
2.5.2	Compositional Components Affecting the Growth Behaviour of Graphite	28
2.5.3	Sulphur in Cast Iron	33
2.5.4	Nitrogen in Cast Iron	37
2.5.5	Titanium in Cast Iron	39
2.6	INGOT MOULD CAST IRONS	42
2.7	EXPERIMENTAL TECHNIQUES FOR THE STUDY OF THE SOLIDIFICATION OF CAST IRONS	45
2.7.1	The Interrupted Solidification Technique	46
2.7.2	Unidirectional Solidification and Decantation	46
2.7.3	The Dip-Stick Method	47
2.7.4	Analogue Methods	47
2.7.5	Tracer Methods	48
2.7.6	Directional Solidification	49
2.7.7	Solidification Under Conditions of Unidirectional Heat Flow	49

3.1	INTRODUCTION	51
3.2	THE FURNACE	52
3.2.1	The Furnace Hot Zone	53
3.3	HEATING ELEMENT CONTROL	56
	Stage 1	56
	Stage 2	56
	Stage 3	57
3.4	THE MOULDS	58
3.5	THE THERMOCOUPLES	60
3.6	THE COPPER CHILL	61
3.7	DEVELOPMENT OF THE CAST IRON MELTING PRACTICE	62
3.7.1	Initial Experiments - Melting Practice A	62
3.7.2	Improved Melting Procedure - Melting Practice B	64
3.8	ALLOY ADDITIONS	66
3.8.1	White Irons	66
3.8.2	Grey Iron Melt Programme	67
3.8.2.a	Carbon Additions	67
3.8.2.b	Sulphur Additions	67
3.8.2.c	Manganese Additions	68
3.8.2.d	Nitrogen Additions	68
3.8.2.e	Titanium Additions	68
3.9	COMPOSITIONAL ANALYTICAL TECHNIQUES	69
3.10	DATA ASSIMILATION	71
3.10.1	The Solatron 'Compact' Logger	71
3.10.2	The Credshire Model 500 Analogue Scanner	71

CHAPTER 4	RESULTS	78
4.1	INTRODUCTION	78
4.2	THE DEVELOPMENT OF THE EXPERIMENTAL APPARATUS AND PROCEDURE	78
4.3	THE GREY IRON MELT PROGRAMME	79
4.3.1	Introduction	79
4.3.2	Cooling Curves for the Grey Iron Melt Programme	80
4.3.3	The Structures of the Low Nitrogen Grey Iron Castings	82
4.3.3.a	Melt A1 - The Base Melt	82
	Melt A1a	86
	Melt A1b	87
	Melt A1c	87
4.3.3.b	The Effect of Sulphur Addition on the Structure of the Base Melt	88
4.3.3.c	The Effect of Titanium Additions on the Structure of the 'Base Melt' (A1)	89
	Melts B1 and C1	90
	Melts E1, F1 and G1	92
4.3.3.d	The Combined Effect of Both Titanium and Sulphur Additions on the Structure of the 'Base Melt' (A1)	94
	Melt B2	95
	Melt B3	96
	Melt C2	96
	Melt C3	97
	Melt E2	98
	Melt E3	98
	Melt F2	99
	Melt F3	100
	Melt G2	100
	Melt G3	101
4.3.3.e	Additional Melts with Both Sulphur and Titanium Additions in the Low Nitrogen Melt Programme	102
	Melt E1a	102
	Melt E3a	103
	Melt F2a	104

4.3.4	The Structures of the High Nitrogen Grey Iron Castings	104
4.3.4.a	The Effect of Sulphur Concentration at the Higher Nitrogen Level	104
	Melt A1'	105
	Melt A2'	106
	Melt A3'	107
	Melt Ala'	108
4.3.4.b	The Effect of Both Sulphur and Titanium Additions at the High Nitrogen Level	109
	Melt B1'	109
	Melt B2'	110
	Melt B3'	111
	Melt C1'	113
	Melt C2'	114
	Melt C3'	115
	Melt D1'	117
	Melt D3'	118
	Melt F1'	119
	Melt F2'	120
	Melt F3'	121
4.3.4.c	Additional Melts in the High Nitrogen Melt Programme	122
	Melt B3a'	122
	Melt C2a'	123
4.3.5	Scanning Electron Microscopy for Inclusion Identification	123
CHAPTER 5	DISCUSSION	
5.1	EXPERIMENTAL TECHNIQUE	125
5.2	THE MICROSTRUCTURES OF THE INGOT MOULD TYPE IRONS	132
5.2.1	Proeutectic Austenite	133
5.2.2	Carbidic Eutectic	134
5.2.3	Streamer Graphite	135
5.2.4	'Grey' Areas	136
	Proposed Mechanism of Formation of Streamer Graphite and 'Grey' Areas	137
5.2.5	Graphitic Cells	139

5.2.6	INCLUSIONS	145
5.3	THE EFFECT OF SULPHUR AND NITROGEN ADDITIONS	145
5.4	THE EFFECT OF TITANIUM ADDITIONS ON THE LOW NITROGEN CASTINGS	151
	Titanium as a Sulphide Former in Ingot Mould Type Irons	157
5.5	THE EFFECT OF TITANIUM ADDITIONS ON THE HIGH NITROGEN CASTINGS	162
5.6	THE EFFECT OF CARBON CONCENTRATION ON THE BASE MELT, Al	169
CHAPTER 6	CONCLUSIONS AND FURTHER WORK	
6.1	CONCLUSIONS	172
6.2	FURTHER WORK	174
REFERENCES		175
APPENDIX 1	THE RELATIVE HEAT CAPACITIES OF THE CASTING AND THE CERAMIC MOULD	
APPENDIX 2	THE MANGANESE-SULPHUR EQUILIBRIA FOR THE INGOT TYPE IRON	
APPENDIX 3	CASE STUDY - THE EFFECT OF COMPOSITION ON INGOT MOULD PERFORMANCE	

Cast irons are one of the most widely used groups of metallic materials available for engineering construction and, in terms of tonnage output, are only exceeded in importance by wrought steels. The output of iron castings in the U.K. has increased steadily since World War II and now stands at nearly 35 million tonnes per annum. The wide usage of cast irons is essentially the result of their cheapness in comparison with all other commercial alloys, combined with their useful, though not outstanding, range of mechanical properties.

Although cast irons clearly constitute an extremely important group of commercial alloys, and have done so for some considerable time, there are many aspects of their microstructure that are far from fully understood. In particular it is only comparatively recently that the effect of trace elements on their solidification, and especially on the mechanism of graphite precipitation, has begun to be appreciated. It is now known that the presence of small amounts of certain constituents in cast irons can have a profound effect on the microstructure and hence the mechanical properties. Nitrogen and sulphur are two such elements which, in small quantities, are believed to exert a powerful influence on the solidification process and, in particular, on the graphite morphology. The introduction of titanium into the melt, prior to casting can negate their effects as a result of the formation of stable titanium nitrides and sulphides.

The purpose of this investigation has been to study the interaction between nitrogen, sulphur and titanium in cast irons and to examine their effect upon the microstructure at various cooling rates. The variation in cooling rates was obtained by a unidirectional solidification method which was developed along with a method for monitoring the results. The work was carried out on a particular cast iron commonly used in ingot mould practices though the nature of the experiments precluded the use of comparable ingot mould cooling times of 48 hours.

2.1 COMMERCIAL CAST IRONS

The amount of material which has been published concerning cast irons is considerable and it is beyond the scope of the present work to attempt a complete review. It is only proposed to present a brief outline of the available literature on the widely accepted general aspects of cast iron solidification, with more emphasis being placed on those areas pertinent to this particular work. It is worth noting that a number of useful general reviews of the literature concerned with the solidification and transformations in cast irons have already been published, notably those of Morrogh^(1,2,3), Wallace⁽⁴⁾ and Hughes⁽⁵⁾.

Cast irons may be defined as that group of high carbon, iron-carbon alloys which exhibit the eutectic transformation during solidification. Unlike steels they cannot be heat treated to produce a homogeneous single phase structure and hence the degree of mechanical working which they can withstand is at best severely limited. For this reason they are essentially used for applications where they can be cast directly into the form of the finished component⁽⁶⁾.

Pure iron forms a eutectic alloy with carbon which, under equilibrium cooling conditions, occurs at 4.25 mass % carbon. Commercial cast irons, in addition to carbon, contain appreciable amounts of other elements and these may affect the composition of the eutectic alloy. The most common elements encountered in cast irons are silicon, phosphorus, manganese and sulphur. In addition they may contain minor amounts of elements such as lead, tin, antimony and bismuth and gaseous elements such as nitrogen, oxygen and hydrogen which, although present in small quantities, can have a powerful effect on the microstructure and hence the mechanical properties of these materials.

Iron, carbon and silicon are generally the most abundant elements present in cast irons and hence it might be reasonable to consider their solidification in terms of the Fe-C-Si ternary system. However, in the presence of upto 3 mass % Si, the binary Fe-C sections of the ternary Fe-C-Si diagram are very similar to the Fe-C binary diagram and hence solidification proceeds in a manner similar to that of the pure two component system⁽⁵⁾. The effect of silicon and also phosphorus on the carbon content of the eutectic are often expressed in terms of the equation⁽⁷⁾ :-

$$(\text{mass \% C})_{\text{eut}} = 4.25 - 0.31 \text{ mass \% Si} - 0.33 \text{ mass \% P}$$

This equation represents the projection of the eutectic valley onto the basal plane of the Fe-C-Si-P phase diagram. For practical purposes the above equation may be presented in a slightly different form in order that the composition of a particular commercial alloy may be expressed in terms of a carbon equivalent value (CEV) and hence related to the position on the Fe-C binary diagram⁽⁷⁾.

$$\text{CEV} = \text{mass \% C} + \frac{\text{mass \% Si}}{3.5} + \frac{\text{mass \% P}}{3}$$

A further complicating feature of cast irons is that they may solidify according to either the stable iron-graphite equilibrium diagram or according to the metastable iron-iron carbide equilibrium diagram. Figure 1 shows the relevant portion of the iron-iron carbide diagram pertinent to commercial alloys. The important features of the iron-graphite diagram are superimposed on this figure and are shown in broken lines. It will be noted that the eutectic temperature of the stable system is slightly higher than that for the metastable system -

an important factor when considering the solidification modes of cast irons.

The existence of two superimposed solidification systems is the explanation for the existence of the two basic types of cast iron:-

- a) Grey cast iron - solidifying according to the iron-graphite system.
- b) White cast iron - solidifying according to the iron-iron carbide system.

Grey irons are the most widely used group of cast irons. In this case the carbon is present in the form of graphite, usually as flakes. Graphite is an inherently soft and friable material, in flake form it exhibits sharp corners which have a detrimental effect on the impact properties of the material, and in commercial alloys it can occupy a significant area of the cross section. It is therefore not surprising that it is the form, pattern and amount of the graphite present which, to a large extent, determines the properties of grey irons. These in turn are controlled by the composition of the alloy, the cooling rate and the thermal history of the melting process⁽⁸⁾. The flake-like form of graphite therefore tends to make commercial grey irons relatively weak and brittle, but they do have good machining and casting properties⁽⁶⁾.

In the case of white cast irons all of the carbon is present in the form of cementite. Cementite is hard (about 1500 VPN) and brittle and hence white iron castings also have these properties, which means that they may only be shaped by grinding. White irons are of little use in themselves but a white layer may be formed on the chilled surface of a grey cast iron in order to render the surface wear resistant, while the component as a whole is tougher and more impact resistant than a totally white casting⁽⁶⁾.

Another use for white irons is as a starting material for malleable iron production. This involves annealing the metastable white iron structure in order to bring about the decomposition of the cementite to form graphite, generally in a nodular form, in a matrix of ferrite or pearlite, as desired. In this form the graphite does not exert such a profound embrittling effect as the varieties found in grey cast irons⁽³⁾.

Malleable iron requires long periods of heat treatment which increases costs. A newer commodity, spheroidal graphite (S.G.) cast iron, is therefore taking the place of grey and malleable irons. In this case the graphite is induced to solidify in a spheroidal form by the inoculation of a low sulphur melt with magnesium or certain rare earth elements. Such irons can be ferritic or pearlitic in the as cast condition, depending upon the elements present. To produce a ferritic iron the base materials must be specially selected; the usual as cast structure is pearlitic and may be rendered more ductile by annealing to produce a ferritic S.G. iron - a material which is amenable to a high degree of mechanical manipulation. Both malleable and S.G. irons in general are tougher and have better impact resistance than grey irons, with a small, but useful, amount of plasticity⁽⁶⁾.

A number of more sophisticated alloy cast irons are also available for specialist uses, their mechanical and physical properties depending, to a large extent, on the influence of the particular alloying elements present and the state and distribution of the carbon.

These briefly are the basic types of alloys which constitute the diverse range of materials known as cast irons. The present investigation has been primarily concerned with solidification characteristics of grey, and to a lesser extent white, cast iron and therefore the next section of this review will be concerned with the solidification modes of these types of iron.

2.2 THE SOLIDIFICATION MODES OF CAST IRON

2.2.1 Grey Cast Iron

Grey cast irons essentially solidify according to the iron-graphite equilibrium diagram. In the case of irons of hypoeutectic composition cooling under equilibrium conditions, solidification begins with the precipitation of austenite dendrites. This is associated with the progressive enrichment in carbon of the remaining liquid, which gradually approaches the eutectic composition as the temperature falls^(1,2,4,8,9). When the eutectic temperature is reached, the remaining liquid, which occupies the interstices between the primary austenite dendrites, solidifies as a eutectic mixture of austenite and graphite from suitable nuclei. Solidification of the individual eutectic cells takes place on an approximately spherical crystallisation front until interference occurs with other growing eutectic cells or with the primary dendritic skeleton of austenite. Growth continues until all the liquid is consumed, so that, immediately after solidification, the primary dendrites of austenite and the austenite of the eutectic mixture are continuous. Distributed throughout the matrix of austenite is a dispersion of graphite, usually in the form of flakes, originating from the eutectic transformation^(4,8,9). On subsequent cooling, the austenite ultimately undergoes the eutectoid transformation producing a matrix of either ferrite or pearlite, depending upon the composition of the alloy and the cooling rate. Maximum hardness is obtained when the matrix is composed entirely of pearlite. The presence of excess ferrite causes a lowering of the hardness due to its weakening effect whilst excess carbide reduces the strength due to its embrittling effect⁽¹⁰⁾.

In the case of hypereutectic irons, solidification commences with the precipitation of primary Kish graphite with progressive denudation

of the remaining liquid of carbon as the temperature falls⁽¹⁾. The subsequent solidification of the remaining liquid by the eutectic reaction, and the decomposition of the eutectic austenite on further cooling, follows a similar pattern to that of hypoeutectic irons.

With commercial irons which contain significant amounts of phosphorus, a phosphorus rich phase segregates to the boundaries of the growing eutectic cells. This ultimately solidifies at a somewhat lower temperature than the iron-graphite eutectic, giving rise to the phosphide eutectic (steadite), which outlines and indicates the limits of the original iron-graphite eutectic cells^(3,8,9).

Most commercially produced cast irons are hypoeutectic in composition and, as a consequence, most of the research work carried out has been concerned with these, rather than hypereutectic alloys⁽²⁾. As stated previously, it is the form, size and distribution of the eutectic graphite which has the dominant influence on the overall mechanical properties of a particular alloy. The formation of the pro-eutectic phase is therefore of relatively less importance than the eutectic reaction which is common to both groups of alloys^(1,8). It is therefore not surprising that it is the mechanism of solidification of the eutectic that has stimulated the most investigatory work. However, it has proved to be such a complex process that even now there is still controversy surrounding certain aspects of the solidification mechanism.

The formation of the eutectic phases proceeds by a nucleation and growth process. In general the nucleation process is considered to be more difficult than the growth process and under practical cooling conditions this difficulty with nucleation manifests itself as a tendency for the alloy to undercool below the equilibrium temperature for the formation of the austenite-graphite eutectic. This tendency for under-

cooling to occur can have a marked effect on the structure of the eutectic graphite and, with sufficient undercooling, can result in the suppression of the graphitic eutectic in favour of the carbidic eutectic^(2,4).

Figure 2 illustrates the type of cooling curve which might be produced by a hypoeutectic iron cooling under practical conditions⁽²⁾. Nucleation of the austenite-graphite eutectic cells commences at some point B, below the equilibrium austenite-graphite eutectic transformation temperature. The melt undercools further with a progressive increase in the number of growing cells until, at a point C, the number and growth of the eutectic cells is often sufficient to cause liberation of heat greater than can be dissipated to the surroundings, and so there is a rise in the temperature to point D. The form of the eutectic arrest shows many variations and may exhibit an extensive horizontal portion⁽²⁾. As the eutectic cells begin to impinge on one another the rate of heat liberation decreases until solidification is complete at E. The degree of undercooling and the form of the eutectic arrest is related to the cooling rate and the degree of nucleation of the melt, as will be discussed later in sections 2.3 and 2.4.

The graphite in cast irons can take a wide variety of forms⁽³⁾. In grey irons however, the most commonly encountered form is that of flake graphite, although the size and distribution of these can be significantly changed by the degree of undercooling. In the A.S.T.M. classification, essentially five types of flake graphite have been identified^(4,11,12) :-

- (i) A - Coarse flake graphite
- (ii) B - Graphite rosettes
- (iii) C - Pro-eutectic or Kish graphite

- (iv) D -)
) Undercooled or eutectiform graphite
- (v) E -)

Of the five types of graphite, type C is fundamentally different from the others in that it refers to Kish graphite encountered in hypereutectic irons. Kish graphite precipitates directly from the melt, generally only in small quantities, in commercial hypereutectic alloys, and hence is not subject to the constraints imposed on the eutectic graphite platelets by the austenite present. For this reason, Kish graphite assumes the characteristic form of straight sided plates, as compared with the more irregular shaped, curved sided forms of eutectic graphite^(3,4,12).

The A, B, D and E types constitute the various forms of the eutectic graphite. Their morphology can be directly related to the degree of undercooling below the equilibrium austenite - graphite eutectic temperature prior to solidification of the eutectic liquid commencing. With increasing amounts of undercooling the form of the graphite flakes changes from A to B to D or E, with ultimately a white iron being produced at the highest degrees of undercooling⁽¹³⁾. The growth rates of the different types of graphite follow directly from the amount of undercooling. With only limited undercooling, type A graphite grows relatively slowly, since the latent heat of fusion of the austenite-graphite eutectic must be removed by conduction out of the solidifying iron. The growth rate is much more rapid in the case of the D and E graphite because the molten iron is sufficiently undercooled that much, or all, of the heat of fusion is absorbed by the remaining liquid, making heat removal no longer a prerequisite for continuation of solidification⁽⁴⁾. The D and E types of undercooled graphite are differentiated by the fineness of the individual graphite flakes and the degree of directionality of the primary austenite dendrites, between which are contained the eutectic cells⁽¹²⁾.

Type B graphite is an intermediate form of flake graphite produced between the two extremes of undercooling. The flakes grow rapidly at the central portion of the cell but the degree of undercooling is less than that required to ensure a fully D or E type structure and so the temperature of the remaining liquid is raised to the equilibrium eutectic temperature by the heat of fusion. Growth then proceeds more slowly producing the type A graphite structure at the outer portion of each cell⁽⁴⁾.

A polished section of a grey iron tends to show the graphite flakes as discrete entities. As a consequence there was once considerable speculation concerning the true nature of the graphite distribution. The true structure of type A graphite was first revealed by certain Russian investigators, and subsequently confirmed by Oldfield⁽⁸⁾, by dissolving away the iron matrix to expose the flakes. They showed that the graphite flakes within a particular eutectic cell originated from a single nucleation site and grew from this point, forming a continuous skeleton which repeatedly branched during the growth of the cell. It was later confirmed by Day⁽¹⁴⁾, using scanning electron microscopy, that the structure of undercooled, D type graphite, also consisted of an interconnected network, differing only from the coarse and medium forms of flake graphite in that the structure was finer and had a greater amount of branching and waviness relative to the thickness of the graphite flakes.

During the formation of a particular eutectic cell the graphite flakes grow normal to the interface with the liquid giving rise to an irregular radial structure. Both the austenite and the flake graphite grow in contact with the liquid, with a tendency for the flakes to project beyond the austenite into the liquid⁽⁵⁾. Although the austenite

SYNOPSIS

UNIDIRECTIONAL SOLIDIFICATION STUDIES OF INGOT MOULD CAST IRONS

by

SARA ANN HORNBY

A furnace has been developed in which liquid iron, supplied from an external source, may be held at elevated temperature whilst solidifying in a cylindrical ceramic mould whose base is supported and closed by a water cooled copper chill.

Readings from a series of thermocouples, monitoring temperatures within the iron, have enabled the establishment of a controlled solidification technique, under unidirectional heat flow conditions, with cooling rates varying from 623°C/min. (at the chill/metal interface) to 4.35°C/min. (near the feeder head). Statistical analysis of cooling rate reproducibility between castings has indicated insignificant variability.

The solidification technique has been used to study the microstructure of an ingot mould cast iron at three sulphur levels (0.02-0.10 mass %) two nitrogen levels (0.005-0.012 mass %) and the interaction of these 6 variations with increasing titanium additions (0.09-0.49 mass %).

Thermodynamic data indicates that the manganese content of the iron (0.8 mass %) should reduce free sulphur to very low values but, even so, the higher sulphur composition (0.1 mass %) showed retardation of graphitic eutectic formation compared with the other two levels.

Titanium's greater affinity for nitrogen rather than sulphur, promoted graphitisation at all sulphur levels in the high nitrogen melts at low titanium concentrations, by virtue of the Ti/N interaction whilst, at low nitrogen, titanium graphitised the 0.10, and possibly 0.05, mass % sulphur melts by virtue of titanium sulphide formation. Increasing titanium promoted the carbide eutectic at contents less than previously suggested by other authors. Titanium also induced complex inclusion clusters as identified by S.E.M. examination.

The castings exhibited Hong's Type I, II and III mottled structures in regions where graphite morphology has been designated streamer 'grey' and cellular respectively. It is suggested that streamer and 'grey' areas result primarily from direct formation from liquid iron as well as decomposition of eutectic cementite.

and the graphite grow side by side the growth of the graphite is anisotropic. The graphite platelets maintain an average interphase separation, governed by the imposed growth rate, as a result of the ability of graphite to change its local growth direction, probably by twinning and sub-boundary formation⁽¹⁴⁾. If the graphite was unable to change its local growth direction, convergent and divergent growth at the solid-liquid interface would lead to termination and the necessity for the graphite to nucleate at, or ahead of, the interface - a process which is not observed in practice.

Whilst flakes are the most common form of graphite in grey cast iron, other forms have been observed. The most well known of these is the spheroidal graphite form^(3,4) (see section 2.2.3). In addition, the graphite has been observed to take the form of plates or needles in a 'pseudo-Widmanstätten' form, as a mesh like distribution, as globules and filaments⁽⁵⁾ and as 'coral' or 'quasi flake' distributions⁽¹⁵⁾. Most of these are the result of compositional effects, the mechanism of which is far from fully understood (see section 2.5).

It will be evident from the foregoing discussion that grey cast iron may exhibit a variety of microstructures defined in terms of the size, shape and distribution of the graphite phase and the matrix in which it is embedded. This variety of structures will in turn give rise to a range of properties. The control of the microstructure is therefore an important consideration and will be influenced by essentially three variables:-

- (i) The cooling rate during solidification and subsequent solid state transformation.
- (ii) The nucleation and growth conditions prevailing during solidification.

(iii) The composition of the alloy.

The effects of these variables on cast iron structure, and in particular grey iron structure, will be discussed in Sections 2.3, 2.4 and 2.5 respectively.

2.2.2 Indirect Graphite Formation

It was once a widely held view that the graphite in grey cast irons was the result of an indirect graphitisation process⁽¹⁶⁾. It was believed that solidification took place initially according to the iron-iron carbide system giving rise to a white iron. The metastable cementite in the structure then underwent solid state decomposition to create the flake graphite observed in practice. The belief that the graphite, and in particular D type graphite, originated in this way persisted well into the 1950's^(3,10,17,18). The historical development of these theories has already been reviewed by Hughes⁽⁵⁾ and it is not proposed to elaborate further on this particular aspect of the development of our understanding of cast iron solidification processes. It is now generally agreed that all the common forms of flake graphite (A to E) form directly from the melt during solidification^(2,19).

While it is accepted that the common forms of flake graphite form directly from the melt, a number of workers have continued to attempt to provide evidence for a theory, championed by Kondic^(20,21), that indirect graphite formation during solidification can sometimes occur. It is known that when cementite is graphitised at 'low' temperatures, compact aggregates of graphite are formed. As the temperature is raised it becomes less compact and, at temperatures approaching the solidus, 'flake-like' forms of graphite can occur by solid state decomposition of the carbide. No demonstration has ever been made however of true flake graphite occurring by this process, except under conditions

where melting could have occurred^(5,22). Evidence has recently been presented however that at least a small proportion of the graphite encountered in mottled structures is closely associated with the cementite phase and may be the product of an indirect graphitisation process^(20,22).

2.2.3 Spheroidal Graphite Cast Iron

Like the ordinary grey cast irons, spheroidal graphite cast irons essentially solidify according to the iron-graphite equilibrium diagram. The change from flake to spheroidal graphite morphology is produced by a change in the crystallographic growth direction, induced as a result of compositional changes in the melt^(3,4).

The atomic arrangement in graphite is that of a simple hexagonal cell. Surface active elements, such as sulphur, are preferentially adsorbed onto the prism planes of the graphite cells, lowering the interfacial energy of these planes with the melt, and thereby encouraging further graphite growth to occur on them. When the surface active element content of iron is sufficiently low, the basal plane has the lowest interfacial energy and growth occurs on these planes. The mode of action of magnesium and other spherodising elements is to react with the surface active elements, and in particular sulphur, to prevent adsorption onto the prism plane and thus allow growth to occur on the basal plane^(3,4).

Due to the action of surface active agents in the melt, flake graphite tends to grow in a direction parallel to the basal plane of the unit cell by adding atoms onto the prism faces. The flakes therefore consist of long sheets of crystals with their basal planes at the top and bottom face. The weak bonding between adjacent basal planes of carbon atoms permits easy relative displacement of the basal planes facilitating the bending, turning and twisting of the flake graphite as it grows^(3,4).

In the case of spheroidal graphite, growth proceeds radially from the centre of nucleation by addition of carbon atoms in the form of additional layers of basal planes. Growth therefore occurs in a direction perpendicular to the basal plane, resulting in a nodule consisting of columnar graphite crystals with their basal plane at right angles to the radial direction of the nodule, and with the basal plane at the surface of the nodule^(3,4).

As a result of the change in graphite morphology there is also a change in the relative distribution of the eutectic phases, austenite and graphite. In hypoeutectic irons the spheroidal graphite nodules grow to a limited extent with the surface in contact with the liquid metal, but are soon surrounded by a solid austenite shell. The growth rate of the graphite nodules therefore becomes dependent upon the rate with which carbon diffuses through this shell and iron diffuses out to make room for carbon atoms. This process is relatively slow and hence these irons are easily undercooled into the metastable region. In hypereutectic irons the graphite spheroids grow in contact with the liquid until the eutectic temperature is reached. The austenite shell is then formed and growth continues in the same manner as in hypoeutectic irons⁽⁴⁾.

2.2.4 White Cast Iron

The white iron structure is the result of solidification taking place according to the metastable iron-iron carbide system. The eutectic alloy solidifies to produce a mixture of cementite and austenite and the proeutectic phases for the hypo- and hypereutectic alloys are austenite and cementite respectively.

The practical problems associated with the study of the solidification

of white irons are somewhat more difficult than those with grey irons. In samples of white iron quenched during the eutectic arrest it is difficult to distinguish between the eutectic solidified before and during quenching. In addition they are of lesser importance commercially than grey cast iron and hence have stimulated less interest. As a result of these factors significantly less is known about white iron solidification than their grey counterparts⁽²⁾.

The white iron eutectic can have either a globular carbide structure, characteristic of ledeburite, or a plate like acicular structure. Very little is known about the factors that determine which type of structure will form. It is believed that the plate structure solidifies after a greater amount of undercooling than is required for the solidification of the ledeburitic structure. A high melting temperature and a very rapid cooling rate consequently tend to promote the plate like structure⁽²⁾ and high sulphur levels are also believed to encourage its presence⁽²³⁾. Under conditions of unidirectional solidification the eutectic may also exhibit a lamellar form⁽²⁴⁾.

It will be noted that on the Fe-C equilibrium diagram, shown in Figure 1, the eutectic temperature for the austenite-graphite eutectic is somewhat higher than that for the iron-cementite eutectic. The formation of the iron-cementite eutectic is therefore dependent upon undercooling the alloy to below the iron-cementite eutectic temperature before the iron-graphite eutectic has nucleated. The factors which tend to render the formation of the austenite-cementite structure more likely may therefore be summarised as follows^(2,5,8) :-

- (i) A reduction in the number of nuclei available for the graphitic eutectic.
- (ii) A reduction in the growth rate of austenite-graphite eutectic cells.

(iii) A high rate of cooling.

(iv) The presence of carbide stabilising elements which reduce the temperature interval between the stable and metastable eutectic temperatures.

Hillert⁽¹⁹⁾ has made progress in rationalising the kinetic theory for the formation of the alternate forms of the eutectic, particularly at temperatures below the carbidic eutectic transformation temperature. He has explained that the graphite eutectic may be more readily nucleated than the carbidic eutectic. Once nucleated however, the growth rate of the latter is much higher and hence white solidification can proceed very rapidly from a single cementite nucleus and spread to all parts of a casting of considerable dimensions. The well known effects of cooling rate on the relative tendency to form the graphitic or carbidic eutectic must therefore be explained in terms of the kinetics of the two alternate reactions⁽¹⁹⁾

2.2.5 Mottled Cast Iron

Under intermediate cooling conditions a part of the eutectic may solidify as graphitic and ^apart carbidic. This leads to a mottled fracture appearance.

Hong and co-workers⁽²⁵⁾, using a unidirectional solidification technique (see section 2.7.6), have identified mottled iron structures in terms of three classifications:-

Type 1: The white iron eutectic cells form first in the melt and the grey eutectic growth occurs in the residual melt between the white cells.

Type 2: The eutectic growth occurs with a high degree of co-operation between the stable Fe-graphite and the metastable Fe-Fe₃C eutectics.

Type 3: The grey eutectic cells form first in the melt and then white eutectic growth occurs in the residual melt between the grey cells.

Whether it is the carbidic or graphitic eutectic which tends to form first depends upon the effects of cooling rate and alloy composition upon their relative kinetics of formation. A subsequent change in the solidification mode may however occur as a result of the preferential segregation of elements to the solid and liquid phases. For example, the white iron structure may form first, as in the case of Type 1 mottled irons, and, due to the preferential segregation of graphite stabilising elements such as silicon and nickel to the remaining liquid, may be interrupted by the graphitic mode of solidification. In such a mottled iron the grey region is confined to the spaces between the white colonies or cells and does not show the characteristic shape of austenite-graphite eutectic colonies^(19,22,25,26).

2.3 THE EFFECT OF COOLING RATE ON THE MICROSTRUCTURE OF CAST IRONS

The effects of cooling rate on the microstructure of cast irons have long been appreciated. It is generally accepted that increasing the cooling rate during solidification tends to favour the formation of finer graphite flakes and ultimately, beyond some critical cooling rate, a white iron will result.

The primary effect of cooling rate is to influence the degree to which the eutectic liquid will undercool below the equilibrium transformation

temperature before solidification commences. The degree of undercooling has a considerable influence on the morphology of the graphite produced and the tendency to form the carbidic eutectic^(1,2,27).

The relationship between the cooling rate and the degree of undercooling is illustrated in Figure 3⁽¹⁾. The equilibrium transformation temperature for the graphitic and carbidic eutectic are represented by the two horizontal lines indicated as T_1 and T_2 respectively. The line XU indicates the effect of increasing cooling rate on the freezing temperature of the austenite-graphite eutectic and WZ the effect of increasing cooling rate on the freezing temperature of the carbidic eutectic. Figure 3 indicates that with increasing cooling rate the eutectic melt undercools progressively further below T_1 before solidification of the austenite-graphite eutectic takes place, until at a certain cooling rate, indicated by point W, the liquid has undercooled below T_2 and solidification of the carbidic eutectic takes place.

As the cooling rate, and hence the degree of undercooling, increases from X to point Y, the number of nuclei from which solidification of the eutectic originates, also increases progressively, resulting in a larger number of eutectic cells of decreasing size. The growth rate of each eutectic cell also increases, the greater the degree of undercooling. The net result is that in a grey iron which has been slowly cooled, a few slowly grown eutectic cells are produced, whereas if the same iron is cooled more rapidly, many more smaller, rapidly grown cells are produced^(1,2,8,27).

The degree of undercooling, and hence the cooling rate, also has a considerable effect on the structure of the graphite. The graphite within each eutectic cell forms a continuous three dimensional network of flakes. With a slow cooling rate there is less undercooling, producing

a slower growth rate with infrequent branching of the graphite network. This results in the formation of coarse type A flakes. With a faster cooling rate there is more undercooling, producing a higher growth rate and more branching of the graphite network. This results in the formation of the finer E and D types of flakes^(1,2,8). The type B rosette graphite is the result of solidification taking place at intermediate cooling rates⁽⁴⁾.

Gadgil and Kondic⁽²⁰⁾ have studied the effect of cooling rate on the graphite morphology in a series of hypoeutectic irons with various silicon contents, but a common carbon equivalent value of about 4.0. A 'unidirectional solidification' technique was used which involved solidification in a vertical, preheated mould, the bottom of which was sealed with a water cooled copper chill. The chill provided the principal means of heat abstraction and supposedly created conditions of unidirectional heat flow, so that the cooling rate of the metal in the mould decreased with distance from the chill. The iron solidifying in contact with the copper chill produced a ledeburitic structure. With increasing distance from the chill, and thus a slower cooling rate, the amount of graphite in the structure increased at the expense of cementite, and the flake graphite morphology changed from type D to B to A. In addition they observed the presence of a highly directionally orientated form of graphite, which they called 'streamer' graphite. This was found in association with cementite in a position between the totally ledeburitic structure and the onset of the type D graphite. Gadgil and Kondic suggested that some of the streamer graphite might be the product of cementite decomposition.

In addition to its effect on the eutectic phases, the cooling rate also influences the structure of the proeutectic phase. The effect of cooling rate on the primary austenite dendrites formed in hypoeutectic

irons has been investigated by a number of Japanese workers using 'unidirectional solidification' techniques^(28,29,30). The primary austenite dendrite spacing was found to decrease with increasing cooling rate and, to a lesser extent, with increasing carbon content of the iron.

In recent years the use of 'unidirectional solidification' techniques has been developed as a means of quantitatively investigating the effect of cooling rate on cast iron structure^(19,20,30,31,32,33). In earlier experiments however, variations in the cooling rate were simply achieved by varying the pouring temperature and the section size of the test piece - the principal factors controlling cooling rate in a commercial foundry operating with a particular moulding practice. With increasing section size and greater distance from the surface of a casting, the cooling rate is slower and hence there is less undercooling, with all the concomitant effects on eutectic morphology. A relatively low pouring temperature produces a high cooling rate through the solidification range and hence a high degree of undercooling^(2,8,34). A high pouring temperature would be expected to produce a slower cooling rate through the solidification range with less undercooling, thus producing coarse, type A graphite structures. Prolonged holding of the melt, especially with a high degree of superheat, does however tend to reduce the number of potential nucleation sites in the melt. In this case there is still a tendency to observe a significant degree of undercooling before eutectic solidification commences, leading to the finer forms of flake graphite⁽³⁵⁾. It has been suggested that this effect may be due to the elimination of oxides such as silica⁽¹⁾ or the dissolution of graphite particles in the melt, which would ordinarily act as heterogeneous nucleation sites^(10,35).

2.4 GRAPHITE NUCLEATION

The generally prevailing opinion is that the graphite present in grey

and S.G. irons nucleates on heterogeneous substrates in the liquid which lower the surface energy requirements for nucleation. The nucleation of both proeutectic and eutectic graphite in grey and S.G. irons is basically similar in nature, although the composition of the nucleating substrate may differ. In addition to the nuclei inherently present, it is common practice to introduce small amounts of an inoculating agent into the melt in order to increase the nucleation rate. There has been intense speculation concerning the origin and nature of the nuclei from which the graphite grows and many theories have been advanced. These have been reviewed by Wallace⁽⁴⁾ who has summarised the possible nucleation substrates for both grey and S.G. irons as follows:-

- (i) Graphite particles which may be deliberately added or are residual in the melt.
- (ii) Dissolved gases or magnesium vapour.
- (iii) Graphite precipitated in regions of silicon supersaturation.
- (iv) Oxidation products of silicon or aluminium⁽³⁶⁾.
- (v) Carbides with non-metallic or salt like structures, such as calcium or aluminium carbides.
- (vi) Boron nitride.
- (vii) Various sulphide particles including those which are the product of spherodising additions.

Some of these theories have enjoyed a fair amount of acceptance while others have not withstood the accumulation of additional data. It does appear however, that more than one type of substrate can serve for graphite nucleation^(4,5,37).

In commercial practice the number of nuclei present may be artificially increased just prior to casting by the introduction into the melt of a

suitable inoculating agent. One of the effects of inoculating the melt is to reduce the amount of undercooling of the eutectic liquid, which takes place at a given cooling rate, before solidification commences. This effect is depicted schematically in Figure 4, in which 'Iron 1' represents an iron which has not been inoculated and 'Iron 2' represents an inoculated material. At a given cooling rate, say R_s , the well inoculated 'Iron 2' undercools much less than 'Iron 1' prior to the start of eutectic solidification and, as a result, can sustain a very much higher cooling rate, R_2 , before undercooling into the region of carbidic solidification⁽¹⁾.

The effect of inoculation on the structure of cast irons follows directly from the degree of undercooling. Increasing the number of nuclei present, and thereby decreasing the degree of undercooling before eutectic solidification commences, causes the graphite to become coarser, giving rise to type A flakes in favour of the undercooled varieties^(4,10,38,39), and also produces smaller eutectic cells^(1,39). The effectiveness of inoculants in decreasing the eutectic cell size has been observed to improve with decreasing carbon equivalent value⁽³⁹⁾. The effects of inoculation are especially beneficial in high strength cast irons, since it ensures the formation of the graphite eutectic without the need to resort to excessively high silicon levels, which would otherwise have an adverse effect on the mechanical properties.

A number of materials have successfully been used as inoculants^(1,2). Graphite itself is a most potent inoculant and is most effective when pure^(5,10,36) with a well developed crystal structure⁽⁴⁰⁾. Silicon containing inoculants include ferrosilicon containing 75 or 80 mass % Si^(1,2,10,36), calcium silicide containing about 60 mass % Si⁽³⁸⁾ and some alloys of silicon with other metals such as manganese, iron, zirconium or copper⁽⁵⁾. For these inoculants to be effective they must be impure,

the principal common impurities being aluminium and calcium in amounts upto about 5 mass %⁽³⁶⁾. Mixtures of commercial ferrosilicon or silicon with aluminium and/or calcium are particularly effective⁽⁵⁾. Aluminium or calcium alone, or cerium as Mischmetal, can also act as inoculants^(5,36). Pure silicon alone is generally believed to have no inoculating power⁽³⁹⁾. It has recently been shown however, that pure silicon is a potent inoculant but that its effect fades rapidly⁽⁴⁰⁾. The amount of inoculant required is generally quite small. As little as 0.05 mass % carbon, added as graphite⁽⁵⁾, or 0.5 mass % silicon, added as ferrosilicon⁽³⁹⁾, have been reported to produce effective results.

The effects of inoculation tend to be somewhat transient. If, after the introduction of the inoculant, the melt is held at temperature, then the inoculating effect, when the melt is ultimately cast, tends to fade gradually with increasing hold time⁽⁸⁾. A high degree of superheat tends to promote the fading effects⁽²⁾. It has also been shown that violent agitation of the melt, by for example gas bubbling, can also result in the destruction of the nuclei⁽²⁾. Decreasing the number of nuclei present in this way tends to increase the amount of undercooling observed prior to the commencement of eutectic solidification at a given cooling rate, thus tending to promote the formation of the more undercooled forms of graphite and, ultimately, the carbidic eutectic⁽³⁸⁾. This tendency for the number of nuclei present in the melt to decrease with holding time and with degree of superheat is also observed with irons which have not been inoculated^(1,10,35).

The effectiveness of inoculants appears to be influenced by the sulphur content of the metal. In low sulphur irons, graphite inoculant additions readily dissolve and their effect fades so rapidly that a ladle addition produces no inoculation. In the presence of normal sulphur levels, the rate of dissolution of a graphite addition appears to be

retarded and it becomes an effective inoculant. Ferrosilicon, strontium containing ferrosilicon and barium containing ferrosilicon have also been shown to be relatively poor inoculants for low sulphur (<0.03 mass %) flake graphite irons. The only ladle inoculants which have been found to inoculate satisfactorily low sulphur flake graphite irons are those containing appreciable quantities of calcium, cerium or magnesium⁽⁴⁰⁾.

In practice there may be limitations on the extent to which inoculation can be applied. Grey cast irons tend to swell on solidification which may result in unsoundness in the form of internal porosity or surface defects⁽¹⁾. The amount of swelling, and hence the probability of developing unsoundness, tends to increase with the number of centres of eutectic solidification. The production of a sound casting with a high degree of nucleation therefore tends to become more difficult. Ideally it is desirable to solidify with as little undercooling as possible, thereby avoiding the formation of the carbide eutectic, and in such a way that the solidification of the graphite eutectic occurs from as few centres as possible to give the best chance of obtaining a sound casting⁽¹⁾. Recently it has been found that strontium silicide, ferrosilicon containing strontium and mixtures of pure ferrosilicon with strontium metal can have a powerful inoculating effect, without adversely affecting the tendency towards increased unsoundness^(1,5). It is thought that the action of strontium is not to increase the nucleation rate but to increase the growth rate of those nuclei already present. By increasing the growth rate without increasing the number of eutectic cells a sounder casting is produced, whilst still ensuring that the degree of undercooling is sufficiently small to avoid the formation of the carbidic eutectic⁽¹⁾.

Sulphides, including the products of spheroidising additions such as magnesium or rare earth metals, show a strong tendency to act as

substrates for nucleation thereby increasing the eutectic cell count and decreasing the tendency to form the carbidic eutectic and the under-cooled forms of graphite^(4,5,37). Manganese sulphide is capable of acting as a nucleation substrate, the optimum degree of nucleation being obtained at 0.75 mass % Mn in the presence of 0.04-0.06 mass % S⁽³⁷⁾.

Wallace^(4,13,37) has suggested that the effectiveness of various sulphide formers in reducing the chilling tendency and increasing the cell count is closely related to the thermodynamic stability of the sulphides formed. Comparison of the behaviour of various inoculants with the free energy of formation of the sulphides capable of being formed by each, shows a close relation with their effectiveness as inoculants. Cerium and strontium have the highest negative free energy of formation, followed by calcium and barium. Titanium and zirconium sulphides have a relatively low free energy of formation, close to that of manganese. Wallace suggests that sulphides can act as substrates for graphite nucleation and that the more stable the sulphide the more effective the inoculating action. Experimental observations appear to confirm that titanium sulphide does not have any significant ability to act as nucleating sites⁽⁴¹⁾. Magnesium also forms stable sulphides and is believed to act as a powerful inoculant. In commercial cast irons however, its effect on the crystallographic growth behaviour of graphite is more important than its inoculating effect⁽⁴⁾.

2.5 COMPOSITIONAL INFLUENCES ON CAST IRON STRUCTURE

The physical and chemical properties of grey cast irons may be varied by alloying with various elements, in a manner similar to that applying to other ferrous materials, in order to control or modify the structure of the metallic matrix. It must be remembered however that it is the graphite dispersion which has the dominating influence on the mechanical

properties of grey irons and that the graphite is derived from the solidification process. The extent to which alloying elements may be deployed to modify the structure and properties of cast irons is partly dependent on their likely effects on the solidification process, though this is not always the case, for example, Nihard Cast Iron is martensitic and during heat treatment manganese affects the transformation characteristics.

The compositional components of grey cast iron may be divided into essentially two groups:-

- (i) Those which affect the relative stability of the graphitic and carbidic forms of carbon in the structure.
- (ii) Those which influence the nucleation and growth mode of the graphite.

General reviews of the elements falling into these categories are presented in sections 2.5.1 and 2.5.2 respectively. The alloying components of especial interest with respect to this particular research investigation are sulphur, nitrogen and titanium and these will be considered separately and in somewhat more depth in sections 2.5.3, 2.5.4 and 2.5.5 respectively.

2.5.1 Carbide Stabilising and Graphite Stabilising Elements

Certain of the alloying elements introduced into cast irons have the effect of increasing the relative stability of either the graphite or the cementite, hence rendering the presence of one or other more likely. In terms of the solidification behaviour of cast irons, these elements manifest their presence by increasing or decreasing the difference between the equilibrium temperature for the formation of the graphitic and carbidic eutectics⁽¹⁾.

Ideally the producer of grey iron castings desires that point W on Figure 3 should be at as high a cooling rate as possible, within the limitations imposed by other factors such as chemical composition, in relation to the specified mechanical properties. The introduction of a suitable graphite stabilising element, such as silicon, will tend to increase the interval between the equilibrium graphitic and carbidic eutectic transformation temperatures (Figure 5). In so doing, the likelihood of undercooling into the metastable region is diminished, thus ensuring that a grey iron structure is produced⁽¹⁾. Silicon is the most powerful graphitising agent usually present in cast irons. Weight for weight, titanium is a much more powerful graphitiser. Other lesser graphite stabilising elements include carbon itself, nickel and copper⁽³⁾.

If a suitable carbide stabilising element, such as chromium is introduced into a cast iron, then the temperature interval between the two possible eutectic transformations will tend to be reduced (Figure 6). The ease with which the eutectic liquid can be undercooled below the carbidic eutectic transformation temperature is therefore increased with the result that the formation of the white iron structure is rendered more likely⁽¹⁾. Increasing the concentration of carbide stabilising elements may eventually lead to the carbidic eutectic becoming the more stable phase in cast iron⁽⁵⁾. The alloying elements which tend to stabilise the carbide structure include chromium and vanadium and, to a lesser extent, molybdenum, tungsten and manganese^(3,4,23).

Some elements, such as aluminium and zirconium, may act as either carbide or graphite stabilisers depending upon the concentration present⁽³⁾. In concentrations upto 3 mass %, aluminium behaves as a graphitiser⁽⁴²⁾, but beyond this amount it behaves as a carbide stabiliser. The effect of aluminium, and also zirconium, at low concentrations may be due to its tendency to react with, and therefore remove from solution, elements such

as oxygen and nitrogen which, as a result of their effect on the graphite growth mechanism, tend to encourage the formation of the carbidic eutectic^(43,44). The behaviour of aluminium in concentrations greater than 3 mass % is associated with the formation of stable aluminium carbides⁽³⁾.

2.5.2 Compositional Components Affecting the Growth Behaviour of Graphite

A peculiar feature of cast irons is their susceptibility to the effect of certain minor compositional components which in other ferrous materials may be unimportant or have only a limited influence, yet in cast irons profoundly modify their structure and properties by their influence on the nucleation and/or growth processes during solidification. The concentration of these elements required to bring about changes in graphite morphology are generally very small - a particularly disturbing aspect for commercial foundries, since their effects are not generally beneficial.

The most widely documented, and also probably the best understood example of the effect of trace elements on graphite morphology, is in the production of S.G. irons. The addition of small amounts of magnesium, calcium or rare earth elements, such as cerium or yttrium, to low sulphur content iron produces a substantial change in the crystal growth habit of the graphite, resulting in the formation of spherulites⁽⁴⁾. Normal flake graphite grows by crystallisation from the melt in a direction parallel to the close packed basal planes. In a graphite spherulite there is a radial array of twisted graphite fibres, each growing normal to the basal plane from a common centre^(1,3,4). There are many theories attempting to explain how the presence of elements such as magnesium bring about this change in morphology. The explanations offered include⁽¹⁾:-

- (i) The occlusion of foreign atoms in the growing graphite.
- (ii) The existence of particular nuclei or nucleating conditions in the melt.
- (iii) The provision or removal of surface active agents at the surface of the growing graphite crystals.

Wallace suggests that the latter theory is probably the one most likely to be correct - see section 2.2.3^(4,37). The amount of the above elements required to bring about the formation of graphite spherulites is very small - in the case of magnesium 0.02-0.04 mass %. As a result of the change in graphite morphology, S.G. irons essentially behave as normal, ductile ferrous materials^(1,6). Unfortunately, not all the trace elements encountered in cast irons have such a beneficial effect.

The presence of small amounts of lead, antimony, bismuth or tellurium may prevent the formation of graphite spherulites by the addition of magnesium, and instead give rise to degenerate forms of graphite^(1,4). The harmful effects of these trace elements may be neutralised by the presence of small amounts of rare earth elements with the magnesium addition⁽¹⁾. It is thought that lead, antimony, bismuth and tellurium tend to collect on the basal faces of the growing graphite cells and thereby encourage growth on the prism planes, thus producing flakes⁽⁴⁾. Rare earth additions prevent the influence of these harmful trace elements on the crystallographic growth direction, so that growth on the basal planes tends to take place⁽⁴⁾. The mechanism involved is not understood and indeed, if no lead, bismuth, antimony or tellurium is present, the rare earth elements themselves can inhibit the development of good spherulites⁽¹⁾.

The sensitivity of graphite to modification by trace impurities is not limited to irons with spheroidal graphite, but also applies to flake

graphite⁽¹⁾. The mechanism of formation of some of these degenerate forms of flake graphite is even less well understood than in the case of spheroidal graphite. In certain irons the graphite may appear as fine plates or needles in a 'pseudo-Widmanstätten' pattern, in addition to the usual graphite flakes. Its appearance suggests a solid state precipitation process, but in iron containing 14-16 mass % Si it may appear as the only form of graphite so that the possibility of a solidification process yielding 'Widmanstätten' graphite cannot be dismissed. Mesh-like graphite may also be the only form appearing in some castings and so is presumably a solidification product, although it is difficult to suggest a solidification mechanism^(5,45). The possibility exists that such abnormal structures may involve considerable solid state diffusion, either during or immediately following solidification, with a complete lack of co-operation in the growth of the phases⁽⁵⁾. These degenerate forms of graphite may significantly reduce the tensile strength of grey irons and are therefore undesirable^(4,46).

The presence of small amounts of lead, bismuth and tellurium are all known to increase the chilling tendency of grey irons and may lead to the formation of 'Widmanstätten' or mesh type forms of degenerate graphite. Lead, bismuth and tellurium have no solubility in solid iron and very limited solubility in liquid iron. It is believed that these elements collect at the surface of the growing graphite, and thereby restrict the growth of the eutectic cells, giving rise to considerable undercooling and degenerate graphite growth modes^(4,13,37,46,47).

Tellurium has a particularly powerful chilling effect and has been deliberately used as a chemical wash to induce the formation of a white iron layer on the surface of castings, in order to improve the wear properties^(37,46). As little as 0.01 mass % Te in grey iron produces

severe undercooling and ^arestraining effect on eutectic cell growth, while 0.02 mass % Te produces a completely white iron. Intermediate concentrations may result in a chilled surface while the interior of the casting exhibits mesh-like graphite or even compact spherulitic forms of graphite. It is believed that tellurium, combined with free 'unbalanced' sulphur, collects at the eutectic cell peripheries and thus impedes carbon diffusion across the boundary, which results in increased undercooling and the formation of degenerate graphite structures⁽³⁷⁾.

Selenium exerts a similar effect to tellurium, although less pronounced. In small amounts in grey irons it increases undercooling and the eutectic cell count, coarsens the graphite flakes and may produce compacted flake structures. Greater amounts of selenium can produce mesh-like structures and other degenerate graphite forms, probably by a similar mechanism to tellurium. Its effects are aggravated by the presence of hydrogen⁽⁴⁸⁾.

Bismuth in grey irons exerts a growth restricting effect and produces appreciable undercooling, although not as marked as with tellurium. As little as 0.05 mass % Bi causes grey iron to undercool an additional 12°C and increases the chill and cell count. Undesirable mesh or lacy types of graphite and poorly formed spherulites have been observed to form as a result of 0.01-0.06 mass % Bi additions, attended by increased amounts of pearlite in the matrix⁽³⁷⁾.

Elements such as lead, bismuth and tellurium may be accidentally introduced into cast iron from non-ferrous alloys, such as bearing metals, or from lead and tellurium containing free cutting steels^(37,46). Their effects are particularly alarming when one considers the concentrations required to induce changes in the graphite morphology. Abnormal graphite structures have been reported with as little as 0.0007 mass % Te or 0.019 mass % Pb⁽⁴⁶⁾.

The addition of rare earth elements to grey iron melts may nullify the effect of the above trace impurities, by preventing their influence on the growth direction and rate of growth of the graphite. However, when present in excessive amounts, rare earth elements themselves may exert a growth restricting effect^(4,40).

In grey irons antimony acts as a strong pearlite stabiliser without influencing the graphite structure. In S.G. iron it also tends to stabilise the pearlite but, as noted earlier, it also causes the spherulites to degenerate into flake-like forms. The pearlite stabilising effect appears to be the result of interference with carbon diffusion to the graphite^(4,37). Tin and copper also exert a strong pearlite stabilising effect⁽¹⁵⁾.

Boron also appears to collect at the eutectic cell boundaries and restricts their growth, increasing both the chilling tendency and the eutectic cell count. The increased cell count is attributed to the formation of boron nitride and its influence as a substrate for graphite nucleation in the melt. The collection of boron at the boundaries of the eutectic cells, in both grey and S.G. irons, results in a cell boundary network of carbides containing some boron nitride, which sharply lowers the strength and machinability. This network becomes more extensive with increasing boron until, at 0.2 mass % B, each cell is surrounded by cementite. Boron, in excess of that required to form boron nitride, exerts a cell growth restricting effect, thereby increasing the number of cells^(4,37).

The presence of phosphorus in the melt is believed to have a beneficial effect on graphite nucleation, giving rise to increased numbers of eutectic cells with decreased undercooling. This is believed to be associated with the significant reduction in interfacial energy between graphite and liquid iron produced by phosphorus additions, thus

lowering the surface energy requirements for nucleation and resulting in an increased number of graphite nuclei in the melt^(5,8,22).

Certain gaseous elements which dissolve in the melt may exert an influence on the graphite growth morphology. Oxygen has been found to increase the chilling tendency of grey cast irons when present in amounts in excess of 0.006 mass %. The normal oxygen levels encountered in commercial practice range from 0.005 to 0.015 mass %⁽⁴³⁾.

Hydrogen pick-up may occur from various sources such as from moisture in green sand moulds or from hydrocarbons. Hydrogen is believed to reduce the growth rate of the eutectic cells producing coarser graphite flakes with an increased chilling tendency^(5,8,9,49). The presence of hydrogen has also been found to accentuate the detrimental effects of lead on grey iron structures, although the mechanism involved is not understood. If lead is present in amounts in excess of 0.003 mass %, and if the hydrogen content is greater than the normal 0.0001-0.0002 mass %, some graphite separates in a pseudo-Widmanstätten pattern which can result in a 50% drop in the tensile strength of the iron⁽¹⁾.

2.5.3 Sulphur in Cast Iron

Sulphur has been shown to exert a considerable influence on the structure and properties of cast irons and, since it is present to varying degrees in all commercial irons, it is perhaps the single most important trace element encountered.

Investigators studying the solidification of Fe-C and Fe-C-Si alloys of high purity ($\ll 0.006$ mass % S) have observed that, when they are graphitic, the structure usually comprises fine type D graphite flakes in a largely ferritic matrix with pearlite restricted to cell boundaries.

At sulphur levels less than 0.002 mass %, the existence of degenerate forms of graphite, described as 'coral' or 'quasi flake' graphite, has been reported⁽¹⁵⁾. The presence of a trace of sulphur however, causes the graphite flakes to coarsen, giving rise to a type A structure in an increasingly pearlitic matrix. This is accompanied by an increase in the number of eutectic cells and an increase in the degree of undercooling of the eutectic liquid before solidification commences. The coarsening effect on the graphite flakes produced by small sulphur additions is so pronounced that Boyles^(9,49) has suggested that this element is solely responsible for type A flake structures, when they occur in commercial cast irons^(4,5,13,23,50). By increasing the sulphur content still further, at a given cooling rate, the degree of undercooling also increases. This tends to cause the graphite flakes to revert back to the more undercooled varieties and, ultimately, leads to the formation of the white iron structure^(2,5,8,9,13,23,37).

The carbide stabilising effect of sulphur at higher concentrations tends to encourage the formation of a pearlitic matrix^(4,13,37). As a consequence, the tensile strength and hardness generally increase with increasing sulphur content, reaching a maximum value in the range 0.04-0.06 mass % S^(4,13,37). With very high sulphur contents the graphite often takes the form of mesh-like or other degenerate forms, which adversely affect the mechanical properties⁽⁵⁾. In malleable irons also, sulphur exerts a retarding effect on graphitisation kinetics, which is thought to be associated with its segregation to the austenite-cementite interface as a result of its surface active nature⁽⁵¹⁾.

The microstructural changes brought about by sulphur additions to cast iron have been explained in terms of the independent effects which this element has upon the nucleation and growth processes involved in the solidification of the austenite-graphite eutectic. Oldfield⁽⁸⁾ has shown

that, at a constant level of undercooling, increasing the sulphur content of an iron increases the number of nuclei and hence the number of eutectic cells which form. This is believed to be associated with the marked effect which sulphur has upon the surface tension of liquid iron and the interfacial energy between liquid iron and graphite. In pure Fe-C-Si alloys, the surface tension is about 1.50 N/m. In the presence of 0.02 mass % S this falls to about 1.18 N/m and with 0.12 mass % S falls still further to about 0.91 N/m⁽⁵⁾. If the interfacial energy between graphite and liquid iron is similarly reduced by sulphur additions, then this would significantly reduce the surface energy requirements for nuclei to form and hence, explains the observed increase in the degree of nucleation in cast irons^(5,8).

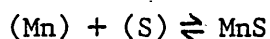
The tendency for small amounts of sulphur to cause the graphite flakes to coarsen is associated with a reduction in the growth rate of the eutectic cells^(5,13,15,41). It is believed that sulphur exerts a growth restricting effect which may also be associated with its surface active nature. Sulphur is insoluble in austenite and as solidification of the eutectic cells proceeds it is rejected into the remaining liquid. Sulphur atoms collect on the surface of the growing eutectic cells and appear to retard further growth by interfering with the transfer of atoms across the liquid-solid interface^(4,13). The reduction in the growth rate of the individual eutectic cells reduces the frequency of branching of the graphite skeleton and thus gives rise to the coarse type A flake structures^(2,15). The continuous enrichment of the liquid in sulphur causes the graphite flakes to coarsen progressively as they grow. This effect has been observed even in very low sulphur content irons⁽⁵⁾.

Associated with the growth restricting effect induced by sulphur is a tendency for the degree of undercooling to increase⁽⁸⁾. As a consequence, the likelihood of forming the metastable white iron structure is greater

in high sulphur content irons⁽⁹⁾.

It has already been noted that hydrogen also exhibits a tendency to reduce the graphitic eutectic cell growth rate, resulting in a coarsening of the graphite flake structure^(5,8,9). The effects of hydrogen and sulphur appear to be accentuated when both elements are present together⁽⁴⁹⁾, but it is not clear what mechanism is involved. It has even been suggested that hydrogen may have no effect at all except in the presence of sulphur⁽⁵⁰⁾.

In commercial cast irons the effects of sulphur are controlled by 'balancing' it with manganese^(4,5,8,13,37,45,50) with which it reacts according to the equation:-



For optimum chill reduction, the amount of manganese required is given by:

$$(\text{mass \% Mn}) = 1.7(\text{mass \% S}) + 0.25,$$

although slight variations on this relationship have been put forward by different investigators⁽¹³⁾.

The effects which sulphur has upon the nucleation and growth processes arise from the free sulphur in solution. This may be decreased, though due to the nature of the equilibrium for the above reaction, never completely eliminated, by increasing the manganese content. The relative amounts of manganese and sulphur present will therefore determine the amount of sulphur in solution in the melt and hence its influence upon the nucleation and growth processes in commercial irons. Even in the

presence of an excess of manganese there will still be a small amount of sulphur remaining in solution and this may be sufficient to account for the existence of A type graphite in normal grey cast iron^(13,50).

In molten iron, the manganese and sulphur are not in direct combination, but, as the temperature of the melt falls during solidification, manganese sulphide particles are precipitated at the eutectic cell boundaries⁽⁴⁵⁾. Opinion varies as to whether precipitated particles of manganese sulphide can act as a nucleating substrate for graphite^(4,5,13).

2.5.4 Nitrogen in Cast Iron

Nitrogen, like sulphur, is also found to varying degrees in all commercial cast irons. Depending upon the melting practice, the melting unit and the fuel, nitrogen contents may range from 20 to 150 ppm⁽⁴⁴⁾. The influence of nitrogen on the solidification mechanism, and hence the structure of cast iron, has not received as much attention as sulphur and hence it is only relatively recently that its effect has begun to be appreciated. The most extensive investigation into the effect of nitrogen on cast iron structure appears to be that undertaken by Dawson⁽⁴⁴⁾ who discovered that by treating the molten iron with fluxed ferrocyanides, cyanamides or similar nitrogen containing compounds, nitrogen contents in the range 30 to 500 ppm could be achieved. Nitrogen was found to exert a strong carbide stabilising influence. In as cast hypoeutectic, hypereutectic and S.G. irons the amount of combined carbon increased with increasing nitrogen content. The graphite flakes were also modified, tending to become shorter, thicker and more curved^(1,5,44,52). It would appear that growth in the direction of the basal plane is progressively discouraged and growth at right angles to this becomes more pronounced, but the mechanism involved is not understood⁽¹⁾. This compaction could

be due to the presence of the element(s) forming the cyanide/ferrocyanides (e.g. calcium, sodium) rather than the nitrogen alone. Attempts to produce compaction by deliberate additions of nitrogen (from high nitrogen ferromanganese, nitrogen gas and calcium cyanimide sources) have failed to produce compacted graphite forms⁽⁶⁸⁾.

It is claimed that the presence of nitrogen favours the formation of a pearlitic matrix in grey irons and also produces an increase in both the tensile and impact strength. This improvement in both tensile and impact strength must be due to the change in the structure of the graphite flakes since the presence of increasing amounts of cementite would be expected to have a detrimental effect^(44,52). The improved tensile strength brought about by nitrogen additions can be quite significant and may be commercially useful. Morrogh reports that increasing the nitrogen content from the normal value of about 50 ppm to 150 ppm can result in a 30% increase in the tensile strength⁽¹⁾. Excessive additions of nitrogen may however lead to porosity in the casting and the presence of undesirable amounts of cementite^(44,52).

Increasing the nitrogen content of S.G. iron also produces increased amounts of pearlite with an accompanying increase in the tensile strength, but a decrease in the ductility of the iron^(44,52).

The carbide stabilising effect of nitrogen is also evident in malleable iron - the time for the annealing process being significantly increased. This is accompanied by an increase in the size and a reduction in the number of nodules formed. All of these effects are clearly detrimental to the production of malleable iron^(44,52). Small additions of aluminium, boron or titanium are commonly made to malleable iron to increase the number of graphite nodules formed, probably as a result of their strong tendency to form nitrides⁽⁵²⁾.

The effects of nitrogen on the structure of ordinary grey and S.G. irons may also be neutralised by the addition of small amounts of aluminium or titanium to the melt. In grey irons, titanium is preferred to aluminium as a nitrogen neutralising additive, since it involves less risk of promoting hydrogen pinhole formation. In practice pinholing is not found to be a problem but aluminium produces a lot of alumina slag which is trapped in the top of the mould. This tendency for alumina formation tends to remove the aluminium from the melt. Aluminium also promotes Kish graphite formation by reducing the carbon saturation. This tends to form a soft top as does the alumina. The neutralising effect of these additions is presumably due to the removal of nitrogen from solution by its fixation as stable nitrides^(44,52).

2.5.5 Titanium in Cast Iron

Titanium, like aluminium and zirconium, may behave as either a graphitiser or a carbide stabiliser in cast irons, depending upon the amount present. When added in small quantities to commercial grey cast irons it behaves as a graphitiser, but shows a marked tendency to refine the graphite structure^(3,53,54,55,56). In larger amounts, titanium behaves as a simple carbide stabilising element by virtue of its ability to form stable titanium carbides^(3,41,55). On the other hand, titanium as a powerful graphitiser, has been found to produce coarse graphite in cast irons cast to large sections. In cupola melted iron this appears to be related to the melting practice which is reducing⁽⁶⁸⁾.

The graphite refining effect induced by small titanium additions has long been appreciated. Norbury and Morgan⁽⁵³⁾ showed that iron normally solidifying to give a coarse flake structure could, by the addition of 0.1-0.2 mass % Ti, be made to yield fine undercooled graphite which produced

an increase in both the tensile strength and hardness⁽⁵⁷⁾. The process was considerably enhanced by bubbling carbon dioxide through the melt prior to casting⁽⁵³⁾. It was initially believed that the graphite refining effect was the result of an inoculation phenomena, due to the formation of titanate inclusions in the melt, and the presence of carbon dioxide was essential in providing suitably oxidising conditions for their formation. It was later demonstrated that the contribution of carbon dioxide was not that of an oxidant, but instead was effectively degassing the melt, thereby removing hydrogen, in particular, which has a growth inhibiting effect on graphitic eutectic cells⁽⁵⁰⁾.

It is now generally believed that titanium is a scavenger of sulphur and will effectively remove from solution, as titanium sulphide, any which is not balanced by manganese. By removing the sulphur from solution in this way, the effects that it would have had on the nucleation and growth processes, as described in section 2.5.3, are nullified. Titanium additions to a cast iron are therefore associated with the production of a low degree of nucleation in the melt, with an increased amount of undercooling. The eutectic cells which form have a much higher growth rate resulting in a finer, more branched graphite network^(5,8,58).

Titanium will also react with any nitrogen in solution, to form titanium nitrides, in a similar way to that described by Dawson for aluminium additions to cast iron⁽⁴⁴⁾. The carbide stabilising effect of nitrogen, described in section 2.5.4, would therefore be neutralised. Small amounts of oxygen in solution in cast iron are believed to encourage the formation of carbidic structures⁽⁴³⁾ and titanium might also be expected to remove this from solution as titanium oxide⁽⁵⁵⁾.

The amount of titanium required to obtain the maximum graphitising effect will depend upon the nitrogen and oxygen contents and also the

concentration of sulphur unbalanced by manganese. Kumar and Das⁽⁵⁵⁾ have examined the effect of additions of upto 2.6 mass % Ti on the structure of hypoeutectic irons with very low sulphur contents and an excess of manganese (3%C, 0.75%Si, 0-0.05%S, 0.5%Mn). Upto 0.6 mass % Ti produced a graphitising effect, but beyond this amount there was an increasing tendency towards carbide stabilisation associated with increasing amounts of titanium carbide in the structure. Morrogh has noted that unless there is at least a slight excess of titanium present in the form of titanium carbide, then no refining of the graphite is produced. When the titanium is completely fixed, as either the sulphide or the nitride, then coarse graphite structures are obtained⁽³⁾.

The tensile strength of grey cast irons decreases with increasing titanium additions, being weakest at 0.04 mass % Ti. At contents greater than this the tensile strength increases. This is probably due to the removal of nitrogen from solid solution in the ferrite and the subsequent formation of titanium nitride. After complete nitrogen removal, the increase in strength is due to the excess titanium causing solid solution strengthening of the ferrite matrix⁽⁵⁹⁾.

Titanium has also been reported to have a deleterious effect on the structure of S.G. iron produced by magnesium additions. When present in amounts greater than about 0.1-0.2 mass %, titanium causes the spheroidal graphite to revert to flake like forms^(47,60), decreasing both the tensile strength and ductility⁽⁴⁾. These effects can be prevented by the introduction of rare earth elements into the melt or by increasing the magnesium addition⁽⁴⁾. The introduction of nitrogen into the melt by additions of calcium cyanide can also induce effective spherodisation again when the titanium levels are excessively high. In this case the excess titanium is removed as titanium nitride, which suggests that this does not have an adverse effect on spherodisation⁽⁶⁰⁾.

Titanium also appears to accentuate the detrimental effects of lead on the graphite structure in S.G. irons. In the presence of 0.1 mass % Ti, as little as 0.005 mass % Pb may cause the graphite to take a mesh-like form, resulting in a significant loss in ductility⁽⁴⁷⁾.

2.6 INGOT MOULD CAST IRONS

An extensive review of the literature concerned with the effects of composition on the structure and in-service behaviour of cast iron ingot moulds has been made by F. G. Wilson⁽⁶¹⁾. It is not proposed to elaborate further on this, but a few of the salient points, with respect to the present work, will be considered here.

In the U.K. the usual composition range of ingot mould cast irons is 3.7-4.0 mass % C, 1.2-2.0 mass % Si, 0.6-1.2 mass % Mn, 0.04-0.2 mass % P, 0.05-0.135 mass % S, the optimum composition depending to some extent upon mould size (for large slab moulds 1.6-2.0 mass % Si, small 1.2-1.6 mass % Si are used). It is reported that minor compositional variations within this range do have an effect on mould performance, depending on the mould design and steelworks operating conditions. The metallographic structure of ingot mould iron is controlled, to a certain extent, by its composition and also by the cooling rate, which is influenced by the size, shape and position within the mould. Usually, the structure of moulds of less than 5t consists of a mainly pearlitic matrix with interspersed iron phosphide and iron carbide complexes and fine, long, curved, randomly orientated graphite flakes. For larger ingot moulds (>5t), the cracking resistance can be improved by increasing the amount of ferrite present which can be brought about by increasing the silicon content. During usage the structure changes, becoming more ferritic with time.

Major failures occur due to cracking which can be minimised by ensuring

a totally ferritic structure with a large amount of coarse graphite. Ultimately moulds have to be scrapped due to craze cracking, if premature failure due to major cracking does not occur. The maximum resistance to crazing is found to be provided by a mechanically hard, growth resistant pearlite and cementite structure, with a small amount of fine graphite, susceptibility to crazing increasing with the amount of ferrite and coarse graphite present. As a consequence, the optimum structure is considered to be a pearlite-ferrite matrix with fine graphite flakes.

Excessively high sulphur levels can lead to the production of mesh graphite, which has a detrimental effect on mould life, and thus a sulphur content as low as possible is desirable. It has been reported that decreasing the sulphur content from 0.08 to 0.05% can increase mould life by as much as 25%, although this benefit is offset by the increased cost incurred in removing the sulphur. In commercial ingot mould irons, the effect of sulphur is neutralised by 'balancing' it with an excess of manganese, leading to the formation of manganese sulphide. Manganese sulphide can, however, breakdown during service due to oxide envelopment and subsequent formation of FeS, resulting in a low melting point FeS-FeO grain boundary network which leads to increased crazing.

The nitrogen content of cast iron is profoundly influenced by the raw materials, the chemical composition and the method of melting^(62,63). Nitrogen contents in ingot mould cast iron are normally in the range 0.004-0.007%. Values of upto 0.019% have however been reported and these have been associated with the utilisation of a high proportion of steel scrap in the charge of hot blast cupolas. The solubility of nitrogen in liquid iron increases with decreasing carbon and silicon contents, as does the solid solubility of nitrogen in iron. The low carbon content of steel scrap is therefore associated with a relatively high nitrogen content which tends to be transmitted to cast iron produced from this material.

Nitrogen strongly stabilises pearlite and eutectic cementite and, as a result, limited amounts of nitrogen are considered beneficial in iron for small ingot moulds, since growth and craze cracking are minimised. Nitrogen contents in excess of 0.007% however, produce compacted graphite which has a deleterious effect on mould life. Slow cooling rates and high ferrostatic pressures are contributory factors favouring compaction, especially at the base of heavy sections. The maximum amount of nitrogen which can be held in solution on solidification is 0.015%. If the nitrogen content exceeds this, the excess is rejected from solution, displacing some of the eutectic liquid and producing interdendritic porosity or blowhole defects.

Nitrogen pickup can be minimised by increased coke charges to the cupola, but much closer control is required to prevent Kish graphite formation and its inherent problems. The more usual method of neutralising nitrogen is by the addition of nitride formers such as aluminium or titanium. An addition of 0.1% of aluminium or titanium is sufficient to eliminate completely compacted graphite, producing irons whose mechanical properties and thermal conductivity are equivalent to those of low nitrogen, untreated irons. Aluminium, being the cheaper of the two, would be the most obvious agent, although hydrogen pickup can be a problem if water is available to oxidise aluminium to alumina. The alumina goes into the slag and complete removal of aluminium often results. The presence of hydrogen can lead to the production of a 'Widmanstätten' graphite structure if lead is present. Hydrogen also can cause pinholing. Aluminium reduces the carbon saturation level in liquid iron, effectively increasing the CEV and rendering the formation of Kish graphite more likely. The presence of Kish graphite causes soft tops, as does the presence of aluminium - the latter, with its high affinity for oxygen, forms an alumina dross which becomes trapped at the mould top. Titanium, added as ferrotitanium

prior to casting to produce a residual 0.03-0.1 % Ti in ingot mould iron, is thus found to be a more effective neutraliser of nitrogen, producing finer, more branched graphite. The normal range used is 0.04-0.06 % as 0.1 % has been found to produce soft moulds⁽⁶¹⁾.

2.7 EXPERIMENTAL TECHNIQUES FOR THE STUDY OF THE SOLIDIFICATION OF CAST IRONS

The major reason for solidification investigations of cast irons has been to obtain accurate interpretations of microstructural features arising from different alloy compositions, impurities and thermal histories, in terms of nucleation and growth phenomena, in order to supplement the practical observations in foundry practice. Several methods have been utilised in previous solidification studies, although not all of them pertain to the practical solidification aspects observed in normal foundry practice. Rather, the methods have been found to be more use for fundamental studies.

Some methods which have been utilised include:-

- (i) The classical interrupted solidification and quenching technique.
- (ii) Unidirectional solidification and decantation to allow examination of the solidification interface.
- (iii) The dip-stick method.
- (iv) Analogue methods.
- (v) Tracer methods.
- (vi) Unidirectional solidification employing a single cooling rate throughout each experiment - essentially a zone melting technique.
- (vii) A combination of the classical interrupted solidification method and a modified unidirectional solidification technique, such that the cooling system allows a variety of cooling rates to be obtained

in each solidified specimen. Solidification actually takes place under conditions of unidirectional heat flow, since unidirectional solidification is not strictly feasible.

2.7.1 The Interrupted Solidification Technique

The classical technique for studying solidification phenomena in cast irons involves obtaining cooling curves, generally for small ingots, and quenching these ingots from various temperatures before, during and after the eutectic arrest^(8,18,21). In the case of a sample solidifying as grey iron, any liquid present prior to the quench solidifies as a white iron, allowing the graphitic eutectic cells to be identified. Study of the solidification of white iron using this technique is more difficult since it is not possible to identify the microstructural components formed before and after the quench⁽²⁾. Whilst most of our knowledge of the solidification behaviour of cast irons has been derived from this technique, it is somewhat limited in that it is difficult to quantify the solidification conditions and relate them to the conditions existing in larger commercial castings.

Use of sample test pieces such as the wedge chill test⁽²⁾ is useful as a quality control check, but not as a means of studying fundamental aspects of solidification behaviour. Undoubtedly foundry-men have developed sufficient experience to enable them to be reasonably successful in their predictions, but their experience has yet to be set on a rational basis in relation to cast iron metallurgy.

2.7.2 Unidirectional Solidification and Decantation

This method involves filling a series of identical moulds with molten metal. The metal is allowed to solidify 'unidirectionally' for pre-

determined times and afterwards the remaining liquid is rapidly decanted, permitting examination of the solidification interface and the thickness of solidified metal, with varying solidification times, to be ascertained. Unfortunately, a number of moulds are required and it is difficult to ensure that all are identical. With wide freezing range alloys, liquid metal is entrained in the pasty region leading to inaccuracies. Also, it is not applicable to the cooling rates encountered in conventional foundry sand or metal moulding practice. It is therefore of more use to the fundamentalists rather than practitioners with respect to analysing grey iron foundry problems⁽⁶⁴⁾.

2.7.3 The Dip-Stick Method

This method is also known as the bar test or as differential sounding. It involves dipping a probe into the molten metal until the solidification front is reached. This allows the position of the solidification front after varying times to be ascertained. Non-planar solidification fronts can lead to misleading results and the presence of the dip-stick may disturb the solidification process. Despite these disadvantages, foundries often use this method as a production control technique.

2.7.4 Analogue Methods

There are two analogue methods, the hydraulic analogue and the electrical analogue, although the former method is not widely used. In the hydraulic analogue, heat flow during solidification is represented by water flow, thermal resistances by the pipe friction factor, and external thermal resistances (radiation from the mould wall or as a result of an air gap at the metal-mould interface) by pipe constrictions. The electrical analogue is a specialised application of an analogue computer where heat

flow due to temperature gradients is represented by the flow of electricity due to a voltage gradient. This has been used by a number of investigators and the method is reviewed by Ruddle⁽⁶⁵⁾.

Performance of the analysis is easy, quick and cheap, but, as a number of analogue sections must be used to represent the solidification of castings, this 'lumping' technique limits the accuracy. Also, the thermal properties required for setting up the analogue are not always available and, furthermore, the technique only produces a theoretical, not a physical, analysis of the system.

2.7.5 Tracer Methods

These involve the addition of:-

- (i) Radioactive tracers, which may be either active, and thus require the obvious safety precautions, or inactive, which can later be irradiated to activate the tracer, although if the casting is large this may prove difficult.
- (ii) Non-radioactive tracers, which usually form phases in the liquid with properties differing from those of the base alloy. These differing properties can be ones of colour, machinability or chemical activity.

The tracer is added to the liquid metal during solidification and thus the solidification front at the time of the addition can be identified. Unfortunately, as only one position of the solidification front can be identified per cast, this method becomes costly and time consuming. Also, the tracer additions may interfere with the nucleation and growth mechanism, disturb the solidification mechanism, and may give misleading results with wide freezing range alloys. The time interval between adding the tracer and its effect on the solidification front must be negligible to be meaningful.

2.7.6 Directional Solidification

The technique variously termed 'controlled solidification' or 'directional solidification' has been applied to the study of the solidification of cast irons by a number of workers^(19,24,25,31,32,33,42). The technique involves melting a specimen, in a long, thin container, in the hot zone of a furnace and pulling it into a colder zone at a constant speed. Solidification takes place at the same position in the temperature gradient and occurs with the same speed as the container is pulled. It is thus possible to predetermine the rate and direction of solidification and to study how the rate will affect the shape of the solidification front and the microstructure of the solidified material. The solidification process may be interrupted by suddenly withdrawing the whole tube from the furnace and quenching it into a suitable medium. As with the previous technique (Section 2.7.2), the cooling rates used have been much slower and the conditions under which melting and solidification takes place are considerably different from those encountered in commercial foundry practice.

2.7.7 Solidification Under Conditions of Unidirectional Heat Flow

Techniques involving the 'unidirectional solidification' of cast iron under conditions of unidirectional heat flow have been employed by a number of workers.

Ogi and Matsuda⁽²⁸⁾ and Ibaraki⁽²⁹⁾ employed a simple technique in which molten iron was cast into a sand mould with a water cooled copper chill in the base. The technique was improved by Gadgil and Kondic⁽²⁰⁾ and Okamoto and Matsudo⁽³⁰⁾ who replaced the simple sand mould with a cylindrical shell mould contained within a preheating furnace. The lower end of the mould was sealed with a water cooled copper chill which provided the principal means of heat abstraction from the metal and hence created

unidirectional heat flow conditions, so that the cooling rate decreased with vertical distance from the base chill. The progressive decrease in temperature gradient with distance from the base gave rise to gradual structural changes, thus allowing a clear picture of the mechanism of formation to be obtained. The cooling rates produced were compatible with those encountered in commercial foundry practice. In addition, the production of various quantifiable cooling rates within a single specimen significantly reduced the amount of experimental work required, in comparison with the other techniques herein described.

Gadgil and Kondic⁽²⁰⁾ used this technique to investigate the effect of cooling rate on the microstructure of grey irons containing various amounts of silicon, but with a similar carbon equivalent value of about 4.0. The results obtained served to prove the usefulness of the technique but, unfortunately, they failed to quantify the cooling rates responsible for the various microstructures.

The quantitative relationship between solidification rate and unidirectional heat transfer rate has been studied for non-ferrous alloys by Moore⁽⁶⁶⁾ and Spinat⁽⁶⁷⁾. In this research, the method of Gadgil and Kondic⁽²⁰⁾ has been combined with the quantitative approach of Spinat⁽⁶⁷⁾, in order to study quantitatively the unidirectional solidification of ingot mould type iron under controlled, reproducible conditions, thus establishing the influence of variations in composition and cooling rate on the structure of these irons. The mechanism by which alloy additions and different heat transfer conditions affect and control the microstructure of these irons has been investigated.

CHAPTER 3

EXPERIMENTAL APPARATUS AND METHOD

3.1 INTRODUCTION

The apparatus and experimental method used in this work was similar to that employed by Gadgil and Kondic⁽²⁰⁾ and also various Japanese authors^(28,29,30), although a number of refinements were introduced subsequent to initial experiments.

The technique involved the controlled solidification of molten cast iron in a vertical, cylindrical, ceramic mould (Figure 7) which was contained within a furnace (Plates 1 and 2). By enclosing the mould inside a furnace, the mould surface temperature may be controlled to minimise lateral heat losses. Unidirectional heat flow, parallel to the mould vertical axis, should be induced by the presence of a water cooled copper chill in the mould base (Figure 9, Plates 3, 4 and 5).

To ensure that unidirectional heat flow was occurring, white iron melts of hypoeutectic composition were introduced ^{to} in the moulds. During solidification of these melts, dendrites, aligned in the direction of the heat flow, were produced, the size of which increased with distance from the copper chill, owing to the progressive decrease in cooling rate. Initial structural and cooling curve evidence showed that some lateral heat loss was occurring where the metal temperature exceeded the furnace temperature. As a result of this, the furnace was sectioned into three separate controllable heating zones and, by trial and error, a standard practice was developed which created conditions closely approaching unidirectional solidification.

Once this had been established the grey iron melt programme was initiated (Table 15). This entailed making six 'base melts' (from Iron III in Table I), consisting of 2 nitrogen contents (0.005 and 0.010 mass %) each with three sulphur contents (0.02, 0.05, 0.1 mass %). These 'base

melts' were to be used as 'controls' to determine the effect of adding four titanium percentages, (0.05,0.1,0.3,0.45 mass %). The observed decrease in cooling rate, proportionate to the distance from the chill, produced a corresponding change in microstructure and thus provided a useful means of studying the effect of melt composition on the solidification process, and hence the final microstructure, at various cooling rates.

3.2 THE FURNACE

General sectional views of the mould furnace are shown in Figures 7, 7A and 8 while more detailed sectional views of the mould in position inside the furnace are shown in Figures 9 and 9A. The furnace and ancillary equipment are shown in Plates 1 to 17.

Dimensional details of the furnace are given in Table 2. The furnace was supported above ground level by a steel frame. This allowed access to the furnace's base for location of the copper chill and water pipes and for connection of the thermocouple leads to the compensating leads and thus, the data logger. An outer, removable, Sandanyo cover provided protection for the exposed heating element ends and electrical connections, both during an experiment and whilst idle (Plates 3, 5 and 6).

An inner Sandanyo box, through which the elements protruded, housed the refractory insulation bricks and hot zone, dimensional details of which are given in Table 2. The brick-work comprised four layers of bricks, the top layer comprising six smaller outer bricks and two central bricks (Figures 7, 7A and 8). Removal of the outer Sandanyo cover enabled the extraction of these two central bricks permitting both access to the furnace hot zone, as shown in Section XX of Figure 7 and in Plates 1 and 7, and accurate positioning of the diffuser and mould. There was a circular hole cut in these bricks which, when the mould was

in position, was sealed with Kaowool to prevent penetration of molten iron into the hot zone should overflow or off-centre pouring occur. Dimensions of the hole and bricks are given in Table 2, and the sealing is shown in Plates 2, 8 and 10.

Initial trials proved that removal and replacement of the Sandanyo access cover was hazardous as, on refitting, the required 'tight fit' caused occasional breakage of the elements. A square hole was therefore, cut in the top of the access cover to permit removal of the bricks whilst the cover remained in position (Figure 7A). A Kaowool insert was then placed directly on top of these bricks (Plates 9, 10 and 11) to re-establish the thermal seal thus preventing unnecessary heat losses. The positioning of the diffuser and ceramic mould was unchanged.

3.2.1 The Furnace Hot Zone

This comprised a central cavity in the lower three layers of refractory insulation brick which was heated by sixteen Crucilite elements arranged in two sets of four pairs, the sets intersecting at right angles as shown in Figures 8, 9 and 9A and in Plates 1, 6 and 7. The dimensions of the hot zone and details of the elements and their axial spacings are given in Table 3. A Triton Kaowool pad was recessed in the Sandanyo furnace base, below the hot zone chamber. This protected the furnace base from over-heating, prevented unnecessary heat loss, and provided a more effective seal between the diffuser and the furnace base.

Initially it was hoped to use a cylindrical Crucilite heating element to ensure a uniform radial temperature distribution existed around the mould. Such an element was not readily available with the required hot zone dimensions and production costs for a non-standard design were prohibitive. Necessity dictated the use of Crucilite rods. It was expected

that use of the rod type heating elements would lead to non-uniform radial temperature distribution about the hot zone's vertical axis. To overcome this, a cylindrical vitreosil diffuser, of dimensions given in Table 2, was placed between the elements and the mould as shown in Figure 9 and in Plates 1 and 7. The radial temperature distribution and hence the thermal diffuser efficiency were determined before proceeding with experimental work.

Using a sheathed platinum-platinum 13% rodium thermocouple (whose length was graduated in millimetres) the profile of temperature versus vertical displacement in the mould cavity was determined for the three different positions shown in Figure 8, namely:

- a) along the vertical mould axis;
- b) along the internal mould wall opposite to the centre of the heating rods;
- c) along the internal mould wall on the furnace diagonal such that the thermocouple was a maximum distance possible from the elements, i.e. 45° from position 'b'.

The method of obtaining these results entailed heating the furnace to operating temperature with the mould and diffuser in position. The thermocouple was introduced into the mould cavity through a hole in an insulating brick which rested over the top two central bricks. To minimise heat losses through the hole in this brick, Kaowool was placed round the thermocouple and hole. After sealing, the thermocouple was allowed to stabilise before a reading was taken. This done the thermocouple was lowered into the furnace in predetermined steps (Table 4) until eleven readings had been obtained. Care was taken to ensure stabilisation prior to each reading. The final reading was at the pseudo chill/metal interface which, in the absence of the chill, would later

form the mould base, was plugged with Kaowool to prevent further possibility of heat loss. The readings were checked by withdrawing the thermocouple to identical positions, allowing time for stabilisation each time. This process was then repeated for the other positions - the results are given in Table 4.

Initially the mould was supported by the vitreosil diffuser so that the top of the chill seat area, incorporated in the mould, was level with the top of the Kaowool insert (Figure 7). Initial experiments showed that complete filling of the feeder head, and temperature maintenance of the iron in this area, was necessary in order to prevent heat losses from the top of the sample. From Figures 7 and 9 it can be seen that the feeder head did not protrude far enough into the hot zone. To correct this the diffuser was shortened, the basal Sandanyo hole widened and the mould dropped (Figures 7A and 9A, and Table 2). As well as widening the basal hole, to accommodate slight diametric variation of the mould chill seat, a slot 25.4mm (1") wide and 50.8mm (2") long was cut in one side of the Sandanyo base adjacent to the hole. This facilitated removal of the thermocouple leads from within the gap between the thermal diffuser and the mould (Figures 9 and 9A) and ensured positioning of the thermocouples on the diagonal as far as possible from the heating elements. Should magnetic currents have been induced by the elements, this latter precaution would minimise interference with the d.c. current produced by the thermocouples. The extent of mould protrusion below the furnace is shown in Figures 7A and 9A and Plates 3 and 4. This facilitated chill seating, removed the possibility of overheating the copper chill and heating in the metal/chill area, whilst exposing the feeder head to more direct heat radiation. To maintain a seal between the mould feeder head and the two removable bricks, a thin layer of brick and insulating cement was applied to the underside of the bricks which increased the internal depth

of the locating hole (Figures 7A and 9A and Plates 1 and 7).

3.3 HEATING ELEMENT CONTROL

Stage 1 When the furnace was built, the 'Crucilite' rods were connected to the power supply using a comparatively simple circuit. Essentially the furnace elements comprised two sets of eight, intersecting at right angles. Each set of eight elements was wired in series and the two sets were connected together in parallel. In this configuration all the elements had to be switched on and off together, independent control of individual element groups being impossible. Experimental results showed that, by simultaneously turning off all the elements, after introducing molten iron into the mould, lateral heat loss through the mould wall occurred as the furnace cooled more rapidly than the solidifying metal. However, by maintaining power to the elements it was possible to heat the metal, especially in the region of the copper chill, where the solidified cast iron was at a relatively low temperature. It was decided that it would be beneficial to control independently the groups of elements at different levels within the furnace.

Stage 2 By consulting the cooling curves obtained using this furnace arrangement an independent temperature control system was developed to give three controllable furnace sections:

- (i) the lower four elements,
- (ii) the middle eight elements, and
- (iii) the top four elements.

The heating elements were controlled by the electrical circuits shown in Figure 10. Circuits for the individual control of the middle and combined upper and lower sections of elements are illustrated in Figures 11

and 12. When power was switched onto all the elements (Figure 10) the circuit was essentially the same as the original circuit. There were two composite sets of eight elements, each set of eight being wired in series and the two composite sets connected in parallel. When the lower four elements were switched off, the remaining circuit comprised the eight middle section elements wired in series and connected, in parallel, to the upper four elements, also arranged in series, but, supplied with half mains voltage (120 volts). When the upper four elements alone were on, power was supplied at half mains potential.

The hot zone temperature was automatically controlled by a mains controller and monitored by two thermocouples. As a precaution the mains controller was linked to two thermal fuses, adjacent to the controller thermocouples, within the furnace. The positions of these are shown in Figures 9 and 9A.

After further study of the cooling curves it was decided to use furnace 'switch-off' times of 15, 32 and 48 minutes, for sections (i), (ii) and (iii) respectively, after teeming the metal into the mould. The duration of an experiment was dictated by the number eight thermocouple (Figure 13) which should have registered 700°C or less before terminating temperature monitoring. Inflections on the resultant cooling curve, caused by heat transfer from the mould furnace to the metal, indicated the need to reduce the element operating times.

Stage 3 Trial and error established the following satisfactory 'switch-off' system:

- (1) the lower four elements immediately prior to teeming the molten metal into the mould,
- (2) the middle eight elements ten minutes after the start of teeming,
and

(3) the top four elements twenty minutes after the start of teeming.

Using this system the duration of each experiment was approximately one and a half hours.

Prior to separating the furnace into three controlled heating zones the controller temperature setting was 1150°C (the figure used by Gadgil and Kondic⁽²⁰⁾). Graphical evidence showed this temperature to be too low and lateral heat flow from the uppermost sample metal, which was in excess of 1200°C , was occurring. During subsequent experiments a 1250°C controller setting was used which produced a temperature of 1180°C in the mould cavity. This discrepancy was due to lack of thermal insulation in the mould, in the absence of metal.

3.4 THE MOULDS

The mould is illustrated in Figure 13, and the dimensions given in Table 5. A feeder head was incorporated in the mould design to compensate for liquid/liquid contraction and any liquid/solid contraction, to facilitate teeming, and to provide a thermal head to negate upward heat losses from the sample head. To obtain a complete interface, between the copper chill and the base of the sample, the lower mould diameter was enlarged. Care was taken to ensure that an insulating cement seal existed between the chill and the mould material to prevent metal penetration between the mould and the chill, and hence minimise downward heat withdrawal from the shell, which would have increased the possibility of lateral heat flow from the metal to the mould. 'K.O.S.' cement was used for this purpose and also provided a means of securing the copper chill in position inside the base of the mould. The cement seal is indicated in Figures 9 and 9A.

The internal profile of the mould was similar to that used by Gadgil and Kondic⁽²⁰⁾, but the sample diameter was increased from 25.4mm (1") to

37.5mm (1.5"). This increase was a result of heat capacity calculations which indicated that a larger volume of metal would decrease the initial cooling effect caused by mould material heat abstraction when the molten metal was introduced (see Appendix 1).

The moulds were made using the Lost Wax Process which necessitated the production of a wax former with the desired sample profile. These formers were made in two parts by casting wax into two appropriately machined aluminium dies - one for the feeder head, the other for the combined sample length and chill sections. Once solid, the two formers were removed from the dies and joined together by gently melting the feeder head base and sample head with a hot spatula and applying pressure. Once joined, the feeder head/sample interface was further secured by building up a slight wax camber.

A molochite shell was produced by dipping the formers into a molochite suspension (Table 6) three times and, after each dip, a coating of 200 mesh molochite powder was applied. A further three dips were applied, this time interspersed with coarse 100 mesh powder. Finally, a sealing solution dip ensured retention of the powder. Care was taken to ensure that each coat was dry before applying the next layer, hence a maximum speed of two dips per day was used, and that the top of the feeder head was wiped clean after each dip. The process produced a 3.2mm (0.125") thick shell in four days. Once dry, the base of the chill seat was removed, using a diamond cut-off wheel, and the wax removed.

Initially wax removal was achieved using a blow torch but longitudinal cracks often resulted from a combination of thermal gradients in the mould and wax expansion. The technique then adopted involved melting out the wax using boiling water. The mould, placed vertically with the feeder head down, was submerged in the boiling water. This produced a

relatively uniform temperature gradient, allowed the wax to run out of the feeder head and prevented variable lateral expansion. Once devoid of wax the moulds were fired at 900°C for a period of two hours to improve handlability.

Locating holes for the thermocouples were initially made an integral part of the wax former by placing aluminium pins at right angles to the sample section at the required positions. This proved to be very unsatisfactory as there was a tendency, during the coating process, for the pins to either fall out or become bent away from the perpendicular thus altering the eventual thermocouple position. It was found that direct machining of the 'green' mould, using a 4mm (0.163") diameter masonry drill, was feasible and this became standard practice.

3.5 THERMOCOUPLES

To monitor the cooling mode at various positions in the iron, a series of thermocouples were introduced through the mould side as shown in Figures 9, 9A and 13 and Plates 12 and 13.

Initially chromel-alumel thermocouples were used in an attempt to reduce costs, but, as trials showed that the temperatures, encountered at the upper end of the solidifying sample, exceeded the operating range for this system, platinum-platinum 13% rhodium thermocouples became standard practice.

A total of eleven thermocouples were used originally, the positionings of which are detailed in Table 8, but the temperature profiles obtained proved that eight thermocouples would suffice. This became standard practice in all subsequent experiments and the positioning of these are also shown in Table 8 and in Figures 9, 9A and 13.

Two equal lengths of platinum and platinum 13% rhodium wires were sheathed in double bored alumina sheaths within 6mm of the hot junction ends. These ends were then welded together using an oxy-acetylene torch. Introduction of each thermocouple into the mould cavity was attained by bending the hot junction end through 90° so that 2mm (0.08") protruded. 'KOS' firebrick cement was then applied to the outside of the mould to hold the thermocouples in position. Care was taken not to dislodge the thermocouples from the right angled position as the temperature record would then not have been representative of the positioning. The protruding thermocouples were initially left bare but the possibility of bending during insertion and/or under the force of the impinging metal necessitated the incorporation of rigid sheathing to within 1mm of the hot junction. As there was no evidence of the thermocouples interfering with the solidification mode, it was decided to increase the sheathed protrusion to 5mm, to assist handling. It was also decided to enclose the bare wires in thermal resistant cement to reduce the chance of metal penetration up the sheath (which might have displaced the hot junction) and to sheath the wires within the mould wall and mould cavity, thus ensuring total sealing of the mould (preventing metal seepage into the furnace hot zone; Plates 14 and 15).

The thermocouples were placed in a vertical line in the mould such that, when the mould was positioned in the hot zone, they were all at the farthest distance from the intersecting elements on the furnace diagonal, Plates 3, 4 and 8.

3.6 THE COPPER CHILL

The water cooled copper chill is illustrated in Figures 9 and 9A and the dimensions are given in Table 7. This was sealed in position

in the base of the mould with 'KOS' cement taking care to maintain an insulating seal between the mould and the chill to prevent heat removal from the mould. This was supported by a clamp stand below the furnace as shown in Plates 3 and 4.

The cooling water was introduced via a plastic tube and copper pipe to within 9.5mm (0.375") of the internal chill cold face. This ensured an adequate water flow across the internal chill face and prevented stagnant layer formation. Two outlet pipes ensured efficient heat abstraction. The water flow rate was accurately monitored to ensure constant cooling conditions throughout all the experiments. It became standard practice to use a flow rate of 114 g/s which represented half scale deflection on a chart recorder. This deflection represented an e.m.f. generated by a propeller, located in the inlet pipe, being turned by the water flow. Care was also taken to ensure that the copper chill surface was clean and dry, prior to introducing the metal, to ensure uniform heat removal and reduce the chance of an 'explosion'.

3.7 DEVELOPMENT OF THE CAST IRON MELTING PRACTICE

3.7.1 Initial Experiments - Melting Practice A

In order to minimise loss of carbon and alloying elements from the melt, a very fast melting time was required. It was thought that a 15 kilowatt melting unit, combined with a parallel sided graphite susceptor of 2.7 kilograms capacity, would suffice. Problems of carbon 'pick-up' from the susceptor were however, anticipated. This problem was investigated by performing similar melts in untreated and 'Zircon X' treated susceptors.

The 'Zircon X' (zirconium silicate) coating was applied by mixing 'Zircon X' powder with isopropyl alcohol to form a semi-fluid suspension.

The suspension was swirled around the inside of the graphite susceptor thus forming a continuous film on the internal susceptor surface. Excess suspension was then removed and the film in the crucible was set alight to vaporise the alcohol. This was repeated four times to obtain a sufficiently thick layer, taking care that the surface was cooled between coats to prevent ignition of the suspension on contact.

The iron used in the trials (Iron III, Table 1) was melted in:

- (i) a cold uncoated graphite susceptor,
- (ii) a preheated uncoated graphite susceptor,
- (iii) a cold zircon coated graphite susceptor, and
- (iv) a preheated zircon coated graphite susceptor.

Samples were taken, using evacuated glass tubes:

- (a) on melting,
- (b) five minutes after melting,
- (c) ten minutes after melting, and
- (d) fifteen minutes after melting.

Occasionally, failure of an evacuated tube resulted in a delay or a sample being lost. However, results obtained (Table 9) seemed adequate enough to allow standardisation of a method for future use.

Similar experiments were performed, using the same sampling times, with a preheated, coated susceptor to determine sulphur and manganese losses on melt down and subsequent holding. Pure iron sulphide and high nitrogen ferromanganese, were the respective sources of the sulphur and manganese, analyses of which are given in Table 1.

From the results obtained (Table 9) a cold or preheated coated susceptor prevented carbon 'pick-up'. Spalling of the wash was observed

in both cases, but no excessive 'pick-up' resulted. When using the preheated washed susceptor in the sulphur and manganese trials the carbon content increased significantly (Table 10). It appeared that addition of the charge to a preheated, coated susceptor would completely disrupt the zircon barrier and thus provide a means of graphitising the melt. The melting practice established for the initial 'unidirectional' solidification experiments was therefore as follows:-

The cold zircon^{coated} susceptor was supported in an induction coil by a refractory brick. A protective layer of moist asbestos was interposed between the coil and the susceptor. The iron charge was then packed into the susceptor and the power, from the 15 kilowatt 'Electroheating' unit, was switched on. The susceptor capacity was 2.7kg of molten iron and 1.9kg of solid charge iron. To produce sufficient molten iron therefore the initial charge had to be partially melted and the remaining charge iron added progressively, as capacity dictated. The charge compositions for melt Nos. 6-17 inclusive are designated in Table 11.

After melt down the iron temperature was measured using a platinum-platinum 13% rhodium thermocouple and, when correct, the susceptor was removed from the coil and carried to the mould preheating furnace (Section 3.2). To ensure that excessive heat loss had not occurred during transfer a further temperature reading was taken. The iron was then teemed into the mould and allowed to solidify directionally (Plate 14).

3.7.2 Improved Melting Procedure - Melting Practice B

After a few trial solidification experiments, using the technique described above, several defects in the original melting technique became apparent:-

1. Cooling curves indicated that heat losses were occurring from the top of the sample. This was thought to be due to incomplete feeder head filling. A charge mass of 3 kilograms was required to achieve filling and, as this exceeded the capability of the graphite susceptor, some 3.5 kilogram capacity susceptors were made. To accommodate these in the heating coil the cavity required deepening. This was achieved by reducing the thickness of the refractory brick support in the base of the unit.
2. Removal of the susceptor from the coil was awkward and sometimes hazardous. The asbestos packing around the susceptor made removal from the coil especially difficult. The time required to loosen and withdraw the susceptor often resulted in excessive heat loss. In such cases the susceptor had to be reintroduced into the coil and reheated. The increased charge mass of the larger susceptor accentuated this and the handling problems worsened as now it was almost impossible to grip the smooth surface with tongs and retain the purchase. To facilitate handling a 25.4mm (1") high, 6.35mm (0.25") deep groove was machined 50.8mm (2") from the top of the susceptor to provide adequate purchase.
3. A melt down time of about one hour was required. This was too slow to minimise alloy losses. It was thought that the 3.5kg susceptor, which could accommodate all the charge, would reduce this but, in practice, this was not the case.

For the above reasons it was decided to abandon the initial melting practice and seek an alternative technique.

The new melting practice incorporated a 50 kilowatt, 'Electroheating', induction furnace. This unit had a self-contained rammed crucible but,

due to its position and size, a transfer ladle was required to move the molten metal to the mould preheating furnace, rather than transferring directly from the induction furnace. The rammed lining composition is given in Table 1.

This system had the following advantages:-

- (i) It eliminated the graphite susceptor and its inherent problems.
- (ii) It had a capacity of 5 kilograms.
- (iii) Much faster melt down times could be achieved.

The use of a transfer ladle required a larger furnace charge to compensate for the metal being lost during the double transfer. A charge mass of approximately 3.5 kilograms became standard practice. Care was needed in choosing charge material since a low surface area to mass ratio was required to minimise the melt down time and hence losses.

Reduction of the carbon content on melt down resulted in the initial grey iron melt (Ala) and, for the subsequent melt, a graphite susceptor was introduced. This induced over graphitisation and a zircon coated crucible was then used. Failure of the zircon to spall during melting impaired regraphitisation and it was decided that direct addition of electrode graphite would be used (see Section 3.8.2 (a)).

3.8 ALLOY ADDITIONS

3.8.1 White Irons

In both melting practices (3.7.1 and 3.7.2) approximately 5.50 mass % chromium was added to the molten metal prior to the transfer from

the high frequency units to the moulds. The additions constituted ferrochrome and pure chromium (Analysis: Table 1) and the melt histories are designated in Table 11 for melts 6 to 17.

3.8.2 Grey Iron Melt Programme

The melting programme (Table 15) based on Iron III (Table 1), necessitated manganese, sulphur, titanium and nitrogen additions to the melts. It was also found that exclusion of graphite susceptors caused a reduction in the carbon content, thus necessitating regraphitisation. The alloy addition compositions are given in Table 1.

3.8.2 (a) Carbon Additions

A 0.50 mass % carbon addition was made to each melt as 25.4mm (1") diameter, 3.2mm (0.125") thick, discs of pure electrode graphite.

Once molten, the iron was superheated to 1500°C, where carbon solubility is 70% greater than at 1420 - 1450°C. The temperature was maintained until complete dissolution occurred. The metal was then allowed to cool to about 1400°C.

3.8.2 (b) Sulphur Additions

0.02 mass % sulphur was achieved in the iron on melt down. Additions of 0.20 and 0.40 mass % iron sulphide produced residual sulphur levels of 0.05 and 0.1 mass % respectively.

The sulphur additions were made simultaneously with manganese at a bath temperature of 1400°C and immediately prior to tapping in non-titanium melts, but prior to titanium additions in titanium melts. Tapping in the latter case was immediately after titanium additions.

3.8.2. (c) Manganese Additions

To raise the base melt composition from 0.2 mass % to the desired manganese content of 0.8 mass %, an addition equivalent to 0.8 mass % manganese was found to be necessary to compensate for melt down losses. The additions were made as 1.0 mass % of high carbon, low nitrogen ferromanganese for the low nitrogen melts, but, for the high nitrogen melts, a combination of 0.61 and 0.386 mass % of high and low nitrogen ferromanganese respectively was used. As the sole source of nitrogen additions was the former ferromanganese, this dictated the amount of manganese available from this source, namely 0.494 mass %. The additions were made as stated in Section 3.8.2. (b).

3.8.2. (d) Nitrogen Additions

The two nitrogen compositions, 0.005 and 0.010 mass %, were chosen as they represent typical melt out figures obtained in industry using pig iron and steel scrap respectively. As nitrogen is notorious for its unreproducibility, both on melting and analysis, the possibility of analysing the effect of a larger number of nitrogen levels was precluded.

About 0.005 mass % nitrogen was obtained on melt down. As nitrogen recovery is poor, an addition of 0.61 mass % of high nitrogen ferromanganese (0.0353 mass % nitrogen) was required to increase the nitrogen content by 0.005 mass %. The addition was made as described in Section 3.8.2. (b).

3.8.2. (e) Titanium Additions

Aluminium has been reported as having a similar effect to titanium when present in cast iron and, since commercially produced ferrotitanium

contains about 3.5 mass % aluminium, an aluminium free ferrotitanium was produced. This was made by vacuum melting pure iron and titanium. The resultant intermetallic, 15 mass % titanium alloy was broken into handlable sizes.

Ferrotitanium produces variable titanium recovery depending upon the amount added. Initially, 0.6 and 0.45 mass percentages of titanium were added as ferrotitanium to produce 0.45 and 0.3 mass percentages of residual titanium respectively. Analysis proved these additions to be insufficient and in subsequent melts of these compositions, 0.75 and 0.6 mass percentages of titanium were added and adequate recovery was observed. Additions to produce 0.1 and 0.05 mass percentages residual titanium were initially 0.25 and 0.15 mass percentages respectively. These produced far higher percentages than required and standard practice for subsequent melts became 0.17 and 0.1 mass % titanium additions. None of the out of composition melts was discarded, thus increasing the number of titanium groups for analysis.

In all cases, the ferrotitanium addition was added immediately after the manganese and sulphur additions, and before tapping. The metal temperature was 1400°C and holding of molten metal in the high frequency melting unit was not possible subsequent to the titanium addition as large losses would have ensued.

3.9 COMPOSITIONAL ANALYTICAL TECHNIQUES

As previously stated in the literature (Section 2.5) compositional variations can have marked effects on the cast iron structure. It was necessary in this work to standardise the base composition (within analytical experimental error) to ascertain the effect of sulphur and

nitrogen additions and the specific effect of introducing titanium to these compositions. To this end melting, alloy addition, sampling and analytical techniques were standardised, as was the base iron.

Two sampling techniques were employed:

1. A chill sample (38.1 x 19.05 x 6.35mm) was cast during the transfer of metal to the mould furnace.
2. A 50 gram sample was turned from the cleaned base of the solidified feeder head.

A spectrographic analyser (Applied Research Laboratories, 29500) was used to analyse the white iron sample for sulphur, silicon, phosphorus, manganese, chromium, aluminium and boron. The experimental errors were $\pm 0.02\%$, $\pm 0.05\%$, $\pm 0.02\%$, $\pm 0.02\%$, $\pm 0.01\%$, $\pm 0.002\%$ and $\pm 0.001\%$ respectively. This method ensured that the analysis was known prior to making a subsequent melt, thus reducing the chance of unnecessary corrective work later. Carbon figures were obtained but, for contents in excess of 3.0 mass %, the composition versus excitation line becomes non-linear and produces unreliable figures. Table 12 shows the methods used for obtaining cross-checks on the above mentioned elements and also for nitrogen and titanium analysis (performed by two further establishments).

It should be noted that nitrogen analysis is highly unreproducible. Variations in time of analysis, personnel and establishments, are known to produce different analyses on the same sample⁽⁶⁸⁾. There is also the problem of titanium intermetallics - the nitrides, sulphides, carbonitrides and the cyanonitrides - masking the true nitrogen analyses. These inherent problems must be considered when assessing the final results.

3.10 DATA ASSIMILATION

The nature of the variable cooling rates within the sample necessitated rapid temperature monitoring, to ensure accurate cooling curve plots, at least in the early stages of an experimental run. It was thought that a chart recorder was inadequate and during the course of this work two data loggers were used:

3.10.1 : A Solatron 'Compact' Logger, and

3.10.2 : A Credshire 500 Analogue Scanner (Plates 5 and 15).

3.10.1 The Solatron 'Compact' Logger

This instrument was capable of monitoring the e.m.f. from a maximum of twenty thermocouples at scanning speeds of 3, 2 or 1 readings per second or one every two seconds. The full scale deflection was 0 - 20 mV with a basic sensitivity of 10 μ V. The output device was a solenoid type LU 1654 Teletype electric typewriter. Channel enumeration beside each millivolt reading was possible but this reduced the scan speed. This method proved to be laborious as millivolt conversion to temperature was necessary, although it was used for the first two experiments.

3.10.2 The Credshire Model 500 Analogue Scanner

This data logger was purchased after the present work commenced. A familiarisation and commissioning programme was performed which highlighted several faults which are discussed later.

Details of the performance data for the analogue scanner and the Model 220 drive cassette unit are detailed in Tables 13 and 14 respectively. Initially it was anticipated that continuous monitoring of the metal

temperature during cooling would be necessary, the faster the monitoring the more accurate would be the cooling curve and hence the calculation of cooling rate. However, the Credshire Logger fast scan of 10 readings per second would have produced readings for an experimental run in excess of the maximum storage capability of the cassette (Table 14). Thus, the results would have been incomplete. Reference to the cooling curves indicated no necessity to employ the maximum scan speed throughout. Since reduction of the scan speed required dismantling of the equipment, which was impossible during an experimental run, the minimum scan speed of seven complete scans per minute was used. It was evident from further data collections that continuous scanning was also unnecessary. There was a manual facility, allowing random selection of channels by a three decade thumb-wheel switch, and a single 'o - n' scan facility, available by manual depression of the start button. The following scan procedure was adopted subsequent to the trials:

TIME PERIOD	SCAN FREQUENCY	SCAN TYPE		TOTAL READINGS
		AUTO	SINGLE	
0-10 mins	Continuous	X		560
10-20 mins	30 secs		X	160
20-30 mins	60 secs		X	80
30-90 mins	120 secs	X		240
		Total readings:		1,040

The input signals were scanned from 'o - n' where 'n + 1' is the preset number of channels.

Inherent in the analogue was a direct temperature read-out for platinum-platinum 13% rhodium thermocouples, coupled with a millivolt read-out for all thermocouple materials. There was an automatic cold junction at the rear of the data logger, operation of which required reproduction of the isothermal box. The circuitry of the patchboard connections and the isothermal box are shown in Plates 15, 16 and 17. The 'iso-box' was produced by replacing the boards at the rear of the instrument, ensuring that the compensating leads were separated to form a continuous foam plastic gland at the centre of the two boards. If air gaps are present the isothermal condition is negated.

The output device incorporated with the Scanner was a model 220 drive cassette unit, details of which are given in Table 14. The maximum accommodation per line is seventy characters. The time display is printed at the end of each data line prior to the system line feed command. Sixty six character spaces per line are subsequently available. From the print-out format one reading occupies nine characters enabling a maximum of six channel scans. The work required eight channel scans, thus four words per line were utilised, resulting in seven complete scans per minute.

The magnetic tape was processed by patching the cassette unit to a computer terminal and impulses from the tape were converted to paper print-out. It was anticipated that the tape could be fed into a computer programme designed to draw the cooling curves and calculate cooling rates for each thermocouple position. Signal problems incurred throughout the work precluded this.

The print-out problems incurred on transposing the magnetic tape data manifested themselves as:

- (i) thermocouple repetition;
- (ii) printing the previous thermocouple number with the following channel's temperature;
- (iii) printing the previous temperature with the following channel number;
- (iv) and temperature fluctuations on channels. (In melt 13 this was up to 600°C).

These faults could have resulted from faulty relays from the logger to the cassette, transposition of the magnetic tape through the computer terminal, metal penetration displacing the thermocouple hot junction up the thermocouple or induced magnetic currents developing in the iron and being superimposed on the D.C. thermocouple readings.

The data relays were checked by simulating thermal data as a variety of known millivolt readings from an external source. Transposition of the data showed a perfect representative print-out thus eliminating the two former suggested error sources.

Attention was then turned to the thermocouples. It has already been stated (Section 3.5) that bare thermocouple wires protruded into the mould cavity for 2mm initially. Later, to minimise bending caused by metal impingement during pouring, the wires were sheathed to within 1mm of the hot junction and protrusion extended to 5mm. Problems were still evident so, to ensure that the hot junction had not been displaced, thermal cement was applied to the gap between the sheath and the hot junction to prevent penetration up the sheath interiors. Though no significant difference appeared on the print-out, this became standard practice thereafter.

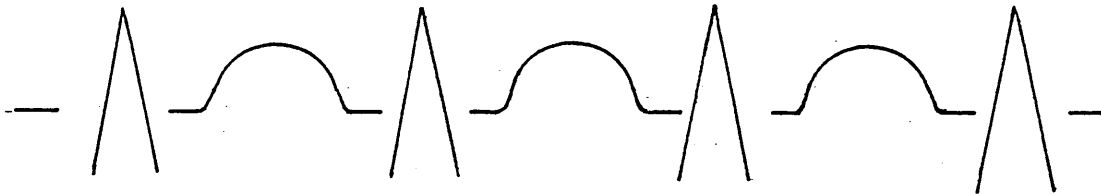
Another thermocouple related error source could have been bridging via the melt. This did not seem likely as the effect was not limited to the lower thermocouples where the separation is small. To make certain, the top two, high temperature thermocouples were completely enclosed in 6mm diameter silica sheaths and the hot junctions cemented in place - touching the internal surface of the sheath. This proved to aggravate the print-out problems, even though the temperature variations were reduced to 10-15°C. It was feared that if lower thermocouples were totally sheathed, delays would be encountered in recording rapid temperature changes and the solidification mode might be disrupted by the large volume of the sheath protruding into the melt. Total sheathing was therefore, not employed.

Finally, attention was directed to the question of induced magnetic currents. The nature of the work required maintaining the current through initially twelve and then four of the heating elements for twenty minutes. This current could cause induced currents which would be superimposed on the direct current thermocouple readings. To ascertain whether or not this was the case, modifications were made to the experimental apparatus and the data logging equipment. These are discussed below.

(a) The high temperature thermocouple (Number 8) was completely earthed, via a cathode ray oscilloscope (C.R.O.) at the input junction on the data logger patch board. This appeared to eliminate all the previously encountered print-out problems. However, attempts to duplicate this on subsequent reheating of the metal to pouring temperature within the mould furnace (thus reducing iron consumption), proved impossible. Temperature variations of 30°C were observed on the 'earthed', Number 8, thermocouple when the furnace controller switched in and out of the circuit.

The C.R.O. connection was transferred to Number 7 thermocouple; the variation also transferred. As no other thermocouples were affected the effect was attributed to the C.R.O.

When the C.R.O. was used solely as a monitoring device the following signal emerged:



It was noted that the vertical height of the signal decreased and the alternating current signal appeared when the heating elements switched out of the circuit. However, despite this signal variation, no print-out malfunction was observed other than the $\pm 1^{\circ}\text{C}$ error.

(b) Earthing the high temperature thermocouple with respect to the data logger (which was earthed with respect to the casing and not ground earth, thus producing floating thermocouple junctions) via the earthing screw on the patch-board was investigated during another melt. This created thermocouple repetition and misprinting in the print-out, although no complete losses or variations were noted.

As no malfunction was evident in the data logger, and none of the above modifications proved completely beneficial, attention was directed towards the experimental apparatus. The metal was in direct and indirect contact with two possible earths - the water and the clamp stand. To 'un-earth' the water from the mains supply a continuous circuit employing a water bath and pump would have been necessary. This being impracticable the clamp was unearthed by placing a Sandanyo board between the stand base and the floor. Excessive temperature variations and reading losses were prevented but repetition and interchanging still occurred. It was

noted that, had the copper stool dislodged during the second C.R.O. earthing trial (thus removing the earth) this could have explained the non-duplication of results. This pointed to the need for a double earthing system in the apparatus.

(c) All methods having failed to correct the print-out errors, it was decided to earth the metal directly by introducing a platinum thermocouple wire into the feeder head metal and earthing this via an external alien piece of apparatus (Plates 10, 11 and 17).

(d) At the same time the compensating and thermocouple leads protruding below the mould furnace (Plates 3 and 4) were encapsulated in aluminium foil throughout their length to the patch board. The foil was then earthed by wrapping a wire coil externally about part of the foiled length (Plate 17) and this was then connected to the same external earth as the metal.

The resultant print-out contained no flaws and this method became standard practice throughout subsequent experimental runs.

4.1 INTRODUCTION

The experimental work was divided into two distinct phases:-

- (i) The development of the apparatus and experimental technique.
- (ii) The investigation of the effects of titanium, sulphur and nitrogen on the solidification mode of an ingot mould type cast iron.

The results obtained from these two stages of the work are described in the subsequent sections - 4.2 and 4.3 respectively.

4.2 THE DEVELOPMENT OF THE EXPERIMENTAL APPARATUS AND PROCEDURE

The initial period of work involved the construction of the mould preheating furnace and its subsequent modification and development to overcome certain limitations inherent to Gadgil and Kondic's⁽²⁰⁾ original design. Concurrently, work was carried out on the development of the mould preparation technique, a suitable melting practice, and the commissioning of a data logger. The work involved in the development of the apparatus and experimental technique, and the measures taken to overcome the problems encountered, have already been described at length in the previous chapter. The results of the initial 17 melts have been summarised in Tables 9, 10 and 11 and it is therefore not proposed to elaborate further on this aspect of the work.

Efforts were made to produce a hypoeutectic white iron structure, the degree of alignment of the primary austenite dendrites with the longitudinal axis of the casting providing a means of assessing the effectiveness of the mould preheating furnace, and operating practice, in creating unidirectional heat flow conditions. Any tendency for

non-unidirectional heat flow to occur resulted in deviation of the austenite dendrites from alignment with the vertical mould axis. Excessive thermal input from the mould preheating furnace was indicated by inflections on the cooling curves obtained from the thermocouples in the melt (See Section 3.3).

Typical microstructures indicating the high degree of directionality achieved with the final practice are illustrated in Plates 25 to 33. Plates 25 and 26 show the structure of the casting obtained from Melt 16 at the chill/metal interface and at 12.7mm from the chill. Rapid nucleation and growth has occurred at the chill surface (Plate 25), the primary austenite dendrites becoming more directionally aligned a short distance from the chill (Plate 26). Plates 28 to 34 show typical microstructures from the Melt 17 casting. The primary austenite dendrites are closely aligned with the vertical axis of the casting, even at 177.8mm from the chill (Plate 33), although not quite as perfectly as at 101mm (Plate 32). The effectiveness of the experimental conditions in creating unidirectional heat flow is clearly indicated by Plate 34 where part of a dendrite is seen close to, and lying parallel with, the casting surface at 177.8mm. The primary and secondary austenite dendrites coarsen with increasing distance from the chill, reflecting the decrease in cooling rate with distance.

4.3 THE GREY IRON MELT PROGRAMME

4.3.1 Introduction

A series of melts with different sulphur, nitrogen and titanium contents were solidified under unidirectional heat flow conditions in order to ascertain the effects of these three elements upon the resulting microstructure. The composition of each melt in the programme is

presented in Table 15. Cooling curves were obtained at a number of positions within each casting (Table 8b). Each casting was subsequently fractured longitudinally, the fractures examined and then prepared for optical and scanning electron microscopy.

The melts essentially fall into two categories - the 'low' nitrogen group and the 'high' nitrogen group. At each nitrogen level the effect of different titanium concentrations at each of the three different sulphur levels was investigated.

The melt identification code was as follows:-

- (i) A, B, C, D, E, F and G indicate melts with different titanium concentrations, increasing from A to G. Melts designated 'A' contained no titanium additions (Table 15).
- (ii) The numbers 1, 2 and 3 denote low, medium and high sulphur contents respectively (Table 15).
- (iii) The high nitrogen content casts are identified by the presence of a prime (').
- (iv) Casts designated a, b and c indicate 'duplications' of the same melt composition.

4.3.2 Cooling Curves For The Grey Iron Melt Programme

The temperature versus time was monitored for each of the thermocouple positions, for each experiment, and the resultant cooling curves are shown in Figures 22 to 60. (The correlation between the experiment and the figure number is shown in Table 15).

The purpose of producing cooling curves for each melt was to

- (a) characterise the cooling of the metal through the solidification

range to ensure that significant variations in cooling rate did not occur (or, if they did, to quantify the differentials) and (b) to quantify the cooling rates pertinent to the observed microstructure.

Two cooling rate assessments were made from all the graphs, for each thermocouple, namely:-

1. The 1160° - 1100°C Range (Table 16). This was chosen for two reasons :

- (i) to monitor the rate of cooling through the arrest and
- (ii) to overcome the inability to define the start of an experiment. The initial temperature could be taken as that immediately prior to casting ($1300^{\circ}\text{C} \pm 10^{\circ}\text{C}$) or the initial temperature recorded in the mould preheating furnace. It was quite obvious that these two temperatures would be quite different for thermocouples 1 to 4 (see Figures 22-60).

2. The cooling rate for the 1160° - 700°C Range (Table 17). This provided an overall cooling rate for the experiments.

The ideal thermocouple positioning (Table 8b and Figures 9 and 9A) was not obtained in some experiments, as was evident from the fractures. Where displacement occurred it was due to chill displacement downwards, effectively displacing the thermocouples upwards, and occasionally, metal impingement during casting forced the thermocouple from the horizontal position. Thus, to assess the variability of the cooling rates, a further two graphs were drawn, one for each temperature range, (Figures 61 and 62) of log. cooling rate versus chill distance after assessing the displacements for each thermocouple (Table 18). As can be seen, the variability is greater for the 1160° - 1100°C temperature

range, throughout the sample distance, as compared with that for the 1160° - 700°C range, where only the first three thermocouples show large variations.

The data obtained from Figures 22 to 60 (Tables 16, 17 and 19) was statistically analysed to ascertain whether the variability was statistically significant from cast to cast (i.e. whether the variability was greater than $(|\bar{x} \pm 1.96\sigma|)$ where \bar{x} is the mean cooling rate, σ is the standard deviation, and $(|\bar{x} \pm 1.96\sigma|)$ is the limit above $(>(|\bar{x} + 1.96\sigma|))$ and below $(<(|\bar{x} - 1.96\sigma|))$ which variability becomes significant). The significance levels plotted on Figures 61 and 62 show that, despite the apparent variability of cooling rates (Tables 16, 17 and 19), the variability is not statistically significant.

4.3.3 The Structures of the Low Nitrogen Grey Iron Castings

The macro- and microstructural features of each of the resultant castings indicated in Table 15 will now be described. The castings obtained showed complex and diverse microstructures. A policy has therefore been adopted of cross-referencing microstructural features common to a number of castings in an effort to represent all the observed features in a reasonable number of photomicrographs.

All distances quoted with reference to the microstructures have been measured vertically from the chill/metal interface. The photomicrographs and the fractures are orientated with the chill/metal interface towards the bottom of the plates.

4.3.3. (a) Melt Al - The Base Melt (3.90%C, 0.02%S, 0%Ti, 0.0064%N)

This melt was made with no additional sulphur, nitrogen, or titanium, utilising electrode graphite as the recarburiser. It

therefore, qualifies as "The Base Melt", to which all subsequent melts can be referred. In view of the importance of this melt, the structural features of the resultant casting will be described in detail.

The fracture, Plate 35, is white in close proximity to the chill/metal interface and, with increasing distance from the chill, becomes mottled a few millimetres up the casting and thereafter increasingly, although never fully, grey. Microscopic examination of the polished and etched casting confirmed these general observations.

At the chill/metal interface a totally ledeburitic structure was observed with the primary austenite dendrites, now transformed to pearlite, predominantly aligned parallel to the longitudinal axis of the casting (Plate 36). A mottled structure was first evident at 12.7mm with the appearance of streamer graphite* at the centre line and 14.5mm from the thermocouple side of the casting (Plates 37 and 38). A number of graphite flakes are evident in the streamer graphite shown in Plate 38, with one particularly large flake stretching across three streamers at 45° to the axis of the casting (Plate 39). The matrix was still ledeburitic with the globular nature of the transformed eutectic austenite being particularly evident in Plate 39.

With increasing distance, the number of graphite streamers increased, eventually impinging on one another to form the irregularly shaped 'grey' areas shown in Plate 40. These areas did not take the form of true graphitic cells but appeared to be confined between the dendrite arms. Close examination of these streamer impingement areas revealed the presence of 'A' type graphite flakes, ferrite grains and inclusions (Plate 41). The commencement of these irregular graphitic areas contained between the streamers will in future be referred to as the 'grey' start.

*Graphite directionally aligned with the unidirectional heat flow as defined by Gadgil and Kondic⁽²⁰⁾.

At 38.1mm, streamer graphite in a ledeburitic matrix was still observed with 'grey' areas of the type described above. At a position 4mm from the thermocouple edge of the casting, the streamers took the form of irregular networks of flake-like graphitic structures associated with ferrite grains and contained between the primary austenite arms (Plates 42 and 43). At positions ranging from 8.5mm to 10mm from the thermocouple edge the graphite contained within the streamers took the form of more conventional 'A' and 'D' type graphite flakes but, again, associated with significant amounts of ferrite (Plates 44 and 45). At 27.5mm from the thermocouple edge the structure was fully ledeburitic. These observations reflect the diversity of structures exhibited by a single traverse across the casting.

At 63.5mm, the first true graphitic cells appeared and the structure became predominantly grey although, ledeburite was still evident. At a position 34.1mm from the thermocouple edge type 'A' graphite, associated with ferrite grains was observed (Plates 46 and 47). Streamer graphite associated with 'D' type graphite was also observed and angular inclusions were noted in the austenite dendrites. At a position 12mm from the thermocouple side, 'D' type graphite in association with ferrite and some cementite was observed and angular and oblong inclusions associated with the primary austenite dendrites were noted. At 34mm from the thermocouple side, the ledeburitic structure had almost disappeared, the structure comprising 'A' and 'D' type graphite flakes in a ferritic and pearlitic matrix (Plate 48).

Ledeburite was still present as a component of the structure at 89mm. The graphite present comprised both 'D' and 'A' type flakes similar to those illustrated in Plate 47, although at a position 27.5mm from the thermocouple edge of the casting, an isolated area of compacted

'A' type graphite was noted (Plates 49 and 50) as were some particularly large 'A' type graphite flakes (Plate 51). In all cases, the graphite was associated with ferrite grains. In some regions extensive areas of ferrite, containing networks of graphite, were associated with the dendrite arms (Plates 52 and 53). Cementite needles are also evident within the areas shown in these latter two plates. Inclusions, probably manganese sulphide, were noted in both the ferrite and in association with individual graphite flakes.

At 127.1mm, the structure was predominantly graphitic with only a small amount of ledeburite. The graphite was similar to that illustrated in Plate 53, but was associated with less ferrite. The majority of the structure was similar to that shown in Plates 47 and 51 comprising 'A' type graphite flakes in a matrix of ferrite and/or pearlite. Large numbers of angular inclusions, probably manganese sulphide, were noted in both the ferrite and pearlite (Plate 54).

At 177.8mm, large 'A' type graphite flakes predominated in association with small amounts of ferrite, in a pearlitic matrix (Plate 55). Large numbers of angular inclusions, probably manganese sulphide, were noted in the pearlite, ferrite and in association with individual graphite flakes. A few isolated areas of streamer graphite, 'D' type flake graphite and cementite needles were also noted.

A large variation in graphite flake size was noted at 185mm. Besides the streamer graphite, similar to that shown in Plates 52 and 53, and normal 'A' and 'D' type graphite, compacted 'A', 'D' and streamer type graphite were also present in a ledeburitic, ferritic, or pearlitic matrix, although the ledeburitic areas were relatively minor (Plates 56, 57 and 58). Large numbers of manganese sulphide inclusions were also present in the structure.

Due to the difficulty in controlling the carbon content in the earlier experiments (see section 3.7.2) three melts were cast prior to the desired Al composition being achieved. These melts were designated Ala, Alb and Alc:-

- (i) Ala resulted from 'melt down' being performed in the 50kW induction unit with an integral rammed lining - excessive decarburisation of the melt occurred.
- (ii) Alb utilised a preheated 'zirconia' coated graphite crucible which failed to spall sufficiently to regraphitise the melt.
- (iii) Alc utilised an uncoated graphite crucible which resulted in over-graphitisation of the melt.

The analysis of each melt is shown in Table 15a, the fractures in Plate 59. The fractures show that with increasing carbon content the fracture became increasingly grey. This was substantiated by microscopic examination, the distance of the streamer, 'grey' and cell starts, from the chill being as follows:- Ala - 17, 54 and 70mm; Alb - (>12.7, <25.4), 20, and 50mm; Alc - none, none, 0mm.

Melt Ala (3.42%C, 0.02%S, 0%Ti, 0.005%N)

The streamer graphite in this casting was significantly larger than that observed elsewhere during the course of this work (Plate 60). The 'grey' start occurred at 54mm and took the form of an isolated irregular graphitic area contained between graphite streamers, similar to that illustrated in Plate 41 for Al, although rather more cementite needles were in evidence. At 74mm, the sample structure was comprised entirely of streamer graphite in a ledeburitic matrix. At 89mm, the

structure had become predominantly one of 'A' or 'D' type graphite in a pearlitic matrix, becoming entirely graphitic beyond 125mm (Plate 61). Very little free ferrite was observed in the structure.

Melt Alb (3.55%C, 0.02%S, 0%Ti, 0.0048%N)

The resultant casting from this melt was, in general, slightly greyer than one would have expected when compared with Al, possibly due to its rather low nitrogen content. The initial size of the streamer graphite was similar to that in Al but the graphitic areas at the 'grey' start were larger but somewhat fewer. At 63.5mm, the structure was comprised almost entirely of 'D' type graphite flakes in a pearlitic matrix, with only a few cementite needles present. At 81mm, a significant amount of 'A' type graphite flakes was evident although 'D' type flakes still tended to occupy the interdendritic spaces (Plate 62). With increasing distance, the amount of 'A' type graphite diminished in favour of 'D' type flakes and even some mesh type graphite was noted at 190.5mm (c.f. Plate 62). The re-appearance of isolated areas of ledeburite in a 'fan-like' configuration (similar to that illustrated later in Plates 86, 111 and 145) were noted at 127mm and 190.5mm from the chill.

Melt Alc (4.02%C, 0.02%S, 0%Ti, 0.0056%N)

Small graphite cells were observed in a ledeburitic matrix in close proximity to the chill/metal interface (Plates 63 and 64), no streamer graphite or 'grey' areas were observed in this casting. Beyond 10mm the structure became fully graphitic. 'A' type graphite flakes and small amounts of ferrite appeared in the structure at 25.4mm, the flakes becoming coarser, and the ferrite more abundant, with increasing distance from the chill/metal interface. Beyond 127.1mm, the

amount of ferrite present gradually decreased. At 177.8mm, the structure appeared similar to that illustrated in Plate 57, although the graphite flakes were generally coarser.

4.3.3. (b) The Effect of Sulphur Additions on the Structure of the Base Melt

Melts A2 (3.8%C, 0.045%S, 0%Ti, 0.0057%N) and A3 (3.8%C, 0.104%S, 0%Ti, 0.006%N) were produced to determine the effect of increased sulphur concentration on the microstructure of the base melt A1 (see Table 15a). The resultant fractures from melts A1, A2 and A3 are compared in Plate 35. With increasing sulphur, the extent of the chilled region appears to increase.

The microstructural features of A2 and A3 were similar, in general, to those of A1 but, as suggested by the fractures, the formation of a graphitic structure appeared to be retarded increasingly by increased sulphur concentrations.

The streamer graphite start for melts A1 (Plate 37), A2 and A3 appeared similar and occurred at distances of 12.7mm, 12.7mm and 27.4mm respectively. (Plate 65 shows a typical area of streamer graphite in A3). At the higher sulphur level, not only was the streamer start delayed but the rate at which the streamer graphite formed also appeared to have been retarded quite significantly. In the medium sulphur level casting, A2, the 'grey' areas observed at 25.4mm (Plate 66) were comparable with similar areas observed in A1 between 12.7mm (Plate 37) and 25.4mm (Plate 40). In A3, comparable 'grey' areas were not encountered until 63.5mm (Plate 67).

The graphitic cell starts for all three occurred at 63.5mm, 63.5mm and 73.5mm respectively, again reflecting the tendency for

higher sulphur to be associated with retarded graphitisation. In general, the structure of A2 was similar to that of A1. However, at positions of 63.5mm and 89mm there was a slight tendency for the structure to become whiter and more dendritic (Plate 68) than was observed with A1 (Plate 49).

In A3, considerable areas of ledeburite were still evident at 177.8mm (Plate 69) with the graphitic areas comprising 'A' and 'D' type flakes (Plate 70). By comparison, A1 and A2, at the same distance from the chill, exhibited structures comprising 'A' type flakes in a pearlitic matrix (Plates 55 and 57). At 182mm in A3, both 'D' and 'A' type graphite flakes were observed and the ledeburitic areas had become only a minor constituent of the structure - the graphite structure being comparable with that observed in A1 (Plate 51) and A2.

4.3.3.(c) The Effect of Titanium Additions on the Structure of the 'Base Melt' (A1)

Melts B1, C1, E1, F1 and G1 (see Table 15a) were produced to determine the effect of increasing titanium concentration on the microstructure of the 'base melt', A1 - the resultant fractures may be compared in Plate 35. In terms of their fractures, the castings fell into two groups:- (A1, B1, C1) group 1, (E1, F1, G1) group 2. In group 1, the fractures are white in close proximity to the chill/metal interface but overall are predominantly of a fine 'cellular' structure. The grey cells exhibited by B1 appear slightly coarser than those in C1 or A1. The group 2 fractures appear almost totally white, with only a few large grey cells being evident towards the top of the castings. There is evidence that the mottled structure in E1, F1 and G1 begins at about the same distance as in B1 and C1 but, the transition is less distinct.

Microstructurally, the castings can be considered in terms of the same two groups i.e. (A1, B1 and C1) and (E1, F1 and G1). In general terms however, it was noted that the degree of graphitisation of the microstructure was retarded progressively with increasing titanium content. For melts A1, B1, C1, E1, F1 and G1 the streamer graphite starts were at 12.7mm, 25.4mm, 26mm, 38.1mm, 38.1mm and 38.1mm respectively; the 'grey' starts were at 25.4mm, 38.1mm, 33.5mm, 44mm, 63.5mm and 75mm respectively and the graphitic cell starts, 63.5mm, 64.5mm, 89mm, 127.1mm, 127.1mm and 136mm respectively. All reflect an increasing trend towards carbide stabilisation with increasing titanium content.

Melts B1 and C1 (see Table 15a)

The resultant casts showed only minor differences from the structures already described for the 'base melt', A1. In close proximity to the chill/metal interface, both castings exhibited a highly directional white iron structure similar to that illustrated in Plates 36 and 37 for A1. The primary austenite dendrites, now transformed to pearlite, were evident throughout the entire length of the casts, becoming coarser with increasing distance.

In B1, streamer graphite, first noted at 25.4mm, was rather finer in structure than that observed in A1. The 'grey' start appeared at 38.1mm (Plate 71) and these areas also were finer than those observed in A1 (Plates 41 and 42). At 63.5mm, areas of particularly large dendrites (like those in A1) were noted along with some fine streamers (Plate 72).

The first isolated graphitic cell appeared in B1 at 64.5mm (Plates 73 and 74), the graphite taking the form of 'D' and mesh type,

with a tendency to outline the dendrite arms. At a similar position in A1, although 'D' type graphite was present, 'A' type predominated (Plate 47). Graphitic cells of a slightly greater size, and concentration, appeared at 89mm although streamer graphite, similar to that shown in Plate 72, in a ledeburitic matrix still predominated (Plate 75). Beyond 89mm, the structure became progressively more graphitic. At 127.1mm, isolated areas were almost entirely graphitic (Plate 76) but the majority of the structure was similar to that illustrated in Plates 75 and 77. This mixture of structures persisted throughout the remainder of the sample though there was a tendency for the graphite, still predominantly 'D' type, to coarsen somewhat (Plates 78 and 79). Nevertheless, the graphite observed, even at 182mm, was still significantly finer than that observed in the previously described casts (A1, A2 and A3) at this position.

The structure of C1 was slightly more comparable to B1 than A1, being entirely ledeburitic up to 26.5mm, where the first very small streamer was observed. The streamer graphite was similar in general appearance to that shown in Plate 37, but with the absence of 'A' type flakes. Plate 80 shows a photomicrograph in the vicinity of the number two thermocouple bead. Dendrites perpendicular to the surface of the bead indicated that slight heat removal, via the thermocouple wires, had occurred.

The 'grey' start, evidenced between graphite streamers, began at 33.5mm in C1, which is earlier than in B1, but still retarded relative to A1. These areas were similar to those illustrated in Plate 40, for A1, but were generally much smaller, areas comparable with those in Plate 40 not being observed until 44mm from the chill. In both B1 and C1, the volume fraction of these areas was less than that

observed at equivalent positions in A1. Structures comprising streamer graphite associated with 'grey' areas, in a ledeburitic matrix with very prominent dendrites, persisted to 89mm from the chill (Plate 81).

The cell start occurred at the same distance from the chill as in B1 (89mm), although much more graphite was evident in the structure (Plate 82). At 127.1mm, particularly broad streamers were still evident (Plate 83). At the same distance certain areas of graphite were associated with ferrite (Plate 84) although more generally the graphite was associated with a pearlitic matrix. Beyond 127.1mm, the amount of ledeburite in the structure decreased, totally disappearing at 177.8mm (Plate 85), only to re-appear as an isolated ledeburitic 'fan' (illustrated in Plate 86) at 181mm. The majority of the structure comprised 'D' type graphite in a pearlitic matrix with prominent pearlitic 'dendrites' and isolated areas of cementite (Plates 85 and 87), and 'A' type graphite (Plates 88 and 89). In general, the flake graphite observed at the top of C1 was coarser than that observed in B1 but finer than in A1.

Melts E1, F1 and G1 (See Table 15a)

Microstructural examination of these casts confirmed the general conclusions derived from examination of the fractures (Plate 35). In all three cases the carbidic eutectic (ledeburite) predominated over significant distances. At positions up to 38.1mm, the structures solely comprised austenite dendrites, transformed to pearlite, in a ledeburitic matrix. In E1 and F1, the dendrites were strongly aligned parallel to the longitudinal axis of the casting, producing structures similar to those observed in many of the previous castings (e.g. Plates 36 and 37). G1 was slightly different in that the strongly aligned primary austenite

dendrites normally present (Plates 36, 37, 44 and 60) were no longer a prominent feature of the microstructure. Instead, the positions occupied by the primary dendrites were replaced by more globular pearlitic areas (Plates 90 and 91). Streamer graphite appeared at 38.1mm in all three castings.

Irregular graphitic areas, constituting the 'grey' start, appeared at positions of 44mm, 63.5mm and 75mm for E1, F1 and G1 respectively. These areas of very fine graphite were generally larger and less obviously associated with the graphite streamers than in any of the previously described castings (Plate 92). The 'grey' areas observed in F1, at the 'grey' start (Plate 92), were significantly larger than in E1 or G1, where areas comparable in size were not observed until 89mm. Some of the 'grey' areas observed further up the castings were quite extensive (Plate 93). Compared with E1, there appeared to be generally more streamer graphite in F1 and G1, although in G1 it tended to be of a finer internal structure. Examples of the streamer graphite in these specimens are illustrated in Plates 94 to 97.

The first isolated graphitic cell was observed at 127.1mm in both E1 and F1. The microstructure of E1 comprised 'D' type graphite flakes associated with areas of both ferrite and pearlite, pearlitic 'dendrites' and isolated area of eutectic cementite (Plates 98, 99 and 100). In some cases the dendrite arms appeared to be outlined by a network of graphite flakes and ferrite (Plate 99). In general, F1 appeared to be less graphitic than E1, at this distance, and the graphite flakes tended to be finer (Plate 101). In comparison, G1 at 127.1mm, still exhibited streamer graphite and pearlitic 'dendrites' in a matrix of ledeburite, similar in appearance to the structure shown in Plate 97, although the dendrites were coarser (as would be expected with the greater distance from the chill). At 136mm, G1 exhibited cells with extensive ferritic

areas at their centres (Plate 102).

At 177.8mm, E1 and F1 exhibited three further graphitic cells each, whilst G1 showed only two. The structure of E1 comprised streamer graphite, similar to that in Plate 94, large pearlitic 'dendrites', ledeburite and 'D' type graphite flakes associated with pearlite and ferrite, similar to that shown in Plate 99, although the areas of ferrite were less extensive. F1 exhibited a structure comprising areas of fine ledeburite and graphitic cells which had ferritic centres (Plates 103 and 104). Some of the pearlitic 'dendrite' extremes in Plate 104 appear to be delineated by a 'layer of ferrite' which, in turn, is outlined by a dense graphite flake network, suggesting that the austenite within the dendritic area has decomposed into ferrite and graphite. The structure of G1 at 177.8mm was similar to that of E1. It comprised streamer graphite, coarse pearlitic 'dendrites', fine ledeburite and 'D' type flakes in a pearlitic matrix. Ferrite, however, was not observed.

4.3.3. (d) The Combined Effect of Both Titanium and Sulphur Additions on the Structure of the 'Base Melt' (A1)

A total of ten melts were cast to determine the combined effect of sulphur and titanium additions on the microstructure of the 'Base Melt' cast iron. Five different titanium concentrations were considered, these being levels B, C, E, F and G at both the level 2 and level 3 sulphur concentrations (See Tables 15a and Section 4.3.1.).

In considering the casts already described, three quantitative criteria have emerged as a means of comparison of the extent of graphitisation obtained. These criteria are the distance from the chill/metal interface at which the following first appear:-

- (i) streamer graphite
- (ii) the 'grey' areas
- (iii) the true, graphitic cells.

These three criteria have been determined for each of the casts in the low nitrogen melt programme and the results are presented in Table 20. In addition, the graphite type existing at the number 8 thermocouple position (177.8mm) has been tabulated, this parameter being chosen as it represents the slowest quantifiable cooling rate produced in the casts.

The microstructures of the individual castings produced will now be considered.

Melt B2 (3.75%C, 0.06%S, 0.091%Ti, 0.004%N)

The streamer graphite closest to the chill/metal interface appeared similar to that shown in Plate 37 for Al, although no coarse graphite flakes were observed in association with it, as was the case in Al. Plate 105 shows an example of the type of streamer graphite observed in B2 at 63.5mm from the chill. The graphitic areas constituting the 'grey' start appeared similar to those observed in B1 but, each 'cluster' was only about half the size of those in B1 (see Plate 71).

The first isolated graphitic cell was observed at 76mm from the chill. The cell comprised 'D' type graphite flakes with a ferritic centre, similar to those illustrated in Plates 103 and 104, and the area around the cell contained large numbers of fine streamers, ledeburite, and pearlitic 'dendrites'. More graphitic cells of a similar form were noted at 106.5mm and 110mm from the chill. Plate 106 illustrates the structure observed at 112mm; streamer graphite, pearlitic 'dendrites' and ledeburite in a more globular form than has been observed previously.

At 127.1mm the amount of graphite present in the microstructure has significantly increased, areas of 'A' and 'D' type flakes (Plate 107) and mesh type graphite (Plate 108) being observed. With a greater distance from the chill, the mesh graphite soon disappeared, the number of 'D' type flakes diminished and 'A' type flakes became the more prevalent form of graphite (Plate 109).

Melt B3 (3.65%C, 0.10%S, 0.0915%Ti, 0.0051%N)

Streamer graphite was again evident. The 'grey' start areas were about twice the size of those observed in B2 and were generally similar in appearance to the 'grey' area shown in Plate 41 but, lacking the obvious 'A' type graphite flake.

The first graphitic cells observed, comprising 'D' type flakes, were also significantly larger than those in B2. Dendrite arms, in the proximity of the graphitic cells, were outlined by a network of 'D' type flakes, and small ferritic areas appeared to be associated with the dendrite arm extremities as in Plate 100.

Between 152.6 and 153.6mm large numbers of angular inclusions associated with filaments of a degenerate form of graphite were observed (Plate 110). 'Fan-like' configurations of cementite plates/ ledeburite were also a prominent feature at this distance and were similar to that shown in Plate 111. Very little cementite remained at 178mm - the structure comprising 'A' and 'D' type flakes in a pearlitic matrix (Plate 112).

Melt C2 (3.80%C, 0.068%S, 0.137%Ti, 0.0049%N)

The primary dendrites were very prominent and streamer graphite, associated with the secondary dendrite arms was noted (Plate 113). The grey start appeared similar to that observed in casting A1 (Plate 40).

Two graphitic cells were observed at the cell start, both being of similar size to that observed in B2. Both cells exhibited 'D' type, interdendritic flake graphite with ferritic areas at the cell centres (as in Plate 103). The remainder of the structure comprised fine streamer graphite, pearlitic 'dendrites' and ledeburite. This overall type of structure persisted to 127.1mm, at which point it became significantly more graphitic. Extensive areas of 'D' type flakes, with some 'A' type flakes, in a matrix of ferrite (no longer confined to the cell centres) were observed. An isolated 'fan' of ledeburite was noted at 145mm (Plate 114).

With increasing distance, the amount of ferrite steadily decreased and more 'A' type flakes appeared. At 177.8mm and 187mm the structure comprised 'A' and 'D' type flakes in a pearlitic matrix, the outlines of the original dendrite arms still being visible (Plates 115 and 116).

Melt C3 (3.80%C, 0.110%S, 0.137%Ti, 0.0046%N)

The streamer graphite at the 'streamer start' was very fine, only just being visible at X16 magnification. The graphitic areas at the 'grey' start were unlike those previously observed as here they resembled 'broad' streamers (Plates 117 and 118).

An isolated cell was observed at the cell start. As with cells observed at an equivalent position in B2, B3 and C2 the cell had a ferritic centre, although there was less ferrite present than in those castings. Again, pearlitic 'dendrites' predominated. The remainder of the structure at this distance comprised pearlitic 'dendrites', ledeburite and streamer graphite. As was observed in C2, with increasing distance the amount of ferrite present initially increased and then gradually decreased ^{until,} at 139mm, the matrix became entirely pearlitic. Plate 119

shows a cell at 164mm which appears to be partially outlined by cementite plates and ledeburite. 'A' and 'D' type graphite flakes were observed at 181mm, the 'A' type flakes becoming more prominent with increasing distance. Pearlitic 'dendrites' still remained a prominent feature of the microstructure and a number of 'fans' comprising ledeburite, similar to those shown in Plates 111 and 114, were noted.

Melt E2 (3.60%C, 0.045%S, 0.316%Ti, 0.005%N)

The streamer graphite start is illustrated in Plate 120 and shows numerous angular inclusions associated with both the pearlite and the graphite. The first graphitic cells observed were similar to those at the cell start in E1 (Plates 98, 99 and 100) although, the 'D' type flakes were slightly finer, and less ferrite was present, than in E1. At 156mm, a ferritic centred cell, similar to that shown in Plate 102, was observed, the dendrite arms again appearing to be surrounded by a layer of ferrite. Extensive areas of ledeburite and streamer graphite, comprising about 50% of the structure, persisted at 181mm. The remainder of the structure at 181mm consisted of pearlitic 'dendrites' with coarse 'D' type and degenerate forms of flake graphite in a pearlitic matrix.

Melt E3 (3.70%C, 0.098%S, 0.316%Ti, 0.004%N)

The structure of this cast was generally similar to those described for E1 and E2. In some areas, however, the streamer graphite appeared to take the form of a coarser, more open network than had been previously observed (Plate 121).

At the cell start the graphitic areas, comprising 'D' type flakes intermediate in size between those observed at the cell start in E1 (Plates 98, 99 and 100) and E2, constituted 50% of the cross section of the casting. The ledeburitic areas at the cell start still exhibited streamer graphite (Plate 122). With increasing distance, the amount of ferrite in the graphitic areas increased though never achieved the proportion observed in E2. Again the dendrite arms appeared to be surrounded by a layer of ferrite bounded by an irregular network of fine 'D' type flakes, similar to that previously illustrated in Plate 102, though the areas of ferrite were less extensive than shown in this Plate. At 177.8mm, the graphitic cells contained 'D' type flakes, whilst the remaining transverse section comprised areas of ledeburite and an isolated 'fan' of ledeburite comparable with Plate 111.

Melt F2 (3.60%C, 0.05%S, 0.390%Ti, 0.0045%N)

The ledeburite in this cast was particularly fine and the cementite plates had a tendency to be more unidirectionally aligned (Plate 123) than those in F1 (Plate 92). As with G1 (Plate 91), the pearlitic 'dendrites' tended to be globular and less obviously directionally aligned. The ledeburite with streamer graphite persisted until 116mm where the first graphitic cell was observed. The cell contained very fine 'D' type flakes associated with both pearlite and grains of ferrite. The dendrite arms again tended to be surrounded by a layer of ferrite. With increasing distance, the ledeburitic areas became progressively smaller until, at 181.5mm, only a very small amount was present. The pearlitic 'dendrites' became coarser and the amount of ferrite present decreased from 116mm to 181.5mm but, there was no significant change in the type of graphite present, this being mainly fine 'D' type flakes, with areas of coarser degenerate forms of flake graphite also being observed

(Plate 124). Large numbers of angular inclusions, mainly in the pearlitic 'dendrites', were noted (Plate 124).

Melt F3 (3.70%C, 0.10%S, 0.377%Ti, 0.0047%N)

The general structure was similar to that of F2. Like F2 and G1, the ledeburitic areas up to about 70mm were very fine, with cementite needles and globular pearlitic 'dendrites' being very prominent (Plate 125). Streamer graphite was also present. At 63.7mm, an area of what appeared to be ordinary streamer graphite, at X16 magnification, was revealed, at higher magnification, to comprise mesh type graphite contained between dendrite arms (Plate 126). Graphitic cells containing 'D' type flakes first appeared at 127.1mm (Plate 127). A number of inclusions are present within the prominent dendritic areas of Plate 127 but no free grains of ferrite are present. At 176.5mm, some of the dendrite extremities were ferritic, similar to those observed in previous castings (Plate 104), but beyond 177.8mm the amount of ferrite present in the microstructure was minimal. At 177.8mm, although 'D' type graphite predominated, small amounts of 'A' type flakes had begun to appear (Plate 128), becoming more abundant at 181mm.

Melt G2 (3.80%C, 0.05%S, 0.408%Ti, 0.003%N)

Longitudinal 'bands' were observed with the naked eye on the sectioned, polished surface of the casting, in both the unetched and etched conditions. Microstructurally, the banding was difficult to discern at or near the chill interface but, further up the casting it became more apparent. The dark bands appeared to be associated with densely packed groups of streamer graphite and pearlitic 'dendrites', separated by ledeburitic zones which gave rise to the light coloured bands (Plates 129 and 130).

The 'grey' start took the form of broadened streamers similar to that illustrated in Plate 117 for C1, rather than the more uniformly distributed form normally observed (Plate 40). At a higher magnification, they appeared similar in structure to Plate 93. Ledeburite was a prominent feature of the microstructure throughout the length of the casting, constituting about 25% of the structure, even at 177.8mm.

As with some previously described castings, the first cells observed exhibited ferritic centres. Although small amounts of 'D' type flakes were observed, the graphite within the cells mainly comprised a mesh-like form (Plate 131). The graphite at 177.8mm exhibited a diversity of forms including degenerate 'D' type flakes (Plate 132) and coarser chain like structures (Plate 133) associated with ferrite or pearlite, and fine flake-like forms similar to that illustrated in Plates 85 and 116.

Melt G3 (3.80%C, 0.10%S, 0.435%Ti, 0.003%N)

The 'banding' phenomenon and the general microstructural features of this cast were almost identical with those of G2. At 182mm, the microstructure of G3 was slightly more ledeburitic than G2, comprising about 40% of the structure and, in addition to the various graphitic forms observed in G2 at 177.8mm, areas similar to that illustrated in Plate 100 were also observed.

4.3.3 (e) Additional Melts with Both Sulphur and Titanium Additions in the Low Nitrogen Melt Programme

The following are melts which, though originally intended to be of a different composition have, as a result of problems on melt down, or with the mould preheating furnace, resulted in duplicate casts being produced. The best three were therefore grouped together, the fourth melt being categorised as an 'additional' melt.

Melt Ela (3.80%C, 0.02%S, 0.293%Ti, 0.0038%N)

The composition of this melt (Table 15a) shows it to contain slightly less titanium and nitrogen but more silicon than the other group 'E' melts. This appears to have produced a more graphitic fracture (Plate 134) than E1, E2 or E3 (Plate 35) although the structure is still cellular towards the top of the casting. The distances for the streamer, 'grey' and cell starts are presented in Table 21. These show the streamer start to occur nearer the chill than any of the other 'E' group casts, the 'grey' start is later than in E1, the same as in E3 and earlier than in E2; whilst the cell start distance is the same as in E1 and E3 but earlier than in E2.

The graphite at the streamer start was much coarser and more abundant than observed in the other group 'E' melts and resembled that shown in Plate 130. The greater abundance of streamer graphite was the cause of the much greyer appearance of the fracture. The 'graphitic' areas constituting the 'grey' start were also coarser than in E1 but were associated with ferrite. The graphite in the 'grey' areas either took the form of that shown in Plate 96 or Plate 99 and these, together with streamer graphite of the form illustrated in

Plate 94, persisted to the cell start. The first cells contained very fine 'D' type graphite and had ferritic centres, as in Plate 102. With increasing distance, the proportion of graphitic eutectic in the structure increased at the expense of ledeburite, although at 89mm, a number of ledeburite 'fans' were noted. The amount of graphitic eutectic in the structure was always greater than at an equivalent position in E1 - at 177.8mm in E1a this was 80% compared with only 50% in E1, though, the structural components were the same. The graphite was a mixture of 'D' type flakes (though these were twice the size of those in E1) and streamer graphite of the type shown in Plate 94.

Melt E3a (3.52%C, 0.120%S, 0.340%Ti, 0.004%N)

Due to problems encountered with the data logger, which prevented any cooling curves being obtained, this melt was held for an excessively long time in the induction furnace. As a result, the carbon content of the melt, when finally poured, was much lower than that of E1, E2 and E3 (Table 15a). The combination of a low carbon content with high sulphur and titanium concentrations resulted in a much whiter fracture (Plate 135) compared with those of E1, E2 and E3 (Plate 35).

Microscopical examination confirmed the general structural trends indicated by the fracture surface. The casting was completely ledeburitic except for one isolated cell which formed around the number eight thermocouple at 177.8mm. Fine streamer graphite appeared at 63.5mm and persisted to the top of the sample, the first 'grey' area only being observed at 177.8mm (Plate 137). The graphite in the cell at 177.8mm was mainly 'D' type flakes but a small amount of more degenerate flake-like forms was also present.

Melt F2a (3.75%C, 0.05%S, 0.39%Ti, 0.0046%N)

The carbon content of this melt proved to be higher than the other 'F' melts (Table 15a) and it has been disregarded from the main low nitrogen melt programme. The fracture (Plate 136) exhibits a slightly greyer appearance than that for F2 (Plate 35). Reference to the streamer, 'grey', and cell start distance criteria in Table 21 support this observation. The graphite of the 'grey' was not as previously observed but resembles that in the ferrite in Plate 106, but, here the matrix was pearlitic. The structure at 64.8mm and 84mm was similar to that in F1 at 177.8mm (Plate 104). There was some graphite surrounding the dendrites as in Plate 138 but, here, the 'D' graphite was larger. At 89mm the structure was similar but more ferritic.

At the cell start the structure was 50% graphitic and the cells appeared similar to those shown in Plates 101 and 103, though the ferrite tended to be less extensive and the graphite flakes slightly coarser. From 145.5mm to the top of the sample the structure was identical to that illustrated in Plate 124 for F2.

4.3.4 The Structures of the High Nitrogen Grey Iron Castings

4.3.4(a) The Effect of Sulphur Concentration at the Higher Nitrogen Level

Three melts were cast with similar compositions to A1, A2 and A3 except that the nitrogen content of each was increased to about 0.01 mass %. The four criteria identified in Section 4.3.3.(d) as a means of comparing different casts have again been utilised for the high nitrogen melt programme, the relevant data being presented in Table 22. The fractures for A1', A2' and A3' are shown in Plate 139.

Comparison of the first columns in Table 20 and 22, and of Plates 139 and 35, leads to the general observation that the increased nitrogen content has tended to stabilise the carbidic eutectic.

Melt Al' (3.80%C, 0.03%S, 0%Ti, 0.012%N)

The structure at the 'grey' start (41.1mm) was similar to that of Al (Plates 40 and 41) although the graphitic areas tended to be slightly smaller. 'Grey' areas of similar shape and size to those depicted in these plates were not observed until 63.5mm where 'A' flakes were again observed, within the general graphitic background, although, the flakes themselves were broader than in Al.

The first cell (89mm) contained much coarser 'A' type flakes than at the cell start of Al, in a pearlitic matrix (Plates 140 and 141). This general structure predominated from the cell start to the top of the casting. Plate 142 illustrates the graphitic structure at 187mm. Unlike Al, whose structure at this distance showed flakes associated with ferrite (Plate 58), Al' showed 'A' type flakes in a resolvable pearlitic matrix. Ferrite associated with flake graphite was rarely observed, but, a typical example is shown in Plate 143.

Though a minor component in comparison with the graphitic areas, ledeburite still persisted in significant amounts to the top of the casting, comprising about 20% of the structure at 187mm. Above 127.1mm, isolated areas of cementite were observed (Plate 144) and at 187mm a number of ledeburite 'fans', similar to that illustrated in Plate 111, were noted. The graphitic flakes at the extremities of cells bounded by cementite plates appeared much finer than at the centre of the cell (Plate 145). Streamer graphite was observed within the ledeburitic

areas, even at the top of the casting, and within individual 'streamers', flake like forms could be identified (Plate 146).

Melt A2' (3.80%C, 0.05%S, 0%Ti, 0.0118%N)

The structure of this cast was very similar to that of Al'. In general, however, there was more ferrite present than in Al', although still not as much as in Al. Also ledeburite persisted in greater amounts towards the top of the casting than in either Al or Al'.

'A' type flakes, which tended to coarsen with increasing distance from the chill, were identified in the streamer graphite at 28.4mm and 38.1mm (Plate 147). The 'grey' start was similar to that observed in Al', comprising graphitic areas similar to those illustrated in Plates 40 and 66, although the component streamers tended to be larger and were present in greater numbers.

The first graphitic cells were of comparable shape and size to those observed in Al' (see Plate 140) but the 'A' type flakes present tended to be much finer, being more comparable to those at the mid-radius position of the cell shown in Plate 145. Small amounts of ferrite associated with the graphite flakes were noted at the cell start. At 127.1mm, ledeburite was still more abundant than the areas of graphitic eutectic. The graphite in the ledeburitic areas had changed from that illustrated in Plate 147 to more compacted, degenerate flake-like forms (Plate 148). The structure of the graphitic cells, at this distance, was generally similar to Plates 103 and 104 though the individual flakes tended to be slightly longer, and more obviously 'A' type, in A2' (Plate 149). This general mixture of 'A' type graphite flakes, in the cellular areas (Plate 149), and degenerate forms of graphite, in the ledeburitic areas (Plate 150), persisted to the top of

the casting. Areas of cementite plates were noted in the cellular areas at 177.8mm and 182mm. Some very large inclusions were noted towards the top of the casting (Plate 151) and ferrite associated with the graphite flakes continued to be a minor microstructural component.

Melt A3' (3.80%C, 0.09%S, 0%Ti, 0.010%N)

This cast was generally much whiter than A1' and A2', the streamer start being retarded (Table 22) and the streamers themselves tended to be shorter and more compact. The streamers increased in size with distance from the chill, eventually forming 'grey' areas at 63.5mm. These were about four times the size of the initial 'grey' areas in A1, and contained compacted, degenerate, flake-like forms of graphite (Plate 152). Progressing further up the casting the graphite in the 'grey' areas became a mixture of flake-like forms, comparable in size with the smaller ones shown in Plate 142, and more degenerate forms, of the type shown in Plates 150 and 152.

The first cells appeared at 127.1mm and constituted approximately 60% of this transverse section. The graphite in the cells was 'A' type associated with ferrite (Plate 153). 'A' type graphite was also observed associated with the streamers at this distance, though these flakes tended to be slightly smaller than those in the cells. At 177.8mm, the structure suddenly became predominantly ledeburitic and the graphite in both the cellular and ledeburitic areas was a mixture of 'A' type flakes and degenerate forms comparable with those in Plates 150 and 151. Ferrite was again associated with the 'A' type flakes which tended to be slightly thicker than those nearer the cell start. At 181mm, the structure became more graphitic, the cellular areas constituting about 60% of the cross section. The graphite was

fine 'A' type flakes, with the occasional areas of more thickened flakes (Plate 154), but very little free ferrite was observed.

Melt Ala' (3.80%C, 0.02%S, 0%Ti, 0.0112%N)

This melt was inadvertently superheated due to a malfunction of the dip thermocouple. Superheating of cast iron (prior to casting) is known to result in the destruction of nuclei for graphitic cells and, as a result, this melt was discarded from the main melt programme. The fracture (Plate 155) however, shows a generally more graphitic casting has resulted possibly due to the slower cooling rate compared with Al'. The 'distance criteria', tabulated in Table 21, show that whilst the 'grey' start occurred slightly earlier than in Al' (Table 22), the cell start has been significantly retarded in Ala'; i.e. superheat has been partly offset by a slower cooling rate (Figures 45 and 46).

The 'grey' areas were similar in shape and structure to those in Al', but tended to be larger. 'Grey' areas comparable in size with those observed in Al' at 63.5mm were observed in Ala' at 46mm. Plate 156 shows the graphite type present within the 'grey' areas at 38.1mm. This graphite type persisted to 63.5mm where small amounts of ferrite appeared associated with the graphite, producing a structure similar to that shown in Plate 143. At 89mm, in addition to the graphite types already described, significant areas of the type illustrated in Plate 130 were noted. The cell start occurred at 127.1mm and beyond this 'A' type flake graphite became the predominant form, even within the streamers. Minor amounts of ferrite were observed associated with the flake graphite towards the top of the casting.

4.3.4. (b) The Effect of Both Sulphur and Titanium Additions at the High Nitrogen Level

A further eleven melts, melts B1' to F3' (see Table 15b) were cast in order to ascertain the combined effect of different sulphur and titanium concentrations on the microstructure of the cast iron at the higher nitrogen level (0.0097 mass % average). The fractures are illustrated in Plate 139 and the streamer, 'grey' and cell starts and the graphite types found at 177.8mm, are presented in Table 22.

Melt B1' (3.80%C, 0.018%S, 0.093%Ti, 0.0084%N)

The fracture (Plate 139) exhibits a predominantly white structure with a number of discrete graphitic cells appearing towards the top of the sample, the number of cells increasing with distance from the chill.

The graphite in the streamers at 75.5mm was a fine degenerate flake-like form, similar to that shown in Plate 148. The graphitic areas at the 'grey' start contained even finer degenerate flake-like forms, which tended to outline the dendrite arms (Plates 157 and 158). The graphite within the first cells was also very fine and similar to that in Plate 158. The pearlitic 'dendrites' in the cells tended to be 'outlined' by a thin layer of ferrite which in turn was surrounded by a band of graphite. At 127.1mm, the graphite in the ledeburitic areas had become more degenerate (Plate 159) but was generally finer than that seen at an equivalent position in the A' melts. At 130.2mm, the microstructure was predominantly graphitic, the graphite taking a form similar to that seen in Plate 158, but two to three times coarser. At 177.8mm, the streamer graphite in the ledeburitic areas

appeared as mesh and degenerate flake-like forms, whilst in the cells 'A', 'D' and degenerate flake-like forms existed and exhibited considerable size ranges (Plate 160). Large areas of cementite were also evident between the cells. The general structure illustrated in Plate 160 persisted within the cellular areas to the top of the sample although it did tend to coarsen. Streamer graphite also persisted to the top, at 182mm taking a form similar to that in Plate 146.

Melt B2' (3.70%C, 0.06%S, 0.091%Ti, 0.0091%N)

Unlike any of the other castings examined, the fracture exhibited a very abrupt transition from a white to a grey structure at about 63.5mm. Microstructural examination revealed streamer graphite and 'grey' areas at positions significantly closer to the chill than 63.5mm (Table 22) and that the apparently abrupt macrostructural transition was associated with the appearance of large numbers of streamers in close proximity to one another (Plate 161).

The graphitic areas at the 'grey' start (Plate 162) were generally larger than those observed in B1' or A1, but their shape was similar, in general, to those illustrated in Plate 40. At 63.5mm, the large streamer 'colonies' shown in Plate 161 were observed. The graphite within the streamers and the 'grey' areas at this distance was mainly of the type illustrated in Plates 162 and 163 but isolated flakes of what appeared to be 'A' type graphite were also noted.

The cell start comprised 'A' type flakes in a mixed ferritic/pearlitic matrix. The ferrite was not confined to the cell centres but tended to be more randomly distributed throughout the cell and, in addition, it was not especially associated with individual graphite

flakes. In the ledeburitic areas, the graphite within the streamers remained similar to that shown in Plates 162 and 163 though slightly finer. At 89mm, the ledeburitic areas still predominated. In the graphitic eutectic areas the 'A' type flakes had increased in size, but remained associated with the mixed ferritic/pearlitic matrix, whilst in the streamers networks of degenerate graphite flakes were observed (Plate 164). Similar structures were seen at 91 and 127.1mm, the graphitic eutectic areas comprising about 50% of the cross-section of the casting at this distance.

At 177.8mm and 181mm, the streamer graphite exhibited open 'chain-like' structures similar to that in Plate 121. The more extensive areas of graphitic eutectic contained mainly 'A' type flakes in a pearlitic matrix (Plate 165) although small concentrations of 'D' type flakes were also observed. The small amount of ferrite present tended to be associated with individual graphite flakes.

Melt B3' (3.65%C, 0.115%S, 0.090%Ti, 0.009%N)

The fracture (Plate 139) and the microstructural criteria (Table 22) indicate that this casting exhibits a graphitic structure over most of its length. The graphite at the streamer start was similar, in size and form (at X16 magnification), to that shown in Plate 164 (at X32 magnification), although, it tended to be more obviously confined between the directionally aligned dendrite arms. At 25.4mm, the graphite appeared much finer as shown in Plate 166.

The graphitic areas at the 'grey' start took the form of broad streamers similar in general appearance to that in Plate 147 but, the internal graphitic structure was much finer. In general there were more streamers present than in B1' but fewer than in B2'. In some

areas degenerate flake-like forms of graphite, of the type shown in Plate 150, were observed. Two quite extensive graphitic areas of an unusual form were noted at 63.5mm (Plates 167 and 168). The graphite in these areas appeared as a continuous network between the dendrite arms with the internal structure of the primary dendrites appearing to be graphitic also.

Two cells were identified at the cell start, the remaining structure (about 75% of the cross section) being ledeburitic. The cells contained compacted 'D' type flakes in a pearlitic matrix. The pearlitic 'dendrite' arms tended to be surrounded by a dense network of compacted flakes and, in some areas, the dendrite arm extremities were again ferritic (Plate 169). By 127.1mm, the graphitic cells had increased in size to occupy about 80% of the cross-section, the remaining ledeburite tending to outline the cell boundaries. 'D' type flake graphite was identified in both the streamers and in the cellular areas which also exhibited 'A' type flakes (Plate 170). Slightly more ferrite was present at this level than is suggested by Plate 170 and more was present at 177.8mm, though ferrite remained a very minor component of the structure. At 177.8mm and 185mm, the areas of graphitic eutectic again constituted about 80% of the cross-section. In these areas, the graphite mainly resembled that shown in Plate 169 with some 'A' type flakes comparable with the larger flakes shown in Plate 170. In the ledeburitic areas large numbers of inclusions were noted especially associated with the cementite; the graphite in the streamers appeared as networks of compact 'D' type flakes (Plates 169 and 171).

Melt C1' (3.60%C, 0.02%S, 0.12%Ti, 0.009%N)

The fracture (Plate 139) suggests that the lower third of the casting has a white iron structure, the middle mottled and the upper third has a cellular graphitic structure. Compared with A1' and B1', the fracture appears generally more graphitic. This is reflected by the streamer, 'grey' and cell starts (Table 22) which all appear earlier than in A1' or B1'.

The general form of the graphitic areas constituting the 'grey' start, and the size and type of graphite present, was the same as that observed in B3'. The 'cell start', an isolated cell at 63.7mm, contained graphite very similar to that in the streamers at the same distance as that shown in Plate 166. At 89mm, the structure was still predominantly ledeburitic, with particularly large pearlitic 'dendrites'. The graphite within the streamers was again similar to, but coarser, in general, than that shown in Plate 166, whilst the cellular areas exhibited a structure similar to but containing less ferrite than in Plate 169. The graphite in the cellular areas at 93mm was again like that in Plate 169 but the amount of ferrite present had increased. At 127.1mm the graphite in the ledeburitic areas was mesh type (Plate 172) whilst the graphitic eutectic areas exhibited small compacted flakes (Plate 173). Even at this distance the ledeburitic areas constituted 60% of the cross-section.

With increasing distance, the amount of ledeburite decreased until, at 177.8mm, it constituted only about 20% of the cross-section. In the graphitic eutectic areas, flake-like forms similar to, and ranging in size from that shown in Plate 110 to that in

Plate 148, were observed. A typical area is shown in Plate 174. In the ledeburitic areas, mesh graphite (ranging in form from that shown in Plate 121 to that in Plate 172) was observed, together with isolated compacted flakes of similar size and form to those illustrated in Plate 148.

Melt C2' (3.70%C, 0.05%S, 0.112%Ti, 0.010%N)

The resultant fracture had, generally, a more graphitic appearance than C1' (Plate 139). In terms of the criteria listed in Table 22 however, it appears similar, in terms of the degree of graphitisation, to C1' and B2'.

Streamer graphite was first observed at 12.7mm, the graphite within the streamers being similar in general form to, but much finer than, that shown in Plate 164. At the 'grey' start, a variety of graphite forms were identified including a much finer version of that shown in Plate 162, and forms similar, in shape and size, to those in Plates 164 and 167. The graphitic areas at the 'grey' start generally took the form of thickened streamers, in common with most of the high nitrogen casts (Plate 157). However, triangular 'grey' areas, more common in the low nitrogen melt programme (Plate 40), were observed at 63.5mm and 64.5mm. These graphitic areas, much larger than any observed in the low nitrogen casts, contained graphite which ranged in form from that shown in Plate 166 to the type shown in the finer graphitic regions of Plate 164.

The cells at the cell start contained graphite comparable with the finer forms illustrated in Plate 164 in a mixed ferritic/pearlitic matrix. The ferrite grains were distributed uniformly

throughout the cells at this distance but at 89mm, the ferrite was confined to the cell centres, similar to that illustrated in Plate 102. In the pearlitic areas of the cells flake graphite, comparable with that in Plate 170, was evident. However, the predominant structure at 89mm was ledeburitic with streamer graphite of the type shown in Plates 148 and 164.

At 127.1mm, cells occupied 60% of the cross-section. These cells contained fine 'A' and 'D' type graphite flakes in a pearlitic matrix producing a structural appearance similar in general, to Plate 170. With increasing distance, the graphite flakes coarsened and the ledeburitic areas diminished in size until, at 186mm, only isolated cementite plates were noted at the cell boundaries. Plate 175 illustrates the type of graphite present towards the top of the sample.

Melt C3' (3.60%C, 0.10%S, 0.13%Ti, 0.009%N)

The fracture (Plate 139) showed cells outlined by white iron towards the top of the casting. In general, C3' appeared 'whiter' than either C1' or C2', an observation borne out by the retarded formation of the streamer and 'grey' starts.

The graphite in the streamers at the streamer start (Table 22) was very fine, comparable in form and overall structure with that shown in Plate 120. At 39.1mm, in addition to this type of graphite, areas of mesh-like graphite, similar to that in Plate 96, were observed. The graphitic areas at the 'grey' start appeared to contain fine streamers in close proximity to one another. Closer inspection revealed the composition of these 'grey' areas to be ferrite and 'D' type graphite.

110

The first cells exhibited ferritic centres. In the ferritic part of the cells, the graphite took a form similar to that shown in Plate 131 whilst in the pearlitic areas it was comparable to that in Plate 99. Between 92mm and 123.1mm the structure was ledeburitic with large numbers of fine graphitic streamers. Four cells (occupying about half the cross-section) with ledeburitic 'fans' between them, were observed at 123.1mm. The cells again exhibited ferritic centres, the ferritic areas being of similar shape to those in Plate 103. The graphite within the cells and the streamers were mainly 'D' type.

The structure became progressively more graphitic with increasing distance until, at 153.6mm, only small amounts of ledeburite remained at the cell boundaries. This ledeburite assumed, a 'fan-like' configuration, producing a structure similar to that illustrated in Plate 145. Fine 'D' type graphite, comparable in size with that shown in Plates 88, 89 and 131, outlined the dendrite arms and occupied the interdendritic spaces, although one area of 'A' type flakes was noted. The small amount of ferrite remaining at this distance appeared to be associated with localised groups of 'D' type flakes, as in Plate 88. This general structure of graphitic cells, containing mainly 'D' type flakes, and outlined by ledeburite 'fans', also was observed at 177.8mm and 183mm (Plate 176). The amount of 'A' type graphite tended to increase however, with increasing distance, as did the coarseness of the flakes.

Melt D1' (3.60%C, 0.026%S, 0.18%Ti, 0.008%N)

The fracture, shown in Plate 139, exhibits a cellular structure towards the top of the casting. It appears greyer than C1' and C3' but as white as C2' which was borne out by the microstructural criteria (Table 22).

The graphite at the streamer start was similar in form to, though slightly coarser than, that seen in B3' (Plate 166). At the 'grey' start the graphite resembled that in Plate 40. At 50mm and 63.5mm, areas of what appeared to be compacted 'D' type flake graphite networks, in both a pearlitic matrix and associated with ferrite, were observed (Plates 177 and 178). However, the bulk of the cast at these distances contained fine ledeburite with a large concentration of streamers.

The first isolated cell, identified at 89mm, comprised 'A' type flakes in a predominantly pearlitic matrix with a small amount of ferrite associated with the graphite (Plate 179). Ledeburite predominated here and the streamer graphite comprised 'mesh-like' forms comparable with those in Plate 178 but with a greater tendency for alignment in the direction of heat flow. With increasing distance, the amount of ferrite present in the cells progressively decreased until, at the top of the casting, very little remained. Small amounts of a degenerate form of graphite (similar to that in Plate 110) existed towards the top of the casting (178.1mm) with predominantly 'A' type flakes. At 181.5mm, small amounts of graphite, of the type observed in Plate 180, was noted with areas of 'D' type flakes producing a structure similar to that illustrated in Plate 154. One isolated ledeburitic 'fan' was seen at 178.1mm.

Melt D3' (3.68%C, 0.115%S, 0.21%Ti, 0.009%N)

The fracture (Plate 139) suggests that the casting is slightly more graphitic than D1' but reference to the microstructural criteria (Table 22) indicates that whilst the streamer and 'grey' starts are slightly earlier, the cell start is identical to that for D1'.

The streamer graphite at 25.4mm and 31mm was similar to that illustrated in Plate 146 but considerably finer, being only about a fifth the size shown in this plate. The 'grey' start comprised mixtures of 'D' type flakes, in a pearlitic matrix, and areas of the type shown in Plate 178. Between the cell start, at 31mm, and 63.5mm the graphite was as illustrated in Plate 132, in a mixed fine pearlitic/ferritic matrix. At 66.5mm, a variety of graphite forms were observed, including examples of the types seen in Plates 132, 146 and 178, around the dendrite arms and in the interdendritic spaces. In some areas ferrite outlined the dendrite arm extremities and small amounts were associated with graphite in the interdendritic spaces.

In the first isolated cell, appearing at 89mm, the graphite was extremely fine, predominantly compacted 'D' type flakes (Plate 181). Slightly coarser flake graphite tended to outline the dendrite arms. Graphite of the type shown in Plate 162 was observed in the streamers in a ledeburitic matrix at this distance. The same type of graphite was also noted in 'grey' areas though, here, it tended to be associated with a mixed pearlitic/ferritic matrix. At 95mm, the structure was essentially ledeburitic with streamer graphite (of the type illustrated in Plates 162 and 178) and 'grey' areas comprising graphite similar to that shown in Plate 182.

At 127.1mm, the microstructure was predominantly cellular with 'D' type flakes occupying the interdendritic areas, and outlining the dendrite arms. The graphite was compacted 'D' type flakes, in general, similar to that illustrated in Plate 181, though one isolated area exhibited 'A' type graphite (Plate 183). Grains of ferrite were associated with the graphitic areas. The streamer graphite at this distance also appeared to comprise compacted 'D' type graphite similar to that illustrated in Plate 181. Plate 183 shows the type of graphite present at 177.8mm. The matrix was a mixed pearlitic/ferritic structure. In some areas ferrite existed at the dendrite arm extremities. 'Fan-like' configurations of ledeburite still constituted about 20% of the sample cross-section at this distance.

Melt F1' (3.60%C, 0.021%S, 0.40%Ti, 0.009%N)

The fracture (Plate 139) exhibited a much more extensive 'white iron' structure than any of the previous casts in the high nitrogen melt programme. Apart from a few isolated graphitic cells, towards the top of the casting, the fracture appeared to be entirely white. Microstructural examination revealed that the streamer start, similar in form to that observed in D3', commenced at 38.1mm. The structure to 127.1mm was essentially ledeburitic with streamer graphite and pearlitic 'dendrites' which coarsened with increasing distance. The streamer graphite appeared to contain very small, compacted 'D' type graphite. No 'grey' start was observed in this cast.

The first graphitic cells appeared at 127.1mm but the ledeburitic structure with fine graphitic 'streamers' still predominated (Plate 184). The cells contained compacted 'D' type graphite, which occupied the interdendritic areas, and outlined the dendrite arms, in a mixed

ferritic/pearlitic matrix. The graphite flakes observed resembled those already observed in Plate 181, but were generally much finer, being about half the size. This general structure, with ledeburite predominating, persisted to the top of the casting. The compacted 'D' type graphite in the cells did coarsen slightly with increasing distance until, at 178.1mm, they were comparable, both in size and form, with that shown in Plate 181. Again, ferrite was associated with the graphite (Plate 185). Some particularly long streamers of very fine graphite were observed towards the top of the casting.

Melt F2' (3.64%C, 0.06%S, 0.38%Ti, 0.0091%N)

The fracture (Plate 139), as with F1', indicated the presence of an extensive 'white iron' structure. Microscopical examination revealed the streamer start to be 38.1mm, the same as in F1' and, similarly, no 'grey' start was observed. Up to 106mm the structure essentially comprised ledeburite, pearlitic 'dendrites' and streamer graphite, of similar form to that illustrated in Plate 184, the streamers and dendrites increasing in size with distance from the chill.

The first cell was observed at 106mm but the ledeburitic structure still predominated. The cell contained 'D' type flakes in the interdendritic spaces, and outlining the dendrites. The matrix was pearlitic. A similar structure existed at 130mm but here, some dendrite arm extremities had transformed to ferrite and 'D' type graphite flakes. The latter formed a band outlining the original dendrite arms. At 177.8mm, the graphitic eutectic predominated with only minor areas of ledeburite and ledeburitic 'fans' trapped between the cells. Pearlitic 'dendrites' were still evident in the cellular areas. The cells contained compacted 'D' type flake graphite of the types illustrated in

Plates 150 and 173, in a pearlitic matrix. Small amounts of a very fine form of graphite were also noted (Plate 186).

Melt F3' (3.65%C, 0.10%S, 0.38%Ti, 0.0091%N)

The fracture (Plate 139) showed evidence of a cellular structure towards the top of the casting. The cells were finer than in F2', but the fracture appeared to be slightly greyer. The criteria (Table 22) show that, whilst the streamer start occurred nearer the chill than in F1' or F2', the 'grey' and cell starts were more retarded than in any other casts. The 'grey' and the cell starts both occurred at 130.2mm. Nearer the chill the structure comprised pearlitic 'dendrites', ledeburite and streamer graphite, the dendrites and the streamers becoming progressively coarser with increasing distance from the chill. In general, the streamer graphite was similar to, but finer than, that observed in F1' and F2'.

At 130.2mm, the first cell, containing pearlitic 'dendrites' and fine compacted 'D' type and degenerate flakes, in a pearlitic matrix, was observed (Plates 187 and 188 respectively). The remaining structure comprised ledeburite with a degenerate form of streamer graphite. This general structure, with the flake graphite coarsening slightly with increasing distance, persisted to 181mm. The structure at 181mm was predominantly cellular with small amounts of ledeburite present as ledeburitic 'fans' trapped between the cells. The graphite was mainly 'D' type but some 'A' type flakes were observed (Plate 189) in an entirely pearlitic matrix.

4.3.4(c) Additional Melts in the High Nitrogen Melt Programme

As in the low nitrogen melt programme, Section 4.3.3.(e), two melts were cast which, due to unforeseen experimental difficulties, resulted in castings which did not meet the precise desired chemical specification or differed markedly in cooling rate from the rest of the group. These are described below:-

Melt B3a' (3.70%C, 0.11%S, 0.094%Ti, 0.015%N)

This cast had a slightly lower carbon content, and a slightly higher nitrogen content (Table 15b), than was intended. The net effect, as evidenced by the fracture (Plate 190) and the microstructural 'criteria' (Table 21), was to produce a much whiter cast than B3' (Plate 139, Table 22).

At the 'grey' start the graphite resembled that illustrated in Plate 166. At 89mm, 'A' type graphite was noted in some of the streamers but, on the whole, the graphite flakes were similar to, though slightly thicker than, those shown in Plate 146. The isolated cell which constituted the cell start exhibited finer 'A' type graphite than that in the streamers at 89mm. At 127.1mm, only one small cell was observed with graphite similar to that illustrated in Plate 170. This graphite was also observed in the streamers at this distance. At 177.8mm, the cellular areas, which contained 'A' type graphite flakes in a pearlitic matrix, constituted about 70% of the cross-section, the remaining structure being fine ledeburite with relatively few streamers. Slightly more ledeburite was present at 184mm, whilst the cells comprised predominantly 'A' type flakes with some degenerate graphite forms.

Melt C2a' (3.57%C, 0.06%S, 0.13%Ti, 0.010%N)

No cooling curves were obtained for this cast. This factor, coupled with the low carbon content, precluded it from the main high nitrogen melt programme. The fracture obtained from this cast (Plate 191) shows a much whiter, more cellular structure than C1', C2' or C3'. The microstructural criteria (Table 21) show the streamer and 'grey' starts to be similar to those for C2' (Table 22), but the cell start has been retarded relative to all the 'C'' melts.

In general, the microstructure was less graphitic than C2'. The streamers at the streamer start, and the graphitic areas at the 'grey' start, were much smaller than in C2' despite their occurrences being at the same distances from the chill. The graphite was similar to that depicted in Plate 118. At 89mm, the graphite took a variety of forms including the types illustrated in Plates 118, 164 and 178. The first cell exhibited a ferritic centre, similar to that shown in Plate 131, although the individual flakes were about two thirds the size of the ones depicted. In the cellular areas at 131mm, the graphite present comprised the types illustrated in Plates 88, 99, and 131, whilst the streamers were similar to those shown in Plate 106. At 177.8mm and 184mm, the graphitic eutectic occupied about 75% of the cross-section, the structure being comparable to that depicted in Plates 87 and 88.

4.3.5 Scanning Electron Microscopy for Inclusion Identification

A variety of inclusions, of varying size, shape, colour and location, were observed in the irons. An attempt was made to identify the composition of inclusions by their colours. Using an optical microscope, the various inclusions were identified, the areas marked

(using a microhardness diamond) and the samples transferred to the scanning electron microscope (S.E.M.) for EDAX chemical analysis. It was not deemed necessary to analyse the inclusions found in all the casts but to utilise a sufficient number of casts to monitor all observed variations. Unfortunately, as the method of indentation marking of the inclusions proved inadequate, scans of approximate areas were produced and the following observed:-

- (i) Titanium formed sulphides of the Ti_2S type as evidenced by the peak height ratios (Plate 193).
- (ii) Titanium was observed to form compounds which were assumed to be cyanonitrides, carbonitrides, nitrides and carbosulphides which cannot be identified as carbon and nitrogen cannot be analysed on the S.E.M.
- (iii) Manganese sulphides existed both on their own, duplexed or triplexed with titanium sulphides and other titanium compounds (Plates 193-204).

The inclusions were located in the austenite dendrites, associated with the graphite flakes, in the interdendritic cementite, ferrite and pearlite, and at all distances from the chill. Those found in close proximity to the chill were mainly in the cementite. The inclusions and composition scans can be seen in Plates 192-204 .

5.1 THE EXPERIMENTAL TECHNIQUE

The technique adopted in this work involved the solidification of a cylindrical casting under unidirectional heat flow conditions such that a large cooling rate variation existed throughout the length of the casting, the cooling rate decreasing with increasing distance from the copper chill. Information gleaned from the English summaries and diagrams in papers by Ogi and Matsuda⁽²⁸⁾, Ibaraki et al⁽²⁹⁾ and Okamoto and Matsumoto⁽³⁰⁾ indicated that they used similar techniques (see Section 2.7.7). The design for the present mould preheating furnace, and its modus operandi, were based on that employed by Gadgil and Kondic⁽²⁰⁾, although modifications were made in order to overcome certain limitations which were apparent at the outset of the work, and some which became apparent during initial experimentation. The principal modifications to the apparatus and technique, described at length in Chapters 3 and 4.2, included:-

- (i) introduction of thermocouples into the melt through the mould wall to quantify the cooling rate variation within the casting and identify furnace control procedures to ensure unidirectional solidification was obtained.
- (ii) centralisation of the water inlet and use of a flow rate which provided a continuous moving film of water over the heat removing portion of the chill.
- (iii) assessment of the cooling rate in each casting and promotion of conditions for unidirectional heat flow by:

- (a) introducing zonal control of the heating elements,
- (b) increasing the temperature of the preheated mould,
- (c) increasing casting diameter (see Appendix 1),
- (d) improving the insulation at the casting top,
- (e) positioning of the ceramic mould such that the feeder head was within the furnace hot zone.

The above modifications constitute a significant improvement in the apparatus and experimental method used by Gadgil and Kondic⁽²⁰⁾ and the Japanese authors^(28,29,30). The high directionality of the primary austenite dendrites in the initial white iron castings (described in Section 4.2) confirmed the effectiveness of the improved furnace and experimental technique in creating unidirectional heat flow.

From the experience gained during the course of this work it is doubtful whether Gadgil and Kondic⁽²⁰⁾ achieved unidirectional heat flow conditions during their experiments ; the degree of directionality they achieved was difficult to assess from the photomicrographs due to their relatively high magnification. It is thought that their use of a furnace preheating and holding temperature of 1150°C, with a switch-off time of 30 minutes, would have led to heat input in proximity to the chill and lateral heat flow from the casting to the furnace at the head of the casting. Their feeder head projected above the furnace hot zone whilst, in the present work, it was within the furnace hot zone. This coupled with Kaowool insulation above it reduced vertical heat loss from the feeder head.

The most important modification to Gadgil and Kondic's technique was the introduction of a number of thermocouples into the moulds. The presence of the thermocouples not only provided a monitor for cooling rates within the casting but permitted derivation of a furnace control technique to ensure unidirectional solidification. The prominent primary dendrites inherent in the initial white iron castings complemented the evidence obtained via the thermocouples - deviation from alignment with the mould vertical axis indicating non-directional solidification. Non-unidirectional solidification would have led to transverse cooling rate variability which would not have been quantifiable, making it difficult to relate structure to cooling rate. It is already evident from the results that a variation in structure has been obtained throughout a transverse section of the casting under unidirectional cooling conditions. The structure is likely to have been even more diverse under non-directional cooling.

Ogi and Matsuda⁽²⁸⁾ used a small sand mould with graduated exothermic insulation which, they claimed, promoted unidirectional solidification and achieved cooling rates of approximately 30-240°C/min over the 1160-1100°C range measured by three thermocouples. Ibraki et al⁽²⁹⁾ and Okamoto and Matsumoto⁽³⁰⁾ used three sheathed thermocouples which projected into the casting contained within a mould, which in turn was supported within a furnace. Extraction of heat through a copper chill at the base of the mould produced cooling rates of approximately 40-60°C/min, over the same temperature range. The present work produced a wide range of mean cooling rates (Table 19) between 4.43 and 635°C/min for the 1160-1100°C range. Careful temperature monitoring via eight thermocouples enabled adjustment of furnace input to achieve directional

cooling. Thus, the structure across the sample (transversely) at any particular point is truly representative of the measured cooling rate. The presence of thermocouples did not cause local disruption of the solidification mode in the light of the metallographic evidence (Plate 80). Clearly the use of sheathed thermocouples, as in the Japanese work^(29,30), would make the thermocouples less sensitive to rapid temperature changes.

The cooling curves for the present work are presented in Figures 14 to 60 (Section 4.3.2). Cooling rates were determined for two temperature ranges:-

- (a) 1160-1100°C - chosen as this represents the approximate solidification range of the ingot mould type iron under investigation, and
- (b) 1160-700°C - used to obtain an indication of the overall cooling rate throughout the course of an experiment.

The data has been presented for each thermocouple in Tables 16 and 17 and graphically in Figures 61 and 62. In these Figures, the cooling rate (derived from the cooling curves) has been plotted versus the actual thermocouple distance from the chill - these being measured directly from the sectioned castings since inaccuracy in drilling the mould or, in some cases, impingement of the metal on the thermocouple beads during pouring, led to displacement from their ideal positions.

Reproducible cooling rates were clearly achieved for thermocouple positions 3 to 8 (Table 19), as indicated by the relatively narrow band constituting the ± 1.96 standard deviation limits shown on Figures 61 and 62. Very much greater cooling rate variation was experienced at thermocouple positions 1 and 2 where the highest cooling rates were observed.

Contributions to cooling rate variability at thermocouple positions 1 and 2 are likely to be from superheating the melts, furnace parameters, thermocouple displacement and air gap formation between the chill/metal interface. Any variation in superheat was monitored by checking the temperature of the metal in the transfer ladle and ensuring it was $1300 \pm 10^{\circ}\text{C}$ prior to pouring. It should be noted that excess superheat will increase the heat removal required and thus alter the duration of an experiment. Care was also taken to ensure that no variability of identified furnace parameters occurred e.g. identical zonal switch-off times, indicated furnace temperatures and water flow rates were used. Appearance of an air gap, formed by contraction away from the copper chill of the white iron resulting from the rapid cooling of the molten metal, would have reduced the rate of heat transfer from the casting. Formation of this gap at the chill/metal interface could not be monitored as this would have required a thermocouple positioned at the back of the copper heat removing surface^(66,67). With a water cooled chill, the indicated temperature is greatly influenced by the water temperature, thus negating any such monitor of air gap formation from the drop in temperature at the back of the chill. Under normal casting practice, air gap formation would detract from unidirectional solidification but, in the present work, the furnace zoning ensured that the molochite mould remained at a temperature closely approximating to that of the metal thus preventing lateral heat flow. Switch-off/^{times}of the zones were pre-determined to ensure that the metal and furnace cooled concurrently at the same rate thus maintaining unidirectional solidification. Should an air gap have formed there would initially have been a variable thermal resistance across the gap which would have contributed to the cooling rate variability experienced in the metal in the vicinity of the first two thermocouples. This var-

iable thermal resistance would have stabilised quickly and this, combined with the increasing contribution of thermal resistance from the already solidified metal, would produce a narrower variation in cooling rate with increasing distance from the chill.

The large variation in indicated cooling rate for thermocouple positions 1 and 2 would have mainly originated from the misalignment of the thermocouples and the possibility of the base thermocouple impinging on the copper stool surface and becoming detached from the casting (e.g. thermocouple 1, cast B2). Therefore, actual thermocouple displacements (Table 18) were determined utilising an optical microscope with a graduated travelling stage. Inaccuracies in these measurements (due to sample alignment problems) are likely, possibly in the order of \pm lmm. In the region nearer to the chill, where cooling rates are changing rapidly with position, any slight inaccuracy in measurement of position will be much more significant and thus account for the greater variability in cooling rates obtained from the output monitored from thermocouples in this region.

There is a slightly greater spread of cooling rate for thermocouple number 8 than for thermocouple number 7 which is accentuated by the logarithmic scale. The likely cause of this variation is the occasional lack of total insulation above the feeder head permitting slight radiation heat loss. This phenomenon is illustrated on Figures 51, 55, 57 by juxtapositioning of the readings from thermocouples 7 and 8.

To carry out the statistical analysis (the results of which appear in Table 19 and Figures 61 and 62) twenty or more readings were required for any particular thermocouple position. Due to thermocouple displace-

ment, readings from a range of positions had to be assigned to the nominal thermocouple positions (Table 19). There are therefore, small inaccuracies inherent in the mean and standard deviation figures and, hence, the limits of significance ($\pm 1.96\sigma$).

The aim of this work was to develop the technique used by Gadgil and Kondic⁽²⁰⁾ to produce a variety of cooling rates to investigate the effect of compositional variation on the structure of ingot mould type iron. The variability in cooling rates exhibited by thermocouples number 1 and 2 was, therefore, not particularly significant since, at these positions (Table 8b and Figure 9), white iron structures were produced.

Information⁽⁶⁸⁾ indicates that complete solidification of an ingot mould may take as much as ten hours, suggesting that the metal within the mould wall cools almost uniformly at an extremely slow rate. The technique adopted in the present investigation has clearly produced, even at the greatest distances from the chill, cooling rates significantly greater than those encountered in commercial ingot mould practice.

During the development of the experimental method, measures were taken to reduce the minimum cooling rate produced in the castings by increasing the section of the castings (see Appendix 1), reducing the water flow rate and increasing the mould preheating furnace temperature. Further reduction in cooling rates was not undertaken so as not to risk significant heat input occurring to the casting within the furnace, thereby incurring non-unidirectional heat flow conditions. To have reduced the rate of heat abstraction still further would also have required significant modification of the chill, possibly by air cooling.

In spite of the differences in cooling rate between the present work and commercial casting and solidification of ingot moulds, the work carried out here does, however, provide a useful general insight into the interaction of sulphur, nitrogen and titanium in ingot mould type irons.

5.2 THE MICROSTRUCTURES OF THE INGOT MOULD TYPE IRONS

During the investigation of the effects of varying sulphur, titanium and nitrogen contents on ingot mould type iron, a variety of structures were obtained. A number of features however, were found to be common to the majority of the melts. These were:-

1. pro-eutectic austenite.
2. the formation of the carbidic eutectic in close proximity to the chill.
3. the formation of 'directional' or 'streamer' graphite (Gadgil and Kondic⁽²⁰⁾).
4. the formation of a graphitic area between impinging streamers and/or dendrites which has been termed the 'grey' region in the present work, and
5. the formation of graphitic regions towards the top of the castings - the areas taking the form of true graphitic cells.

5.2.1 Proeutectic Austenite

The proeutectic austenite dendrites are a pre-requisite of solidification in hypoeutectic irons^(1,2,4,8,9) and were nucleated at numerous sites at the chill/metal interface (Plate 36). On subsequent cooling the austenite underwent transformation to pearlite, which is seen in all the photomicrographs, but, in some cases, there was partial transformation at the dendrite arm extremities to ferrite and graphite. At the chill interface the dendrite orientation was random due to nucleation and growth of dendrites of various orientations on contact with the chill. This random orientation only existed over a short distance as those dendrites with a favourable orientation for growth rapidly crowded out those less favourably aligned (Plates 36 and 66). The dendrites were very directional over the majority of the casting lengths (Plates 44, 81) and often were clearly visible in graphitic areas towards the top of the castings. In these regions the dendrites tended to be more randomly orientated. It is thought that this was due to lower temperature gradients and the influence of growing eutectic cells rather than significant departure from unidirectional heat abstraction (Plates 69, 85, 88, 114, 127 and 128). It is clearly visible in Plates 176 and 186 that cells have interfered with growth.

In close proximity to the chill the dendrites were very fine (Plates 36, 37, 66, 90 and 161) but, as expected with the lower cooling rates prevalent at greater distances from the chill, the dendrites coarsened (Plates 44, 60, 67, 81, 105, 113 and 130). In all of the castings, except for G1, the primary dendrites were very prominent. However, in G1, the dendritic appearance is not as marked (Plates 90 and 91). A feature very prominent in the high, but also evident in the

low, nitrogen melts was the ferrite at the dendrite arm extremities (Plates 53, 74, 84, 102, 103, 104, 126, 169 and 182). From the microstructures it would appear that, at these extremities, austenite in contact with interdendritic graphite has decomposed to give ferrite and graphite.

5.2.2 Carbide Eutectic

All but one cast examined in the present work showed the carbide eutectic at the chill/metal interface (Plate 36). The exception was the hypereutectic iron (Ala), which resulted from overgraphitisation, and exhibited a mottled structure at the chill interface (Plate 63).

Evidence exists of the rapid nucleation and growth of the carbide eutectic (ledeburite) at the chill (Plate 36), where excessively high cooling rates exist, the rate of nucleation and growth decreasing with increasing distance from the chill (Plate 37). The ledeburite, like the austenite dendrites, coarsened with distance from the chill (Plate 113). Once the graphitic eutectic began nucleating, at the lower cooling rates, the amount of ledeburite decreased although in numerous cast^{ings} the ledeburitic structure existed throughout the sample length. The kinetics of formation of the different eutectics (graphitic and carbide), as explained by Hillert⁽¹⁹⁾, show that, even in regions where the graphitic eutectic is nucleating, the speed at which the carbide eutectic grows, even from a single site, far exceeds that of the graphitic eutectic and often precludes a totally graphitic structure. This is why the carbide form exists at the top of the samples in most cases and, in part, might explain the existence of occasional carbide 'fans' (Plates 111 and 145). These 'fans', found in the intercellular regions, are believed to be due to the nucleation and growth of ledeburite from single carbide nucleating events and have grown at a far greater rate than the graphitic cells.

Since the eutectic has resulted from a single nucleating event it is not surprising that it has assumed a 'fan' shape. Growth of these fans would be further encouraged by the rejection of carbide stabilising elements from the graphitic cells⁽⁷⁾. The formation of the ledeburite and the carbidic 'fans' in the intergraphitic cellular liquid might constitute the Hong Type III mottle structure⁽²⁵⁾ (See Section 2.2.5).

5.2.3 'Streamer' Graphite

Strongly directional forms of graphite (termed 'streamers' by Gadgil and Kondic⁽²⁰⁾ were the first form of graphite to appear^(20,21,22). The 'streamer' start was very fine and appeared, at low magnification, as a darkened pearlitic dendrite, very directionally aligned. A typical area, showing a number of streamers in the initial stages of formation, is shown in Plate 37. However, in many samples, these graphitic areas were much smaller and less dense than indicated in this plate and verification at high magnification was often required (Plates 65, 94, 96 and 146).

With increasing distance from the chill (decreasing cooling rate) these areas increased in size whilst remaining directionally aligned (Plates 52, 60, 67, 72, 97, 105, 113, 129 and 130) and were sometimes evident at sample extremes where they often coexisted with cellular graphitic areas (Plates 68, 71 and 73), with the carbidic 'fans' (Plates 83, 114, 145 and 186) and sometimes just in a carbidic region (Plate 69). Gadgil and Kondic⁽²⁰⁾ have suggested that this graphite form may be attributed to cementite decomposition. As in their work, in many cases the streamers appeared in ferrite (Plates 42, 43, 53, 56 and 122) and pearlite and in association with ledeburite (Plates

42, 60, 77, 81 and 106). Closer examination of the streamer areas (Plate 37) showed flake-like structures within the more general streamer graphite areas (Plates 38, 145, 146 and 147). Plate 37 shows an 'A' type graphite flake at 12.7mm (0.5in) from the chill. The structure of the flakes is similar to those flakes found in the more conventional cellular graphitic areas which would lead one to conclude that these flakes have formed directly from the melt. In the low nitrogen castings the streamers coexisting with the cellular structures were very fine. In the high nitrogen castings there was a great similarity between the streamer graphite and the cellular graphite (Plates 152, 153, 164 and 170).

The mechanism of streamer graphite formation is obviously very complex and appears to involve both the formation of flake-like graphite forms from the melt and the high temperature decomposition of the cementite.

5.2.4 'Grey' Areas

Originally it was the intention to utilise the fractures to measure the degree of graphitisation obtained in the castings. However, the mottled areas evident on the fracture surfaces, close to the chilled end of the castings, were found, on microstructural examination, not to be true graphite cells, in most cases, but irregular graphitic areas associated with the streamers, here termed 'grey' areas, the streamers in fact not being evident on the fracture surfaces. These 'grey' areas were found generally to take two forms. In some cases they appeared to have formed between two or three impinging dendrites (Plates 40 and 41). Similarly shaped areas appeared in other castings where a large number of dendrites produced a 'grey'

region though in these cases, the ledeburitic matrix was evident between some of the streamers (Plates 66 and 161). The second type of grey area was less obviously associated with streamers and appeared to have formed between the dendrite arms (Plates 81, 92, 93, 117, 123 and 157). Closer examination showed flake-like structures within these 'grey' areas (Plates 40, 41, 117 and 118).

Proposed Mechanism of Formation of the Streamer Graphite and 'Grey' Areas

It has already been shown that evidence exists for the formation of streamer graphite from the high temperature decomposition of eutectic cementite. A possible mechanism of formation of both the streamers and more particularly, the 'grey' areas directly from the melt is as follows:-

Hong⁽²⁵⁾, using a unidirectional solidification technique (Section 2.7.6) has identified three types of mottled structure (Section 2.2.5). A Type I mottled structure is one in which the white iron eutectic forms first and the graphitic eutectic forms in the residual melt between the white iron 'cells'. It is possible that, in the present work, the structure in those areas of the castings exhibiting streamer graphite constitutes a Type I mottle structure. The cooling rate at the chill/metal interface is rapid and therefore, conducive to the nucleation and growth of the white iron structure. Due to the directional heat transfer, the growth is vertically upwards from the chill and the possibility exists of liquid entrapment (i.e. areas of residual melt) between the rapidly growing white iron. Subsequent solidification of these small volumes of liquid could lead to flake-like graphitic forms, of the type illustrated in Plates 38, 145, 146 and 147.

158

Formation of such graphite would also be encouraged by rejection of graphite stabilising elements into the liquid from the carbidically solidifying metal, although, due to the high cooling rates and hence growth rates, there is probably insufficient time for solute rejection to proceed to its maximum extent. Any interdendritic liquid entrapped by the rapidly growing white iron structure and enriched in graphite stabilising elements would, however, tend to promote the formation of streamer graphite and, with increasing distance, 'grey' areas. It is also feasible that latent heat of solidification of the surrounding carbidically solidifying areas would locally increase the liquid temperature such that graphitic nucleation occurs, although nucleation would need to be rapid as this latent heat would be dissipated rapidly. Hillert⁽¹⁹⁾ has suggested that graphitic eutectic nucleation is much more rapid than for the carbidic eutectic, but that the growth rate of the latter is much more rapid and would, therefore, consume a large amount of the liquid, thus limiting the extent of graphitic eutectic growth in the remaining trapped liquid. Flakes which have grown from the liquid in this manner could act as nucleation sites suitable for subsequent decomposition of eutectic cementite to give streamer graphite. The graphite resulting from this decomposition is finer and more continuous than that forming directly from the melt and follows the honeycombe outline of the cementite of the original carbidic eutectic. (Plates 39, 41 and 53). (Rejection of carbon from supersaturated austenite above the eutectoid temperature, and the eutectoid transformation of austenite to ferrite and graphite, would also contribute to the thickening of the graphite.)

With increasing distance from the chill the cooling rate decreases and white iron growth is retarded hence presenting an opportunity for the more easily nucleated graphitic eutectic to grow in the residual liquid⁽¹⁹⁾. The 'grey' regions (Plates 40, 41, 71 and 137) may possibly be considered as the embryos for cell formation - there is no longer sufficient white iron forming rapidly enough to isolate small volumes of liquid and thus the graphitic eutectic nucleated from the liquid has a longer time, and a greater volume, in which to grow. Eventually these graphitic areas become encircled by the white iron. This would constitute a Hong Type II mottled structure.

5.2.5 Graphitic Cells

The graphitic eutectic was observed at the top of all castings. The degree of graphitisation varied from casting to casting, depending on the amount of carbide stabilising elements present. In a large number of castings the cells (which were clearly different from the 'grey' areas as they took a spherical form) were obvious from the mottled fracture surface (Plate 35, Fractures B3, C1, C3, E1, E2, E3, G1, G2, G3 and Plate 139, Fractures B1', C1', C3', D1', D3', F1', F2' and F3'). In these castings, the carbide stabilising elements outweighed the slower cooling rates and effectively promoted a higher degree of undercooling, which resulted in mottled structures as opposed to a continuous graphitic structure. In some cases, in the absence of a large concentration of carbide stabilising elements, the cellular nature was not as obvious due to the impingement of the growing cells which reduced the delineation of cell peripheries (Plate 35, Fractures A1, A2, A3, B1, B2, C2 and Plate 139, Fractures A1', A2', A3', B2', B3' and C2'). Some cells were large enough to be seen by the naked eye

but the finer ones were only visible at higher magnifications on polished and etched sections (Plates 119, 140, 145). There was one isolated case where, on the polished and etched section, a mottled structure was observed at the chill/metal interface. (Plate 59). This was the overgraphitised melt Alc (See Sections 4.3.3 and 5.6).

In general the first cells exhibited 'D' type (Plates 74, 82, 84, 98, 99, 100, 101, 127, 158, 169, 173, 179, 181 and 187), degenerate (Plates 108, 110, 148, 185, 188) and mesh type (Plates 108, 131 and 172) forms of graphite. In some melts, Al and Al', the first graphite form appearing was 'A' type graphite (Plates 46, 47, 48, 140 and 141). The graphite tended to coarsen with increasing distance from the chill (due to the decreased cooling rate) and, ultimately, the coarse 'A' type graphite was observed in the low sulphur and titanium melts (Plates 49, 50, 51, 54, 55, 57, 58, 70, 78, 89, 109, 115, 142, 143, 144, 145, 149, 153, 165 and 175). However, the trend with the higher sulphur and titanium melts was the retardation of the graphitic eutectic start (Tables 20, 21 and 22) and, as a result of this retardation and the presence of titanium and sulphur, the predominant forms of graphite at the sample extremes were 'D' and degenerate types (Plates 79, 85, 86, 87, 88, 103, 104, 112, 116, 124, 132, 137, 150, 151, 154, 160, 171, 174, 176, 180, 183, 186 and 189). Similar forms of graphite were observed in the high nitrogen melts. The nitrogen appears to have caused compaction of these flake forms and also to have modified the smooth outline of the graphite flakes which now exhibit irregularities (Plates 142, 143, 148, 150, 151, 153, 154, 159, 169, 170, 173, 174, 175, 180, 181, 183 and 185).

The graphitic cells have nucleated and grown by the accepted methods as described in Section 2.2.1. The 'D' type flakes are the result of a greater degree of undercooling inherent at higher cooling rates while, at the lower cooling rates, the presence of such elements as sulphur and titanium in the melt reduce the cooling rate necessary to produce the same degree of undercooling. The 'A' type graphite flakes are the result of lower growth rates associated with less undercooling and hence slower cooling rates. The irregularities at the edge of the flakes could be due to the carbon atoms plating onto preferential lattice growth planes⁽¹⁾. Due to the curvature of the original flake surfaces, suitable growth planes might not be uniformly distributed causing the carbon deposition process to occur in more localised areas leading to the serrated appearance characteristic of the high nitrogen melts .

The matrix was, in general, pearlitic. However, in some samples, significant amounts of ferrite were present. This ferrite was observed at various locations:-

1. at the cell centres - sometimes these areas were quite extensive either forming dense central regions (Plates 103, 104 and 131) or taking more dispersed forms (Plate 102).
2. associated with individual flakes (Plates 47, 48, 49, 50, 51, 52, 54, 55, 57, 58, 70, 107, 115, 140, 143, 149, 153, 165, 175 and 179).
3. at the dendrite arm extremities - here the austenite at the dendrite extremities had transformed to ferrite and graphite.

In all three cases, the ferrite has probably resulted from the direct decomposition of austenite at the eutectoid temperature, the graphite contributing to the already existing flakes in the vicinity.

In general, the amount of ferrite present at the cell centre was a maximum at, or slightly above, the cell start position and decreased with increasing distance. In most cases the matrix in the graphitic areas was entirely pearlitic at the top of the castings. One would have expected that with decreasing cooling rate the ease of austenite decomposition to ferrite and graphite would increase. This behaviour is probably the result of competition between time at temperature, and the distance over which diffusion would have to occur. With fine graphitic structures (e.g. 'D' type graphite) the amount of graphite is more widely dispersed and carbon within the austenite has a shorter distance to diffuse at the eutectoid temperature, during the austenite decomposition to ferrite and carbon. With coarse 'A' type graphite the fewer, larger flakes increase the distance over which carbon must diffuse to enable deposition on existing graphite.

It has been suggested in the previous section that streamer graphite is a manifestation of a Hong Type I mottled structure⁽²⁵⁾ (see Section 2.2.5) and that the 'grey' areas constitute a Hong Type II mottled structure. Hillert⁽¹⁹⁾ suggests that mottled structures are due to the relative kinetics of solidification of the two different eutectics. The graphitic eutectic is more readily nucleated than the carbidic eutectic but the latter grows more quickly. The graphitic eutectic nucleates and grows forming well defined cells which reject carbide stabilising elements to the intercellular liquid within which the carbidic eutectic may ultimately nucleate, and more rapidly grow to occupy the intercellular spaces. This would constitute a Hong Type III

mottled structure and accounts for the 'fan' configurations discussed earlier (Plates 92 and 111, Section 5.2.2). With very slow cooling rates, the graphitic eutectic can nucleate and grow surrounded by large amounts of liquid, permitting the spherical shape usually associated with the graphitic eutectic (Plates 102, 151). Growth would ultimately be restricted by impingement on other cells. This would occur prior to the carbidic eutectic nucleation having a chance to occur and would produce a true Grey Iron structure.

5.2.6 Inclusions

An attempt was made (Section 4.3.5) to identify the variety of inclusions microstructurally evident (Plates 43, 48, 53, 55, 56, 58, 89, 100, 104, 108, 110, 115, 116, 120-124, 126, 127, 132, 133, 137, 150-154, 159, 162-166, 169, 171-175, 177-179, 181-184, 187-189, 192) by way of microhardness tests and EDAX scans on the S.E.M. (Plates 193-204). Manganese sulphide (MnS , Plates 194, 196-202, 204), titanium sulphide (Ti_2S , Plates 193, 195, 197, 199-201), titanium manganese sulphide ($(Ti, Mn)S$, Plates 196, 197, 199, 200) and complex titanium (Plates 196-202, 204) inclusions were evident from these scans.

In the titanium containing melts examined (Plates 193-204), approximately equal numbers of simple MnS and Ti_2S inclusions were observed with very few $(Ti, Mn)S$ inclusions. The majority of the titanium inclusions were of a complex nature - typically about four times as many as compared with Ti_2S and MnS . With the EDAX equipment available it was not possible to identify the other elements in association with the titanium in these inclusions. In steels, and especially in austenitic stainless steels, titanium carbosulphide inclusions have been observed frequently associated with $Ti(CN)$ ⁽⁷⁰⁾. It is also believed that

Ti_2S is impure and is more likely to also be a carbonsulphide stabilised by iron and perhaps oxygen and nitrogen in solid solution, and would therefore have the form $(Ti,Fe)_2(S,C)$ ^(71,72). The oxygen content of cast iron is probably too low to be a contributing factor in inclusion formation but it is possible that the complex inclusions observed are the result of Ti-N-C-Fe-S interaction. The EDAX equipment was not able to identify nitrogen, carbon or oxygen and hence, this could not be positively confirmed.

General controversy exists as to the exact stoichiometry of titanium sulphide inclusions but it has been stated ⁽⁷²⁾ that sulphides with the least sulphur content are more likely to occur as inclusion phases in steels. In this work Ti_2S appeared to be the only stoichiometric form observed (Plate 193), i.e. the tau phase ^(20,71,72). In addition in steels a variety of sulphide stoichiometries have been observed:-

- | | |
|--|---|
| 1. TiS_n (where $n = 0.25-3$) | } relatively stable, melting points (2000-2100°C) |
| 2. Ti_2S_3 ⁽⁶⁹⁾ | |
| 3. TiS_2 ⁽⁶⁹⁾ - this is relatively unstable as it decomposes at 300°C. | |
| 4. Ti_6S - not usually present as an inclusion due to the difficult crystalline structure ^(71,72) . | |
| 5. TiS_{1-z} (where $0.2 < z < 0.3$) ^(71,72) . | |
| 6. $Ti_{1-x}S$ (where $x = 0-0.11$) ^(71,72) . | |

In texts, titanium sulphide is usually quoted as TiS which would incorporate 1, 5 and 6 above if $n = 1$, $x = z = 0$. As already stated here, sulphides with the least sulphur are more likely to occur as inclusions ^(71,72) which would mean Ti_2S is more likely to occur than TiS .

5.3 THE INFLUENCE OF SULPHUR AND NITROGEN ON THE STRUCTURE OF THE

'BASE MELT' CAST

The structure of the 'Base Melt' casting, and the effect of introducing more sulphur at two different levels is fully described in Section 4.3.3.(a) and Section 4.3.3.(b) respectively. All of these melts were performed at the low nitrogen level.

The general microstructural features were similar but the increasing sulphur level retarded graphitisation. The tables of the distances at which the three criteria appeared (Tables 20(a), (b) and (c)) show that the streamer, 'grey' and cell starts were at the same distance for melts A1 and A2 but for A3 these were retarded. Despite these starts being at the same distance for both A1 and A2, the growth rate for the graphitic forms in A2 was retarded as compared with those in A1 and, as a result, the 'grey' regions of comparable size appeared later in the sample. In A3, not only were the starts retarded but also the growth rates of the graphitic forms were retarded, when they occurred, leading to finer graphite forms than evidenced in A1 or A2 (see Section 4.3.3.(b)). The amount of carbidic eutectic present/ from the chill increased with increasing sulphur.

The effect of sulphur on the microstructure has been attributed in the past, to the independent effects that it has on nucleation and growth processes (see Section 2.5.3). With increasing sulphur, to 0.12 mass percent, there is a decrease in surface tension in Fe-C-Si alloys. If the interfacial energy between the graphite and liquid iron is similarly reduced by sulphur then the surface energy requirements for nuclei formation would be significantly reduced, explaining the increase in the degree of nucleation^(8 and 16). A further effect of sulphur is to restrict

the growth mechanism of the graphitic flakes. As sulphur is insoluble in austenite, it is rejected to the liquid as dendrites grow and is thought to be adsorbed on to the eutectic cell surface and there prevents the further growth as it restricts the transfer of atoms across the liquid solid interface^(35,39,46). Growth rate reduction of individual cells reduces the branching frequency of the graphite skeleton and gives rise to the coarse 'A' type flakes⁽⁵⁹⁾, also observed in low sulphur content irons⁽⁴⁶⁾. Lakeland and Hogan⁽⁷⁴⁾ have observed that absence of sulphur at the austenite dendrite allows it to act as a nucleation substrate for graphite which forms^a discontinuous boundary to the original dendrite. However, in the microstructures they presented to corroborate their theory, the austenite had obviously transformed to ferrite and graphite and the carbon, as previously discussed in this work in Section 5.2.5, had diffused towards the interdendritic graphite and outlined the dendrites. In the present work, the phenomenon of graphite nucleating at, or in close proximity to, the dendrite surface is evident not only where partial decomposition of the dendrite arm extremities has occurred (Plates 52, 53, 74, 84, 99, 100, 104, 169 and 186) but also where no decomposition has occurred (Plates 74, 76, 79, 82, 85, 87, 88, 124, 127, 128, 137, 158, 160, 176 and 187). This phenomenon is observed in high sulphur, high titanium melts (Plates 70, 124, 127, 128, 137, 169, 176, 185 and 187) as well as in non-titanium and low sulphur castings (Plates 63, 74, 76, 82, 158 and 160).

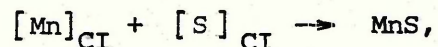
Associated with this growth restricting mechanism is the tendency of sulphur to increase undercooling and, hence, promote the formation of the carbidic eutectic. The effects of sulphur are only attributed to free sulphur in solution. The sulphur levels quoted in Table 15 (0.02-0.10 mass percent) must be assessed with reference to the manganese

present (about 0.8 mass percent) as manganese, during solidification, combines with some of the sulphur present in solution (see Section 2.5.3). The manganese in these base melts is capable of effectively controlling free sulphur in solution, thereby preventing excessive undercooling of the melt and limiting the growth restricting effect of the excess sulphur.

Reference 46 suggests an empirical relationship for the manganese content necessary for optimum 'chill reduction':-

$$\text{mass \% Mn} = 1.7 \times \text{mass \% S} + 0.25$$

For the three sulphur levels considered (optimally 0.02, 0.05 and 0.10 mass percent) the values are 0.28, 0.335 and 0.42 mass percent manganese respectively. Clearly, in this ingot mould type iron, the excess manganese will tend to encourage the sulphur in solution to be removed to a low level and the excess manganese might exert a mild carbide stabilising effect. This stabilising effect should however, be more than offset by the removal of sulphur, which should produce a graphitising effect. Since manganese does not have a relatively high affinity for sulphur, some residual sulphur will always remain in solution to ensure the formation of 'A' graphite with adequate cell nucleation rates (see Section 4.3.3(a) and (b) and Plates 54, 55). An estimate of the residual sulphur in solution for the reaction



can be obtained from thermodynamic data. Such a calculation has been performed in Appendix 2 and the sulphur concentration in equilibrium with various residual manganese concentrations in solution has been presented in Figure 66. On the basis of the calculations shown in Appendix 2, for a total manganese content of 0.8 mass percent in the melt, and for total sulphur concentrations of 0.02, 0.05 and 0.10 mass

percent, equilibrium manganese concentration^{ion} would be expected to be 0.766, 0.716 and 0.631 mass percents respectively. Purely from consideration of Figure 66, such residual manganese concentrations are potentially capable of lowering sulphur contents to extremely low levels. In reality, the actual residual sulphur concentration is unlikely to be as low as this for three reasons:-

1. the reaction may not have come to equilibrium in the time available,
2. sulphur is notoriously surface active and will tend to segregate preferentially to suitable interfaces where its partial molar free energy will be lower than in the bulk liquid where, as a consequence, the reaction with manganese will be less thermodynamically feasible, and
3. rejection of sulphur on solidification may lead to the accumulation of this element at an interface, this process being controlled by diffusion in the solid, and convective mass transfer in the liquid phase.

All of these factors will tend to contribute to there being a higher residual sulphur concentration in the liquid than would simply be expected from thermodynamic data. Certainly microstructural evidence tends to confirm this since, if such low sulphur concentrations as suggested by Figure 66 existed, one might expect that the graphite would take on a spherical form as in magnesium or cerium treated S.G. irons where the affinity of these elements for sulphur is much greater (3,4) .

It has also been shown in Appendix 2 that, for a total manganese content of 0.8 mass percent, the residual sulphur content will increase with increasing total sulphur content. It is reasonable to assume that the true residual sulphur concentration in the liquid will also tend to follow a similar trend. It is this change in residual sulphur concentration which gives rise to the observed effects on graphitic eutectic retardation, as evidenced in Table 20 for A3. Little change was observed between the A1 and A2 castings due to the smaller difference in the residual sulphur levels. There is also a smaller change in equilibrium sulphur levels for the 0.02 and 0.05 mass percent levels from 0.0000425 to 0.0000453 mass percent respectively, compared with that for the 0.05 and 0.10 mass percent levels of 0.0000453 to 0.0000512 mass percent respectively.

Boyles^(9,49) has shown that a minimum of 0.012 mass percent sulphur is required to generate 'A' type flake graphite. One would expect more realistically that residual sulphur concentrations, at least in the vicinity of the growing graphite flakes, should be near this value, if not in excess, in order to produce 'A' type flakes of the type illustrated in Plates 51 and 55.

Observed practice with malleable irons shows that sulphur retards the decomposition of iron carbide⁽⁵¹⁾. If iron carbide decomposition, near to the eutectic temperature, is indeed a contributory mechanism for streamer and 'grey' area formation, as discussed in Section 5.2.4, then this would account for the retardation of the streamer and 'grey' regions at the higher sulphur levels.

The same general trend occurred at the high nitrogen level. That is, with increasing sulphur the castings became more carbidic and all the criteria were retarded (Table 22(a), (b) and (c)). In all cases, the high nitrogen 'A' casts are more carbidic, at each sulphur level, than their low nitrogen counterparts. This must be due to the carbide stabilising effect of the nitrogen present.

The carbide stabilising effect of nitrogen has been known for a long time^(44,52) but no adequate explanation has been postulated for the mechanism involved. Increasing nitrogen content is known to decrease the graphitic eutectic temperature and the amount of recalescence during eutectic solidification, which means less undercooling is required to promote carbidic eutectic solidification⁽⁵²⁾.

Nitrogen also promotes shorter, thicker, more curved, more round edged graphite flake forms. Some of these forms with rounded edges were identified in the high nitrogen castings in this work (Plates 147, 151, 158 and 181), as were some flakes which had irregular edges (Plates 148, 150, 154, 180 and 188). Compacted graphite flakes such as these have been identified in commercially produced thick sectioned castings, which have been allowed to solidify at slow cooling rates^(44,52,62). Flakes with irregular edges could be the result of plating of carbon, from super-saturated austenite and from austenite transformation, onto preferential crystallographic planes of the graphite flakes. Morrogh⁽¹⁾ has suggested that thickening of graphite flakes in high nitrogen castings may be due to the nitrogen changing the growth direction of the graphite from the basal plane orientation to one perpendicular to the basal plane. In the present work, these compacted forms of graphite were evident in A3' but not in A1' and A2'. This suggests that nitrogen

and sulphur may have a complementary effect in producing these forms of flake graphite. It has already been stated in the literature^(1,37,46,48) that trace elements often have no effect on their own on microstructure, but do have an effect when another trace element is present. Sulphur would be present in trace amounts in the presence of excess manganese (see Appendix 2). The residual sulphur in solution increases with increasing total sulphur present and would therefore, be more likely to complement the effect of nitrogen in the A3 melt.

5.4 THE EFFECT OF TITANIUM ADDITIONS ON THE LOW NITROGEN CASTINGS

In addition to the three 'A' series melts described in sections 4.3.3.(a) and (b), a further fifteen melts were cast containing titanium additions at the B, C, E, F and G levels at each of the three sulphur levels considered (See Table 15a).

Nominal Sulphur		Titanium (mass %)				
Level	mass %	B	C	E	F	G
1	0.02	0.091	0.143	0.330	0.390	0.490
2	0.05	0.091	0.137	0.316	0.390	0.408
3	0.10	0.0915	0.137	0.316	0.377	0.435
Mean Ti Concentration		0.0912	0.140	0.321	0.386	0.444

The nitrogen concentration ranged from 0.003 to 0.0064 mass %, the highest values (0.0057-0.0064 mass %) being observed in the non-titanium containing 'A' melts and the lowest values (0.003-0.0051 mass %) in the titanium containing melts. As previously noted (Section 3.9), the latter values might not be truly representative of the inherent nitrogen

levels due to the well known relative stability and insolubility of titanium nitrides, carbonitrides and cyanonitrides^(52,59).

The intention of the series of melts was to monitor the effect of possible interaction between sulphur and titanium on the microstructures of these ingot mould type cast irons. The microstructures of the resultant castings are described in Sections 4.3.3.(c) and (d). Due to the number of, and the range of structures exhibited by, each casting in the low nitrogen programme, discussion of the effects of titanium on a cast by cast basis would prove very cumbersome. A more immediate overall impression of these effects can be gained by considering the tabulated microstructural distance criteria defined in Section 4.3.3.(d) and presented in Table 20. Furthermore, using the mean cooling rate versus distance data (Figures 61 and 62) obtained from the cooling curves (Sections 4.3.2. and 5.1.) these distances have been converted to cooling rates through the solidification range (1160-1100°C), thus giving them a wider relevance. These cooling rates, associated with the appearance of the three criteria, are summarised in Table 23, along with the graphite present at the number 8 thermocouple position, and presented graphically in Figures 63(a), 64(a) and 65(a). The inaccuracies already described regarding Figures 61 and 62 (Section 5.1) will, therefore, be incorporated in these figures.

Although slight anomalies exist, the general trend indicated in these Tables (23a, b and c) and the Figures (63a, 64a and 65a) is that, with increasing titanium concentration, a progressive decrease in the maximum allowable cooling rate necessary for the formation of streamer graphite, 'grey' areas and cellular graphitic eutectic is experienced. With increasing titanium concentration the white iron structure is more easily formed and, therefore, becomes more extensive, suggesting that

less undercooling is required to form the carbidic eutectic and, hence, titanium behaves essentially as a simple carbide stabilising element by virtue of its effect on the equilibrium carbidic eutectic temperature (See Section 2.5.5.). A similar trend is identifiable with the type of graphite present at 177.8mm in each casting. In the titanium free low sulphur melts, 'A' type flake graphite forms at the slowest cooling rates but, with increasing titanium and/or sulphur content, there is a marked tendency towards the formation of more under-cooled 'D' type graphite, with degenerate forms appearing where both titanium and sulphur are present at the highest concentrations considered in this work.

At no titanium concentration is there any marked regraphitisation of the melt to the degree observed by Kumar and Das⁽⁵⁵⁾. The only indication that slight regraphitisation might have occurred is in castings C2 and C3, both of which appear, from Table 20, to be slightly more graphitic than B2 and B3 respectively. Only the 'grey' start exhibits a similar effect in the case of B1 and C1 however. There appears therefore, to be some degree of influence of sulphur on this behaviour as depicted by Figures 63a, 64a and 65a. Considering Figure 63a, there is a continuous decrease in the cooling rate with increasing titanium concentration for the level 1 sulphur but, for levels 2 and 3, the cooling rates for the cell starts at 0.14 mass % titanium (C2 and C3) is greater than those at 0.09 mass % titanium (B2 and B3) respectively. Similar trends are evident in Figures 64a and 65a, especially for the level 3 sulphur, where there appears to be a more pronounced graphite stabilising effect over the same titanium range. Since the strength of the graphitisation response increases with increasing sulphur level, it is reasonable to assume that the graph-

itising phenomenon observed is due to the lowering of the residual sulphur concentrations, by titanium, i.e. sulphide formation. Nitrogen also exerts a carbide stabilising influence and its removal from solution as titanium nitrides, a reaction which is thermodynamically favourable (See Section 5.6), would have been expected to produce a graphitising effect at all three sulphur levels. Complex titanium inclusions have been identified in the castings on S.E.M. examination, suggesting that the titanium/nitrogen interaction does occur. The nitrogen content of these castings is, however, very low and it is possible that such low concentrations do not exert a significant effect on the microstructure. It would appear, therefore, that the titanium/sulphur interaction is the dominant factor in producing the minor graphitising phenomenon observed at the low nitrogen level.

The graphitising effect observed in these castings is a weak one, however, and some doubt must be expressed as to whether it is indeed a real phenomenon. The difficulty of identifying the first streamers, due to their often minute size, introduces a degree of inaccuracy into the use of this criteria as a precise comparative criteria. Similarly, the formation of the first 'grey' areas depends, to some extent, upon the chance impingement of dendrites, and possible entrapment of liquid during solidification. The use of the cell start cooling rate probably gives the most reliable means of quantitative comparison of castings but, this too has limitations, in that isolated eutectic cells frequently occurred slightly ahead of the bulk of the graphitic eutectic (e.g. melts B1, G1, F3, Sections 4.3.3. (c) and (d)). The fact that all three criteria do indicate a graphitising tendency over the same titanium range, and especially at the level 2 and 3 sulphur levels, suggest that it is a real phenomenon.

Compositional variation of the other elements in the melts, notably carbon, silicon and manganese, will have an effect on the microstructural distance criteria but, these are extremely difficult to quantify. A superficial examination of such compositional variations inherent in the melts would suggest that there will be no significant change to the trends indicated in Figures 63, 64 and 65.

In the light of the foregoing discussion, and on the consideration of the microstructural criteria (Tables 20, 23 and Figures 63a, 64a and 65a, and the Fractures (Plate 35)), the low nitrogen castings can be considered in terms of three groups as shown in Tables 24a, b, c and d. Each group is characterised by a different type of titanium interaction in the melt and will ultimately provide a useful means of comparison with the high nitrogen castings.

The Group I castings (the three non-titanium 'A' melts described in Sections 4.3.3.(a), (b) and 5.3) all exhibited a 'mottled' structure over much of their length (Plates 46, 52, 56, 68, 69) but became almost entirely graphitic, exhibiting 'A' type flakes towards the top of the castings (Plates 51, 55, 57, 58, 70). Increasing sulphur has tended to retard graphitisation and given rise to the presence of 'D' type flakes, in addition to 'A' type flakes, in A3 (Plates 69 and 70).

The Group II castings, comprising the 'B' and 'C' level titanium castings described in Section 4.3.(c), represent an intermediate stage between the Group I and III castings, and are similar, in terms of the microstructures, to those in Group I but are, in general, slightly more carbidic. All exhibit extensive or even totally graphitic areas

towards the top of the castings, comprising 'A' and 'D' type flakes. At a given sulphur level, the cell starts all occur at equivalent, or slower, cooling rates than the Group I castings but at significantly higher rates than those in Group III, all being at less than $12.33^{\circ}\text{C}/\text{min.}$ for the $1160-1100^{\circ}\text{C}$ range. Similar, though less distinct, trends are evident for the streamer and 'grey' starts but, at the highest sulphur level, an increase in the critical cooling rate for their formation is evident. Once cell formation commences, the nucleation rate appears to be high, producing what appears to be an entirely graphitic iron in the upper areas of the fractures (Plate 35), the cellular nature being obvious microstructurally, but not to the naked eye (Plates 73, 74, 75, 82, 83, 86, 119). The characterising feature of this Group is, as already discussed, that the titanium present over the range 0.09-0.14 mass % appears to exert a slight graphitising effect, especially at the higher sulphur levels, which can be attributed to the lowering of the residual sulphur concentration in solution as a result of titanium sulphide formation. The need for the presence of a minimum amount of titanium before titanium sulphide formation (and hence graphitisation) is probably due in part to the low residual sulphur levels created by the manganese present (See Section 5.5.) and, also, the combination of titanium with the small amount of nitrogen present.

Group III comprises the higher titanium level melts E, F and G (Section 4.3.3.(d)). In this Group the dominant microstructural feature is the extensive white iron structure, the cell starts in all cases being at cooling rates of less than $7.03^{\circ}\text{C}/\text{min.}$, and mostly of similar cooling rates of $6.28^{\circ}\text{C}/\text{min.}$ (Figures 63a and Table 23c). Even when cellular graphite growth occurs, the individual cells tend to be isolated and visible to the naked eye (Plate 35) suggesting a low

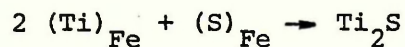
nucleation rate. The graphite type within the cells at the top of the castings tends to be of the more undercooled, 'D' type variety and, within the main Group, there appears to be a sub-group of higher titanium and sulphur melts (F2, F3, G2 and G3), where degenerate forms of graphite become particularly prominent (Plates 124, 132 and 133). There appears to be no microstructural dependence on sulphur concentration (Figures 63a, 64a and 65a) suggesting that a relatively low residual level has been achieved as a result of 'balancing' with both the manganese and titanium present. The dominating interaction is therefore, that of titanium with carbon, thereby encouraging stabilisation of the white iron structure by decreasing the undercooling necessary to form the carbidic eutectic^(3, 41, 55). The extent of the white iron structure in the Group III castings only appears to increase slowly with the increasing titanium concentration, probably reflecting the nature of the titanium concentration dependence of the carbidic eutectic temperature.

To summarise, the dominant effect of titanium additions at the low/nitrogen level is to produce a carbide stabilising effect, although, at higher sulphur levels, a minor graphitising effect is observed over the range 0.09-0.14 mass % titanium, associated with titanium sulphide formation. It should be noted that no apparent graphitisation has been seen for level 1 sulphur but this might have been observed had a lower titanium value been achieved.

Titanium as a Sulphide Former in Ingot Mould Type Irons

Evidence has been presented that, in the Group II castings, titanium may behave as a graphitising agent as a result of titanium sulphide formation. Titanium is certainly capable of forming stable compounds with sulphur and indeed the S.E.M. investigation of selected castings (Section 4.3.5.) revealed the presence of titanium sulphide

inclusions of the stoichiometry Ti_2S . Unfortunately, the combination of these two elements in the melt,



cannot be considered in isolation since this ingot mould type iron contains about 0.8 mass % manganese which, as discussed in Section 5.3., will react with sulphur to form manganese sulphide inclusions. Indeed, large numbers of MnS inclusions were identified (See Section 4.3.5 and Plates 151, 188, 192, 194, 196-203), sometimes in association with titanium sulphides (Plates 190, 192, 196, 197, 199 and 201). The amount of manganese present is potentially capable of lowering the dissolved sulphur to a low level (as described in Section 5.3 and Appendix 2) and therefore, the introduction of titanium into the melt will lead to competition between the manganese and titanium for the available sulphur present, once any requirement for titanium nitride formation has been met. The behaviour of titanium, with respect to the sulphur in the melt, will therefore, depend upon its relative affinity for sulphur, compared with that of manganese.

Opinion varies as to whether titanium can be regarded as a strong^(5,8,58) or a medium^(3,41,55) sulphide former. Unfortunately no thermodynamic data pertaining to the Ti_2S formation appears to exist. However, some inference may be drawn from the experimental observations here. It is generally believed that titanium is a moderately powerful sulphide former, comparable with manganese, and experimental evidence here would tend to substantiate this.

a

If titanium had been/much more powerful sulphide former than manganese, then one would have expected behaviour similar to that demonstrated by magnesium, calcium and cerium etc.^(4,5,8,13,37,41,45,50) The titanium would have combined with free sulphur (not balanced by manganese) and reduced the manganese sulphides already in existence,



With titanium levels less than those required to combine completely with 'all' the sulphur in the melt, manganese sulphide would have formed and the manganese content of the iron would then have ultimately determined the equilibrium sulphur remaining in solution at solidification. With optimum titanium levels, the free sulphur content of the melt would have been reduced to a very low level, producing spherodisation of the graphite, as is the case with magnesium etc. and, with an excess of titanium, carbide stabilisation would have been achieved. In all the castings, flake graphite forms were observed. Even at the highest titanium level, where pronounced carbide stabilisation was occurring, spherodisation never occurred.

If titanium were a weaker sulphide former than manganese, the sulphur concentration in the melt, established by equilibration with the manganese in the iron, would be less than that at equilibrium with titanium. Once any requirements of nitride formation had been satisfied, the titanium present would simply exert a stabilising effect on the white iron structure. Obviously this cannot be the case since titanium sulphide inclusions have been identified in the solid castings using the S.E.M. and, in addition, some degree of microstructural dependence on both titanium and sulphur has been observed in the Group II castings. This would suggest that the titanium addition has encouraged further reduction of the sulphur in solution by further precipitation of titanium sulphide, complementing the effects of manganese. Presumably, at the lower titanium level, the dissolved sulphur level is primarily being determined by the much higher concentration of manganese. This would account for the need for a minimum

titanium concentration (0.09 mass %) to be present before any graphitising effect is noted at the higher sulphur levels, although some may be consumed in TiN formation (due to its greater affinity for nitrogen). At the lowest sulphur level considered, the residual sulphur concentration in equilibrium with the manganese present, is presumably sufficiently low that it is either less than that in equilibrium with the titanium additions made or, that the extent of the titanium/sulphur interaction is so slight as to have no microstructurally observable effect. This together with the large concentration of carbon present, ensures that the titanium/carbon interaction has the dominant effect on the microstructure of the sulphur level I castings, producing a continuous increase in carbide stabilising tendency with increasing titanium addition.

These observations suggest that titanium and manganese are comparable in terms of their tendency to form sulphides. The introduction of titanium into the melt therefore, complements the effects of the manganese present and this, to some extent, accounts for the duplexed manganese/titanium sulphide inclusions identified in the S.E.M. and microstructural analyses of the castings (Plates 124, 193-203). The further removal of sulphur from solution as Ti_2S , as well as the MnS, will effectively reduce its growth restricting effect on cellular graphite formation. For streamer graphite and 'grey' area formation, carbide decomposition is also an important factor. Sulphur is known to act as a retardant for carbide decomposition in malleable irons (51) and its further removal from solution as Ti_2S would tend to encourage this form of graphitisation. Even at the highest titanium contents, however, there was only half as much present compared with manganese and, therefore, with similar affinities for sulphur, the

higher manganese level would still tend to have the dominating effect on the sulphur concentration in solution.

The introduction of small titanium additions to low nitrogen ingot mould type iron compositions is expected to have only a slight effect on the microstructure as a result of combination with sulphur. Addition of titanium in larger amounts would result in carbide stabilisation and, especially at high titanium and sulphur levels, the presence of degenerate forms of graphite. There would appear to be no economic or thermodynamic advantage for partial replacement of manganese by titanium. In addition, the margin for error is diminished in terms of its carbide stabilising tendency. Whilst an excess of manganese can be tolerated, by virtue of its mild carbide stabilising tendency, no such excess of titanium could be, since this would lead to white iron structures.

Unlike manganese sulphide,⁽³⁷⁾ there would appear to be no advantage in titanium sulphide formation as a nucleating agent. There is no evidence of increased cell nucleation rate as a result of titanium sulphide formation, or if it does occur, the effect must fade rapidly. Indeed, at higher titanium levels there appears to be a marked decrease in the cell count associated with the decreased degree of undercooling required to form the carbidic eutectic.

5.5 THE EFFECT OF TITANIUM ADDITIONS ON THE HIGH NITROGEN CASTINGS

The effect of titanium additions (at the B, C, D and F levels) to a further series of melts containing 0.02, 0.05 and 0.10 mass % sulphur, but with a total nitrogen content of approximately 0.01 mass %, was investigated (see Table 15b and Section 4.3.2.).

Nominal Sulphur		Titanium (mass %)			
Level	mass %	B	C	D	F
1	0.02	0.093	0.120	0.180	0.410
2	0.05	0.091	0.112	-	0.380
3	0.10	0.090	0.130	0.210	0.380
Mean Ti concentration		0.0913	0.121	0.195	0.390

The range of nitrogen levels (0.008 to 0.0118 mass %) alone might be expected to produce microstructural variations in the castings but it is well known that nitrogen determination in cast irons is difficult since the nitrides present, especially in white cast irons, are insoluble⁽⁵²⁾. The spectrographic samples obtained were, by necessity, all chill samples, though check analysis was performed also on iron removed from the feeder head and produced the same degree of variability in reported nitrogen content. Therefore, some doubt must exist regarding the accuracy of the nitrogen analysis results and the assumption that the nitrogen levels were the same for all melts, and about twice that of low nitrogen melt programme, must be made.

The fractures and the microstructures of the resultant castings have been described in Section 4.3.2. The microstructural distance criteria are presented in Table 22 and, with the aid of Figure 60, these have been converted to a cooling rate through the solidification range to produce Table 25. These results are also represented graphically in Figures 63b, 64b and 65b. On the basis of these results the high nitrogen castings can be conveniently considered in terms of the three groups defined in Table 26 - each group being characterised by a different type of interaction with respect to the titanium present. In general terms, these groups coincide with those defined in the previous Section (Table 24) and therefore, in addition to Figures 63, 64 and 65, provide a means of comparison between the high and low nitrogen castings.

The Group I castings again comprise the 'A' melts, to which no titanium addition was made. As discussed in Section 5.4, they exhibit a tendency towards carbidic eutectic stabilisation with increasing sulphur content and, at a particular sulphur level, they are distinctly more carbidic than their low nitrogen counterparts.

The Group II castings comprised the B, C and D titanium level melts, the only exception being B1' which will be considered later. The dominant feature of this group is that the maximum cooling rate through the solidification range at which streamer graphite, 'grey' areas and cells form are all greater than for the Group I castings at a particular sulphur level, suggesting that the titanium addition is having a graphitising effect. This behaviour is particularly well illustrated in Figures 63b, 64b and 65b which indicate that maximum graphitisation is achieved by an addition of about 0.1-0.2 mass % titanium. This behaviour is very much

more pronounced, and also occurs at all three sulphur levels, compared with the Group II low nitrogen castings, where only a slight graphitisation tendency was noted at the higher sulphur levels. The Group II castings at the high and low nitrogen levels are similar, however, in terms of the appearance of the fracture surface (Plates 35 and 139) and the graphite type at the number 8 thermocouple position i.e. 'A' and 'D' type flakes, although the flake graphite in the high nitrogen castings tended to be of a compacted form (Plates 146, 150 and 152).

The only anomaly, with respect to the observations pertaining to the Group II high nitrogen castings, is melt B1' which appears to have yielded a casting very much more carbidic than any other Group I or II casting (Tables 24 and 26). Although there are minor compositional variations from the norm, in terms of titanium and nitrogen, these are small and unlikely to account for the observed behaviour (Table 15b), and the casting does not appear to have cooled excessively quickly through the solidification range (Table 16). Because of this doubt concerning B1', it has been excluded from consideration with the other Group II castings.

The Group III castings constitute a return to carbidic eutectic stabilisation and comprise only the 'F' level titanium melts at the high nitrogen level which are very similar to the low nitrogen Group III castings. In both cases the fractures exhibit extensive areas of white iron structure with the graphitic areas being distinctly cellular in appearance (Plates 35 and 139). Microstructurally, the 'A' and 'D' type flakes present at 177.8mm, in both sets of Group II castings, have been replaced by 'D' type flakes with more degenerate forms of graphite

in Group III (Tables 24 and 26). Comparison of the cooling rate through the solidification range for all three graphitic areas, at both nitrogen levels, in Figures 63, 64 and 65 suggests that, at the higher titanium concentrations, consistent with Group III, the results are very similar and might easily be superimposed on a common graph, and that there is no dependence on the sulphur concentration in the melt.

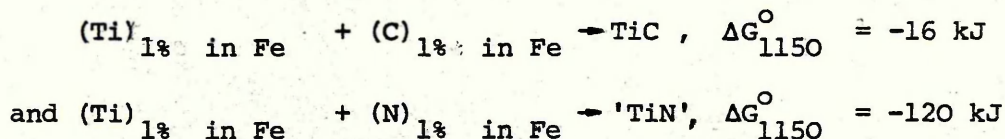
The behaviour exhibited by these Groups is attributable to the differing degree of interaction of titanium with the nitrogen, carbon and free sulphur present in the melt. The Group I castings contain no titanium and, therefore, the free sulphur remaining after manganese sulphide formation, and especially the nitrogen present, can exert their full carbide stabilising effect on the microstructure, producing castings which are more carbidic than their low nitrogen counterparts.

The removal of nitrogen and free sulphur from solution, as titanium nitrides and sulphides, thereby removing their carbide stabilising influence, has produced the pronounced graphitising effect observed in the Group II castings. The low nitrogen Group II castings exhibited only a minor graphitising effect at the higher sulphur levels and, since one would expect that the degree of titanium / sulphur interaction would be no greater in the high nitrogen castings than in the low nitrogen ones, it must be assumed that titanium nitride formation is the dominant reaction taking place in the high nitrogen Group II castings. The higher initial nitrogen content has thus resulted in a much more pronounced graphitising effect when removed from solution as titanium nitrides and has also produced a displacement in the Group II/III boundary from about 0.2 Mass % titanium, for the low nitrogen castings, to 0.3 mass %, for the high nitrogen castings, reflecting the increased titanium required to neutralise the nitrogen. Some degree of titanium / sulphur interaction

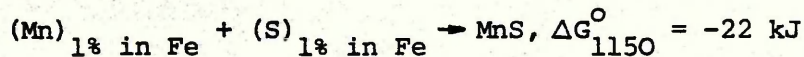
must however, still be occurring since Ti_2S inclusions have been identified under S.E.M. examination and also the higher sulphur level castings in Group II appear to be slightly more carbidic, an effect which diminishes with increasing titanium concentration.

In the Group III castings there appears to be titanium present in excess of that required for reaction with nitrogen and sulphur, producing a marked carbide stabilising effect, with respect to the Group I and II castings, by virtue of the affinity of titanium for carbon.

The above observations, made on the basis of microstructural evidence, would appear to be in agreement with thermodynamic data for the reaction of titanium with nitrogen, carbon and sulphur. For the following reactions at $1150^{\circ}C$ ⁽⁷³⁾ :-



although Jørgensen and Thorngren express doubt concerning the stoichiometry of TiN. No data exists for the free energy/formation of Ti_2S , but, as discussed in the previous Section, it is probably similar to that for the formation of manganese sulphide for which data does exist ⁽⁷³⁾ :-



The above data is based on ^aHenrian standard state of one mass % in iron and, although the reactant elements will not be in their standard state in the molten cast iron, and indeed equilibrium may not be achieved, it does provide a useful means of comparing the relative affinities of carbon, nitrogen and sulphur for titanium. Clearly from the above equations, titanium has the highest affinity for nitrogen followed by sulphur and finally carbon.

In theory, therefore, titanium would react preferentially with nitrogen, removing it from solution as stable titanium nitride, and as such, titanium additions will be a very effective means of controlling the carbide stabilising effects of nitrogen. With sufficient titanium present, combination with sulphur and carbon would also occur, in that order, as defined by the free energies of formation. The distribution of the titanium additions between nitrides, sulphides and carbides will, to some extent, depend on the concentration of reactant elements present, but the quantification of the interactions involved would be difficult, even if equilibrium were achieved.

In practice, as discussed in the previous sections, the amount of free sulphur in solution will tend to be dominated by the manganese / sulphur equilibrium. Also, while nitrogen has a high thermodynamic affinity for titanium it is only present in small concentrations, whereas carbon, with less affinity for titanium, is present in relatively high concentrations, which will tend to encourage TiC formation, even at relatively low titanium concentrations (not to mention the complex carbo- or cyanonitrides or carbosulphides). This is in agreement with S.E.M. identification of the inclusions present. Complex inclusions comprising titanium, in association with what was thought to be carbon and/or nitrogen, but which could not be identified with the EDAX equipment available, were generally much more abundant than simple titanium or manganese sulphides (See Section 5.2.6).

With such high affinity for nitrogen, one would expect the titanium additions to be capable of lowering the nitrogen content of the melt to a sufficiently low level that its effect on the microstructure would be insignificant. That this situation, and therefore, the attainment of equilibrium, is never achieved is reflected in the morphology

of the graphite. Even at the highest levels of titanium, in the high nitrogen melt programme, there is evidence of flake graphite compaction (Plates 180 to 188), suggesting the presence of a slightly higher residual nitrogen content in the melt at solidification than in the low nitrogen melts. The retention of compacted flake graphite, whilst eliminating the carbide stabilising effects of nitrogen is, however, considered to be beneficial with respect to ingot mould life⁽⁶⁸⁾.

To summarise, the effect of titanium would appear to be that it behaves as a graphitising agent in the high nitrogen castings up to about 0.2 mass %. At the low nitrogen level, titanium additions only produce a weak graphitising effect over the range of 0.09-0.14 mass % titanium at the 0.05 and 0.10 mass % sulphur levels. At titanium concentrations greater than 0.14 and 0.20 mass %, for the low and high nitrogen melts respectively, titanium promotes the formation of a white iron structure by decreasing the undercooling necessary to form carbidic eutectic.

5.6 THE EFFECT OF CARBON CONCENTRATION ON THE BASE MELT, Al

In Section 4.3.3.(a) the microstructural features of the Base Melt (Al) were reported, as were those of three additional melts (Ala, Alb and Alc) which constituted the initial attempts to produce the base melt composition, Al. These attempts failed due to problems incurred in recarburisation when melting in the 50kW electroheating unit. The carbon contents of Ala, Alb, Alc and Al were 3.42, 3.55, 4.02 and 3.90 mass % respectively (See Table 15a). One would expect the microstructures of the castings to be more graphitic with increasing carbon content, i.e. Ala, Alb, Al and Alc. Reference to Tables 20 and 21 shows that this is so for the streamer start. However, the 'grey' and cell starts occur earlier in Alb than Al which might have resulted from composition variations between the four melts. Silicon varies from 0.97 to 1.17 mass % from Al to Alb, whilst nitrogen varies from 0.0048 to 0.0064 mass % from Alb to Al respectively. Silicon is a strong graphitiser, though only one third as powerful as carbon, whilst nitrogen is a carbide stabiliser which also induces compacted graphite. Alc and Alb have approximately the same silicon contents, with the content of Al between these two and Ala. It is suggested that the silicon variation is significant in promoting more graphitisation in Alb than Al, the latter also having a higher concentration of nitrogen acting as a graphitisation retardant. There is no apparent reason, therefore, why the streamer graphite should be less retarded in Al than in Alb in the light of the composition variability.

Since the first streamers were generally minute it is feasible they started earlier in Al than was originally thought, and these earlier streamers were not identified. From previous discussion, streamer and 'grey' areas form directly from the melt and by decomposition. It is possible streamer graphite formation is more depend-

ent on the initial carbon content of the melt rather than the other compositional elements (e.g. silicon and nitrogen), thus the streamer start follows the predicted trend and varies directly with the carbon content. It is possible the 'grey' and cell starts are more dependent on the overall composition and, as the cooling rates decrease with distance from the chill, rejection of graphite stabilising elements from the melt would be favoured, and any variation in composition would become more significant. Hence, Alb would become more graphitic than Al.

With regard to graphite type at 177.8mm, melts Ala and Alb exhibited predominantly 'D' type graphite flakes with Al and Alc exhibiting 'A' type and large 'A' flakes respectively. 'D' type graphite flakes are promoted by undercooling, which in turn is promoted by carbide stabilising elements. Silicon on the other hand affects the flake population as opposed to the shape of the graphite flakes. It therefore follows that Alb would be more graphitic than Al, due to the high silicon content promoting more graphite flakes but the predominantly 'D' type flakes in Ala and Alb, have arisen due to the effective increase in undercooling due to the low carbon content. The high carbon content of Al, however, has promoted 'A' type flakes, despite the comparatively low silicon content compared with Alb, and the highest nitrogen content, which would respectively promote fewer flakes and promote compaction of the flakes. In Alc, the high carbon and silicon by far outweigh the effect of nitrogen and promote very large 'A' type flakes.

It can thus be seen that the effects of carbon cannot be assessed to the exclusion of any slight variability in other compositional elements. With respect to the present work, examination of the carbon, silicon, manganese and sulphur variations throughout

the castings suggested no significant change in the trends shown in Figures 63, 64 and 65 would occur as a result of these variations.

CHAPTER 6

CONCLUSIONS

AND

FURTHER WORK

A furnace has been developed which produces unidirectional heat flow by differential control of the heating rods in the furnace, whilst cooling the casting from the base by means of a water cooled copper chill. The unidirectional cooling has been verified by a combination of microstructural examination of white irons and thermal analysis of the metal via eight Pt./Pt.13% Rh. thermocouples introduced directly into the metal through the mould. The unidirectional cooling has produced variable cooling rates within one casting ($635-4.43^{\circ}\text{C}/\text{min.}$), the cooling rate decreasing with increasing distance from the chill. This variable cooling rate allows the structure versus cooling rate to be quantified and permits the effect to be studied on varying chemical compositions in fewer melts than required if one cast/cooling rate was needed.

The cooling rates achieved were much larger, even at the greatest quantified distance from the chill, than those found in large commercial sand castings, particularly Ingot Moulds where the solidification arrest extends over a period of ten hours. Statistical analysis of the reproducibility of an experimental run shows that the variability is not statistically significant except in the regions of the two highest quantified cooling rates, where the odd results produce significant variability.

Evidence obtained from studying the interaction between sulphur (0.02-0.10 mass %), titanium (0.09-0.49 mass %) and nitrogen (0.003-0.012% mass %) shows that the manganese content (0.8 mass %) was adequate to neutralise the effect of low and medium sulphur (0.02 and 0.05 mass % respectively) and that titanium is only comparable to manganese in its affinity for sulphur. However, the affinity of titanium for nitrogen is much greater than for sulphur and, in the high nitrogen melts, titanium displayed a graphitising effect due to the removal of nitrogen, and, hence,

the major carbide stabilising element. At the low nitrogen level (0.0055 mass %), titanium appears to act as a slight graphitiser up to 0.14 mass % at the level 3 and, possibly the level 2 sulphur, associated with the titanium sulphide formation, thereafter becoming a carbide stabiliser at all levels of sulphur.

The microstructures observed in all the castings can be characterised in terms of Hong's Type I, II and III mottled structures, designated in the present work as streamer, 'grey' and cellular structures with regard to graphite morphology. It has been suggested that the two former graphitic areas are both the result of direct formation from the melt and decomposition of preeutectoid cementite.

The technique developed during the present work has proved valid for experimental work considering the effect of compositional variation at various cooling rates.

(a) It is not believed that the technique developed during the present work could be used to produce a solidification arrest period of ten hours to study the Ingot Mould type solidification. It is suggested that the apparatus be modified by replacing the water cooled copper chill by an air cooling system and the use of this means of heat removal, coupled with zonal mould preheating furnace temperature control, be manipulated to produce lengthy arrest times. It might even be feasible to use a large sectioned sand casting.

(b) Three graphitic areas have been identified,

(i) Streamer graphite

(ii) 'Grey' areas

(iii) Cellular graphite

It has been suggested that the streamer graphite and the 'grey' areas form as a result of both direct formation from the melt and high temperature decomposition of cementite. Further work is required to determine the mechanism of formation of graphite in the two former areas, and that of the more degenerate forms of graphite observed i.e. the mesh type graphite.

(c) Evidence shows that the apparatus produces castings with statistically non-significant cooling rate variability, i.e.

$$>(|\bar{x} - 1.96\sigma|), <(|\bar{x} + 1.96\sigma|)$$

However, this variability might prove to be significant microstructurally. It is suggested therefore, that numerous identical castings should be made with statistically insignificant cooling rate variability and the castings should be examined microstructurally to ascertain whether the variation has affected the structure. Steps should also be taken to quantify the minimum variability which can be sustained prior to the microstructure being affected.

REFERENCES

2. H. Morrogh - British Foundryman, 1960, May, p.221.
3. H. Morrogh and W.J. Williams - J.I.S.I., 1947, 155, p.321.
4. J. F. Wallace - I. & S. Soc. of A.I.M.E., 1974, 32, P.202.
5. I. C. H. Hughes - The Solidification of Metals, I.S.I. Pub. 110
1968, P.184.
6. E. R. Petty - Physical Metallurgy of Engineering Materials,
Pub.: George Allen and Unwin, 1968.
7. A. Moore - B.C.I.R.A. Journal Report 1038, 1971, July, P.310.
8. W. Oldfield - B.C.I.R.A. Journal, 1960, March, 8 P.118.
9. A. Boyles - Trans. A.F.S., 1938, 46, p.297.
10. J. T. Eash and N. J. Bayonne - Trans. A.F.S., 1941, 49, p.887.
11. A. B. Everest - Modern Castings, 1962, April, p.86.
12. Metals Handbook - 7, 8th Edition, Chairman: R. F. Mehl,
Pub.: Am. Soc. of Metals.
13. K. M. Muzumdar and J. F. Wallace - A.F.S. Trans., 1973, 81, p.412.
14. M. G. Day - J. of M., 1969, April, p.31.
15. E. Campomanes and R. Goller - Modern Casting, 1976, March, p.71
16. K. Honda and T. Murakami - J.I.S.I., 1920, 102, (11), p.287.
17. A. Berman and V. Kondic - J.I.S.I., 1954, April, p.385.
18. H. Morrogh and W. J. Williams - J.I.S.I., 1954, April, p.375
19. M. Hillert and V. V. Subba Rao - The Solidification of Metals,
I.S.I. Pub. 110, p.204.
20. V. A. Gadgil and V. Kondic - British Foundryman, 1969, Oct., p.392
21. J. E. Harris and V. Kondic - Foundry Trade J., 1957, Feb., p.267.
22. H. Fredriksson and M. Hillert - British Foundryman, 1971, Feb.,
p.54.
23. W. J. Williams - J.I.S.I., 1950, April, p.407.
24. T. Ohide et al - British Foundryman, 68, (5), p.118.
25. C. P. Hong et al - J. of Crystal Growth, 1976, 34, p.61.

26. W. S. Owen - J.I.S.I., 1951, Feb., p.117.
27. M. Doi et al - Imono, 1971, 3E 43, (5), p.366.
28. K. Ogi and K. Matsuda - Imono, 1971, June, 43, (6), p.454.
29. M. Ibaraki et al - Nippon Kinzoku Gakkaishi, 1968, 32, (4), p.396.
30. T. Okamoto and H. Matsumoto - Imono, 1970, Feb., 42, (2), p.104.
31. J. C. Ruth and M. Turpin - Memoires Scientifiques Rev Metallurgy, 1969, LXVI, (9).
32. J. S. Prasad and T. Watmough - A.F.S. Cast Metals Res. J., 1967, Dec., p.173.
33. M. P. Wilkinson and A. Hellowell - B.C.I.R.A. J. Report No. 699, p.439.
34. G. A. Timmons and V. A. Crosby - Trans. A.F.S., 1941, 49, p.225.
35. A. Di Giulio and A. E. White - Trans. A.F.S., 1935, 43, p.531.
36. D. J. Swinden and C. F. Wilford - British Foundryman, 69, pt.5, May, '76.
37. R. L Naro and J. F. Wallace - A.F.S. Trans., 1970, 78, p.229.
38. A. Boyles and C. H. Lorig - Trans. A.F.S., 1941, 49, p.769.
39. H. D. Merchant et al - Trans. A.F.S., 1961, 69, p.241.
40. A. Moore - from 77th A.F.S. Congress, April 30th - May 4th, 1973, Montreal, p.219.
41. R. Ozaki et al - Imono, 1971, 43, (8), p.639.
42. T. Carlberg and H. Fredriksson - Met. Soc. Pub. 192, 1979, P.115.
43. S. Matoba and S. Banya - Bull. of the Res. Inst. of Min. Dressing & Met., Tohoku Univ., 1957, 13, p.71.
44. J. V. Dawson et al - B.C.I.R.A. J., 1953, 4, Res. Rep. No. 355, p.540.
45. H. Morrogh - J.I.S.I., 1946, 154, (2), p.399.
46. G. E. Morton - B.C.I.R.A. - J. of Res. and Dev., 1956, 6, Dec., p.436.
47. J. V. Dawson - B.C.I.R.A. J. Res. Rep. No. 423, p.180.

48. J. V. Dawson - A.F.S. Cast Metal Res. J., 1969, (3), Sept., p.138.
49. A. Boyles - Metal Technology, 1937, 4, April, Tech. Pub. 809.
50. J. V. Dawson et al - B.C.I.R.A. Journal Res. Rep. No. 428, p.249.
51. M. Pope and P. Grieveson - Metal Science, 1977, April, p.137.
52. Private communications - B.C.I.R.A.
53. A. L. Norbury and E. Morgan - J.I.S.I., 1936, (2), p.327.
54. S. Nishi et al - Imono, 1970, 42, (10), p.831.
55. R. Kumar and N. K. Das - Trans. Indian Inst. of Metals, 1968, March, p.24.
56. R. Mrdjenovich and R. J. Warrick - Modern Casting, 1975, Oct., p.37.
57. G. F. Comstock and E. R. Starkweather - Trans. A.F.S., 1938, 46, p.353.
58. K. Matsuda and Y. Matsubara - Imono, 1969, Sept., p.731.
59. BSC Special Steels Division, Private Communication.
60. Y. Kondo et al - Nagoya Univ., Govt. Indus. Res. Inst., 1973, March, 22, (3), p.92.
61. F. G. Wilson - BSC Product Res. Group, Process Section - Private Communication.
62. F. A. Mountford - British Foundryman, 1966, April, p.141.
63. M. Johansson and B. Thyberg - I.B.F. Journal, 1974, May, p.128.
64. B. Chalmers - Trans. T.M.S. - A.I.M.E., 200, 1956, p.519.
65. B. Ruddle - The Solidification of Metals, Inst. of Metals Monograph and Report Series, (7), London, 1957.
66. A. Moore - PhD Thesis, Sept. 1966. Imperial College. Heat Transfer in Metals Solidifying with Linear Heat Flow.
67. E. Spinat - PhD Thesis, 1971. London University. Heat Transfer During Controlled Solidification of Binary Alloys and Eutectics.
68. Private Communication - BSC Product Research Group, Process Section - Dr F. G. Wilson and K. Wilford.

69. K. Narita - Tetsu to Kagaku, July 1966, 32, p.1098.
70. Institution of Metallurgists, Monograph 2, Inclusions.
71. R. Keissling - Metal Society Publication in Collaboration
with Nils Lange - Non Metallic Inclusions in Steel, Part I-IV
p.137.
72. N. Jellinek - Arkive Kerni, 1963, 20, p.447
73. C. Jörgensen and I. Thorngren - Thermodynamic Tables for Process
Metallurgists. Pub. Almgrist and Wiksell, Stockholm
74. K. D. Lakeland and L. M. Hogan - I.S.I. Publication 110. Iron
and Steel Institute, p.213.

.....
APPENDIX I

THE RELATIVE HEAT CAPACITIES OF THE CASTING

AND THE CERAMIC MOULD

The temperature to which the ceramic mould is preheated prior to an experiment is always less than the temperature at which the molten metal is poured. The mould therefore, exerts a slight chilling effect on the molten metal. In Gadgil and Kondic's work⁽²⁰⁾ a 25.4mm (1in) diameter test piece was cast. Whilst a similar technique to that developed by Gadgil and Kondic has been utilised in the present work, it was thought it would be beneficial to increase the test piece diameter to 38.1mm (1.5in) and hence increase its heat capacity, in order to reduce the chilling effect of the mould.

The heat capacity of the cast iron test piece, Q_{CI} , will be proportional to its (mass x specific heat capacity), i.e.

$$Q_{CI} \propto \left[\pi \cdot \frac{d^2}{4} \cdot h \cdot \rho_{CI} \cdot C_{CI} \right]$$

where d = diameter of the test piece

h = height of the test piece

ρ_{CI} = density of the molten cast iron

C_{CI} = specific heat capacity of the molten cast iron

By increasing the test piece diameter from 25.4mm (1in) to 38.1mm (1.5ins) its heat capacity is increased in the ratio:-

$$\frac{\pi \cdot \frac{(38.1)^2}{4} \cdot h \cdot \rho_{CI} \cdot C_{CI}}{\pi \cdot \frac{(25.4)^2}{4} \cdot h \cdot \rho_{CI} \cdot C_{CI}} = \frac{2.25}{1}$$

The heat capacity of the mould, Q_M , is also proportional to its (mass x specific heat capacity).

i.e.

$$Q \propto \left[\pi \left\{ \frac{d_o^2}{4} - \frac{d_i^2}{4} \right\} \cdot h \cdot \rho_m \cdot C_m \right]$$

where d_o and d_i = external and internal mould diameter

ρ_m = density of the mould material

C_m = specific heat capacity of the mould material

and h = height of the mould

In both cases the mould wall is approximately 6mm (0.24in) and, hence, by increasing the diameter of the test piece from 25.4mm (1in) to 38.1mm (1.5ins) the mould's heat capacity is increased in the ratio:

$$\frac{\pi \left[\frac{(50.1)^2}{4} - \frac{(38.1)^2}{4} \right] \cdot h \cdot \rho_m \cdot C_m}{\pi \left[\frac{(37.4)^2}{4} - \frac{(25.4)^2}{4} \right] \cdot h \cdot \rho_m \cdot C_m} = \frac{1.41}{1}$$

Hence, by increasing the diameter of the test piece the ratio of the heat capacity in the mould to that of the molten metal test piece is reduced by a factor of:-

$$\frac{1.41}{2.25} \quad \text{or} \quad \frac{0.63}{1}$$

This can also be considered with absolute values rather than as a simple ratio.

$$\begin{aligned} \rho_{CI} &= 7 \times 10^3 \text{ kg/m}^3 & C_{CI} &= 0.471 \text{ kJ/kg } ^\circ\text{C} \\ \rho_m &= 1.950 \times 10^3 \text{ kg/m}^3 & C_m &= 1.17 \text{ kJ/kg } ^\circ\text{C} \end{aligned}$$

For a 25.4mm (1in) diameter test piece the heat capacity of the metal is:

$$\begin{aligned} Q_{CI} &= \pi \left[\frac{(25.4)^2}{4} \times 10^{-6} \right] (7 \times 10^3) \times (0.471) \text{ kJ/}^\circ\text{C} \\ \underline{Q_{CI}} &= \underline{1.671 \text{ kJ/}^\circ\text{C}} \end{aligned}$$

and for the mould is:

$$Q_m = \pi \left\{ \left[\frac{(37.4)^2}{4} - \frac{(25.4)^2}{4} \right] 10^{-6} \right\} (1.950 \times 10^3) \times (1.17) \text{ kJ/}^\circ\text{C}$$
$$\underline{Q_m = 1.35 \text{ kJ/}^\circ\text{C}}$$

The ratio of heat capacity of the metal to the heat capacity of the mould is:

$$\underline{Q_{CI} : Q_m = 1.24 : 1}$$

For a 38.1mm (1.5in) diameter test piece the heat capacity for the metal is:

$$Q_{CI} = \pi \left[\frac{(38.1)^2}{4} \times 10^{-6} \right] (7 \times 10^3) \cdot (0.471) \text{ kJ/}^\circ\text{C}$$
$$\underline{Q_{CI} = 3.76 \text{ kJ/}^\circ\text{C}}$$

and for the mould is

$$Q_m = \pi \left\{ \left[\frac{(50.1)^2}{4} - \frac{(38.1)^2}{4} \right] \cdot 10^{-6} \right\} (1.95 \times 10^3) \cdot (1.17) \text{ kJ/}^\circ\text{C}$$
$$\underline{Q_m = 1.897 \text{ kJ/}^\circ\text{C}}$$

The ratio of the heat capacities for the metal and the mould is therefore:

$$\underline{Q_{CI} : Q_m = 1.98:1}$$

Thus it can be seen that increasing the test piece from 25.4mm (1in) to 38.1mm (1.5in) has effectively halved the chilling effect of the mould.

APPENDIX 2

CALCULATION OF THE EQUILIBRIUM
RELATIONSHIP BETWEEN MANGANESE
AND SULPHUR

For the reaction:-



where

$$K = \frac{a_{\text{MnS}}}{a_{[\text{Mn}]} \cdot a_{[\text{S}]}} = \frac{a_{\text{MnS}}}{Y_{[\text{Mn}]} \cdot m\% [\text{Mn}] \cdot Y_{[\text{S}]} \cdot m\% [\text{S}]} \frac{100 M_{\text{Mn}} 100 M_{\text{S}}}{M_{\text{Fe}}^2 \gamma_{\text{Mn}}^\circ \gamma_{\text{S}}^\circ}$$

i.e. Converting Raoultian to Henrian mass % activities

a_{MnS} : Raoultian activity of manganese sulphide.
Assuming MnS is pure then $a_{\text{MnS}} = 1$

$Y_{[\text{Mn}]}$: Henrian activity coefficient of manganese in the melt

$$\log_{10} Y_{[\text{Mn}]} = e_{\text{Mn}}^{\text{Mn}} \cdot [m\% \text{Mn}] + e_{\text{Mn}}^{\text{C}} \cdot [m\% \text{C}] + e_{\text{Mn}}^{\text{P}} \cdot [m\% \text{P}] + e_{\text{Mn}}^{\text{Si}} [m\% \text{Si}] + e_{\text{Mn}}^{\text{S}} [m\% \text{S}]$$

Taking base melt composition, i.e. Al:-

3.9%C, 0.02%P, 1.01%Si, 0.80%Mn

From Bodsworth:-

$$e_{\text{Mn}}^{\text{Mn}} = 0, \quad e_{\text{Mn}}^{\text{P}} = -0.02, \quad e_{\text{Mn}}^{\text{Si}} = 0, \quad e_{\text{Mn}}^{\text{C}} = -0.01, \quad e_{\text{Mn}}^{\text{S}} = -0.044$$

$$\begin{aligned} \log_{10} Y_{[\text{Mn}]} &= 0 - 0.01 \cdot 3.9 - 0.02 \cdot 0.02 + 0 - 0.044 [m\% \text{S}] \\ &= -0.039 - 0.0004, -0.044 [m\% \text{S}] \\ &= \underline{-0.039 - 0.044 [m\% \text{S}]} \end{aligned}$$

$Y_{[\text{S}]}$: Henrian activity coefficient of sulphur in the melt.

$$\begin{aligned} \log_{10} Y_{[\text{S}]} &= e_{\text{S}}^{\text{S}} \cdot [m\% \text{S}] + e_{\text{S}}^{\text{Mn}} \cdot [m\% \text{Mn}] + e_{\text{S}}^{\text{C}} \cdot [m\% \text{C}] + e_{\text{S}}^{\text{P}} \cdot [m\% \text{P}] \\ &\quad + e_{\text{S}}^{\text{Si}} \cdot [m\% \text{Si}] \end{aligned}$$

$$e_{\text{S}}^{\text{S}} = -0.028, \quad e_{\text{S}}^{\text{Mn}} = -0.025, \quad e_{\text{S}}^{\text{C}} = +0.25, \quad e_{\text{S}}^{\text{P}} = +0.042, \quad e_{\text{S}}^{\text{Si}} = +0.065$$

$$e_S^P = 0.042, \quad e_S^{Si} = +0.065$$

$$\begin{aligned} \log_{10} Y_{[S]} &= -0.028[m \% S] - 0.025 \cdot 0.8 + 0.25 \cdot 3.9 \\ &\quad + 0.042 \cdot 0.02 + 0.065 \cdot 1.01 \\ &= -0.028[m \% S] - 0.02 + 0.975 + 0.008 - 0.066 \\ &= -0.028[m \% S] + 1.022 \end{aligned}$$

The standard free energy change for the reaction is defined by Kubaschewski and Evans by the relationship:-

$$\Delta G^\circ = -265\,500 + 64.40T \text{ J/mol based on Raoultian standard state.}$$

$$T = 1423\text{K i.e. taking eutectic temperature of } 1150^\circ\text{C}$$

$$\begin{aligned} \Delta G^\circ &= -262\,500 + 64.40 \cdot 1423 \\ &= -170.9 \text{ kJ} \end{aligned}$$

$$\Delta G^\circ = -RT \ln K = -2.303 RT \log_{10} K$$

$$\begin{aligned} \therefore \log_{10} K &= \frac{170.9 \times 10^3}{8.314 \cdot 1423 \cdot 2.303} \\ &= 6.271 \end{aligned}$$

$$\text{Now, } K = \frac{a_{\text{MnS}}}{Y_{[\text{Mn}]} [m \% \text{Mn}] Y_{[\text{S}]} [m \% \text{S}]} \cdot \frac{100 M_{\text{Mn}}}{M_{\text{Fe}}^2 \gamma_{\text{Mn}}^\circ} \cdot \frac{100 M_{\text{S}}}{\gamma_{\text{S}}^\circ}$$

Atomic masses :-

$$M_{\text{Mn}} = 55.0, \quad M_{\text{S}} = 32.1, \quad M_{\text{Fe}} = 55.9 \quad (\text{g/mol})$$

Roultian activity coefficients at infinite dilution :-

$$\text{Fe-S : } \gamma_{\text{S}}^\circ = 7.0$$

$$\text{Fe-Mn : } \gamma_{\text{Mn}}^\circ = 1.38$$

$$\begin{aligned} \log K &= \log a_{\text{MnS}} + 4 + \log M_{\text{Mn}} + \log M_{\text{S}} - \log Y_{[\text{Mn}]} \\ &\quad - \log [m \% \text{Mn}] - \log Y_{[\text{S}]} - \log [m \% \text{S}] - 2 \log M_{\text{Fe}} \\ &\quad - \log \gamma_{\text{Mn}}^{\circ} - \log \gamma_{\text{S}}^{\circ} \end{aligned}$$

$$\begin{aligned} 6.271 &= 0 + 4 + \log 55.0 + \log 32.1 + 0.039 + 0.044 [m \% \text{S}] \\ &\quad - \log 0.8 + 0.028 [m \% \text{S}] - 1.022 - \log [m \% \text{S}] \\ &\quad - 2 \log 55.9 - \log 1.38 - \log 7.0 \end{aligned}$$

$$\begin{aligned} 6.271 &= 4 + 1.740 + 1.507 + 0.039 + 0.044 [m \% \text{S}] \\ &\quad + 0.097 + 0.028 [m \% \text{S}] - 1.022 - \log [m \% \text{S}] \\ &\quad - 3.495 - 0.140 - 0.845 \\ &= 1.881 + 0.072 [m \% \text{S}] - \log [m \% \text{S}] \end{aligned}$$

$$\therefore \log [m \% \text{S}] - 0.072 [m \% \text{S}] = -4.390$$

Assuming that $[m \% \text{S}]$ is sufficiently small that $0.072 [m \% \text{S}]$ is negligible :-

$$\log [m \% \text{S}] = -4.390 \cong \bar{5}.610$$

$$\therefore [m \% \text{S}] = 0.0000407 \text{ mass \%}$$

and hence the above assumption that $[m \% \text{S}]$ is very small was reasonable.

But total Mn present = 0.8m %

and for total S present = 0.02m %, assuming that residual sulphur

≈ 0.00 mass % :-

$0.02 \text{ m \% S} \cong \frac{0.02}{32.1} \times 55.0 \text{ m \% Mn} = 0.034 \text{ m \% Mn}$, consumed in forming MnS.

Hence Mn in solution = $0.8 - 0.034 = \underline{0.766 \text{ mass \% Mn}}$

Iterating the calculation with $[\text{mass \% Mn}] = 0.766$ to improve the accuracy of the result yields:-

$$\underline{[\text{mass \% S}] = 0.0000425}$$

A second iteration yields no further improvement in the accuracy of the result.

The calculation has been repeated for various total sulphur concentrations and hence various residual manganese concentrations in the melt, and also various temperatures, to produce the data presented in the accompanying table. This data has also been presented graphically in Figure 66.

In calculating the activity coefficients for manganese and sulphur in the melt, interaction parameters taken from Bodsworth have been used. These are only strictly applicable to dilute solutions and some slight inaccuracy may have been incurred in their application to such concentrated solutions as molten cast irons. In the absence of more relevant data this is considered to be the most accurate estimate of equilibrium manganese and sulphur levels possible at the present time. The Raoultian activity of manganese sulphide has been assumed to be unity. Complexing of the MnS with other elements would have the effect of reducing the Raoultian activity of MnS which would further reduce the equilibrium concentration of sulphur in the solution.

References:

C. Bodsworth - Physical Chemistry of Iron and Steel Manufacture,
Longmans, 1963.

I. Kubaschewski and E. Evans - Metallurgical Thermochemistry, Pergamon, 1958.

Equilibrium [S] concentrations for various residual [Mn] levels after MnS formation

<u>Total [m & S]</u>	<u>Egm. [% Mn]</u>	<u>Equilibrium [mass % S]</u>		
		1150°C ("eutectic temp.")	1300°C (Teeming temp.)	1400°C (Mn addn. temp.)
0.02	0.766	0.0000425	0.000352	0.001170
0.05	0.716	0.0000453	0.000376	0.001247
0.10	0.631	0.0000512	0.000425	0.001409
0.20	0.463	0.0000692	0.000574	0.001905
0.30	0.294	0.0001076	0.000893	0.002965
0.40	0.125	0.0002506	0.002080	0.006902
0.50	Manganese deficient i.e. insufficient Mn to balance S			

The following case study was formulated by the collaborating industrial establishment, British Steel Corporation, for assessment as part of the MSc in Industrial Process Metallurgy Module 4.

PH.D CASE STUDY

Foundry 'F' manufactures ingot moulds from 5-40 tonnes, together with some bottom plates. Its main customer is a large integrated Steelworks situated nearby.

The foundry melts in two hot blast cupolas (20-25 tonnes per hour) alternatively over campaigns of 2-3 weeks. The burden has been changed several times over the past five years for commercial and technical reasons but has mainly been based on a Workington pig iron with varying amounts of steel scrap and broken moulds. Ferrotitanium (FeTi) has been added to the burden in varying amounts or not at all.

Attached are details of ferrotitanium additions made and costs incurred in so doing, along with economic data for mould production and costs per cast. Utilising the data given assess:-

- (i) How changes in the burden and FeTi additions have affected performance and mode of failure.
- (ii) What implications, if any, the mode of failure has on Steelworks operation.
- (iii) How the mode of failure is related to mould metallurgy and
- (iv) Whether a FeTi addition should be made under the present operating conditions.

1. INTRODUCTION*

During ingot mould production there are many variables which can affect the subsequent mould performance:-

- (i) Cupola charge.
- (ii) Sand Technology.
- (iii) Stripping practice and, possibly,
- (iv) Titanium additions.

(i) Cupola Charge

The cupola charge at this particular iron foundry usually consists of pig iron (Workington), steel scrap and foundry returns. The variation of this has been shown to affect the mould performance considerably. If high steel scrap is utilised it has been shown that the resultant nitrogen content in the mould iron, produced by hot cupola production, can be as high as 0.019 mass % despite the nitrogen content in steel scrap being only 0.006 mass%. This is due to the increased solubility of nitrogen in the low carbon iron which is initially produced on melting the scrap. Regression analysis figures have shown nitrogen to be proportional to the carbon content by the equation:-

$$N \text{ total (p.p.m.)} = 160 - 26.8 \text{ mass\% C} + 22$$

It is thought that high nitrogen contents reduce the resistance of the moulds to cracking due to nitrogen promoting 'compacted' graphite structures resulting in premature failure. Nitrogen dissolves in ferrite producing solid solution strengthening. It has been shown to increase the 0.2% proof stress and fracture stress in low carbon ferritic iron according to the formulae $(3800 + 760 \times \% N_2)$ N/mm² & $(7000 + 2200 \times \% N_2)$ N/mm² respectively. If nitrogen is decreased by 0.006 mass % by increasing residual titanium, from 0.016 to 0.038 mass %, the 0.2% proof stress decreases by $22.8 + 4.5$ N/mm² and the fracture stress decreases by $42 + 14$ N/mm² theoretically. From stoichiometry 0.025 mass % titanium is required to neutralise 0.006 to 0.007 mass % nitrogen, though it is usual to add an excess of titanium to compensate for any "float-out" that may occur. Titanium recovery is proportional to the carbon content or carbon equivalent value if the silicon content varies. At carbon contents in excess of 4.2 mass % there is 80% recovery but below this it drops rapidly and at 3.5 mass % carbon the recovery is only 48%. Titanium's power of fixing nitrogen has been found to follow a logarithmic curve. 0.02% titanium has proved inactive in nitrogen removal and it has been assumed that the titanium is tied up with oxygen and carbon.

* Information made available by the Co-operating Industrial Organisation.

Hot blast cupola practice has been found to lead to decreased mould life if the carbon equivalent value is less than 4.3, due to vertical splitting caused by stubby compacted graphite associated sometimes with free cementite. 'Normal' lives are attained if the carbon equivalent value is equal to or greater than 4.3. However, if no pig iron is used to produce these carbon equivalent values, lives are decreased for medium and large moulds (10 to 12 tonnes). The extent of the decrease in life has been found to be proportional to melting shop practice. The B.O.S. practice is more arduous than the O.H. practice. It has been found that life expectancy utilising a charge with no pig iron can be expressed, for the two steelworks practices, as follows:-

- (a) B.O.S. - (life) no pig iron = 51% (life) with pig iron, and
- (b) O.H. - (life) no pig iron = 80% (life) with pig iron.

These also reflect the difference in severity of the two steel practices. The effect of pig iron has been attributed to the inherent 'high' titanium content (0.12 - 0.2 mass %) which fixes the excessive nitrogen.

(ii) Sand Technology⁽⁴⁾

During sand moulding the sand must be sufficiently uniform in rigidity and strength to ensure that the mould is free from defects and of the required dimensional accuracy.

The source and the constitution of the sand has been found to be of little consequence provided that the final properties are of the required standard. There are two methods of compaction utilised by the co-operating establishment:-

- (a) Jolting:- This is performed whilst the sand is still moist and permits a high uniform hardness at the base of the mould which begins to decrease at half the height up the mould and decreases to a minimum at the top of the mould.
- (b) Slinging:- When using this method substantial porosity often results subsequent to poor ramming and an uneven hardness distribution. This form of hardness variation assumes a wave form and is detectable on the sand core face as rippling.

(iii) Stripping Practice

Stripping practice should be taken into account when considering ingot mould performance. Controlled stripping should be utilised all the time but this is often not the case. When stripping is controlled the casting is allowed to slow cool to subtransformation temperature, i.e. below 700°C, prior to stripping the cast from the sand mould. Structures resulting from this are coarse graphite in a coarse pearlitic matrix. This produces a weak iron which ultimately fails from torn seats or stickers.

If uncontrolled stripping is used the cooling rate is more rapid through the transformation temperatures, thermal cycling is therefore increased and transformations occur in the ingot mould which leads to the formation of irresolvable pearlite and poor resistance to cracking hence, premature failure. The effect of stripping can be seen in Table 1.

(iv) Titanium and its effect

Titanium is a powerful graphitiser (0.1-0.15 mass % titanium being equivalent to 0.7 mass % silicon) despite its stable carbide form. Comstock (5) has said this is due to titanium's deoxidising power though no mechanism was postulated. Titanium is also capable of refining the graphite flakes which is thought to be due to its affinity for sulphur (which coarsens graphite) thus removing the coarsening effect.

Titanium increases the tensile strength in iron with more than 3.7 mass % carbon due to its refining power and decreases the strength of lower carbon iron due to its graphitising power. Minimum strength in the mould is achieved at 0.04 mass % titanium. In excess of this the strength increases. The initial decrease in strength is due to nitrogen removal by titanium (nitrogen is known to increase strength) as previously explained. When all the nitrogen is combined, the 'free' titanium then begins to increase the strength by:-

- (a) Solid solution strengthening the ferrite, and
- (b) Promoting areas of fine graphite.

The tensile strength increases to 230 N/mm^2 for a 1 mass % titanium addition. This increase has a linear relationship thus, for an increase of 0.038 mass % to 0.197 mass % a theoretical increase of 37 N/mm^2 should be experienced (in practice it is only 33 N/mm^2).

If a 100% steel scrap charge is used the nitrogen content of the iron is increased, sometimes to the maximum of 0.019 mass %. This increase in nitrogen content reduces the iron's resistance to cracking. An addition of up to 0.1 mass % titanium neutralises this effect. The resultant iron, if cooled slowly, induces a coarsening of the graphite and a ferritic matrix. Experience shows that the iron is weak and is prone to failure by torn seats.

Titanium is an expensive additive, especially if no benefit is to be derived with regard to increase in mould life. It has been found to decrease slab mould life but increases the lives of 7 tonne moulds. 'Normal' ingot moulds are predominantly pearlitic and titanium weakens them by:-

- (a) Coarsening the graphite flake, and
- (b) Increasing the ferrite content.

- (i) How have changes in burden affected (a) performance and (b) mode of failure?

(a) Burden versus performance

Initially the burden figures were listed in order of increasing number of moulds in the burden group (Tables 2 and 3). For each group the lives of moulds, steelworks practice the moulds were subjected to, whether deliberate titanium additions had been made to the mould iron or not, the mode of failure of the moulds and the residual titanium levels were noted. The average life for each burden group was then calculated.

The burdens were then listed in order of decreasing performance (Table 4a). As this showed no apparent trend, the groups were broken down into those moulds to which deliberate titanium additions had not (Table 4b) and had been made (Table 4c).

From the list of burdens having no ferrotitanium additions it can be seen that high steel scrap and returns burdens show, as would be expected, the lowest average life, whilst the 50/50 pig iron/steel scrap exhibits the largest average performance which was not expected. From previous findings (Table 1) a 60/20/20 burden is the better composition, the high pig iron burden origin mould subjected to uncontrolled stripping conditions is the next best and the lowest average life is exhibited by a high pig iron mould with no ferrotitanium additions and subjected to controlled stripping. It is surprising to find the lower life average occurring under controlled stripping conditions as this should ensure longer life than uncontrolled where thermal cycling would be expected to decrease lives.

As the data analysis for the present exercise appears to contradict previous knowledge regarding the burdens which should lead to longevity, there must be other significant factors affecting life which have not been presented with the figures. The main factor would be stripping practice; the detrimental effect of uncontrolled stripping can be offset by the presence of titanium in the mould.

From the burden groups with the ferrotitanium addition moulds, experience shows (1-5) that the order of decreasing life is derived from moulds of the following burden origin:-

- (i) 70/80% pig, 20% max. steel scrap, returns the rest.
- (ii) high steel scrap, uncontrolled stripping.
- (iii) high pig iron, controlled stripping.

Ferrotitanium additions increase the mould life when steel scrap is a large proportion of the burden as the titanium nullifies the detrimental high nitrogen associated with the high steel scrap burden.

It can be seen from the data analysis in the present work that the first three burden groups concur with experience. The next burden groups would have been expected to be those with the high steel scrap but this was not so. Again it would appear that other significant factors affecting mould life have not been supplied to allow full determination of trends.

(b) Mode of failure versus burden

The figures were broken down cross referencing burden grouping with method of failure, designating the number of moulds in each group, their lives and the steelworks practice they were subjected to (Table 2). The bracketted figures represent those moulds used for ingot production by the Basic Oxygen Steelmaking practice, those without were used in the Open-Hearth steelmaking plant.

The largest failure group is that of vertical cracking. The percentage with respect to the total number of moulds in each burden group was calculated and the total overall percentage failure in each failure mode group was found (Table 3). The burdens were then listed in decreasing percentage failure by the vertical cracking mode (Table 5).

Vertical cracking accounted for 55.04% of failures, crazing 15.50%, torn seat due to teeming effect 9.11%, horizontal cracking 6.98%, broken lugs caused by mechanical damage 4.26%, cold shuts 3.88%, mechanical damage 2.13%, torn seats caused by foundry defects 2.91% and further teeming defects accounted for 0.19%, (The total failure from torn seats disregarding the cause is 12.02%).

Cracking occurs in irons where resistance to thermal shock is low. From experience (1-7) this occurs in irons having an irresolvable pearlitic matrix with either fine or coarse graphite. It is usually associated with uncontrolled stripping and occurs in moulds produced from both high steel and high pig iron charges with or without ferrotitanium additions.

Of the burden groups considered 75% contained 50% or more failures by vertical cracking. Only 10% consisted of 50% or more crazing failures. Of the remaining 15%, 10% failed with a slight majority of vertical cracking followed by crazing and torn seat failures. The other 5% was biased towards crazing then cracking and torn seats. It can only be assumed that those moulds which have failed predominantly by vertical cracking have been subjected to uncontrolled stripping as this, in previous observations, seems to be the determining factor.

Those moulds which have been subjected to controlled stripping have failed by crazing which would account for 85% of the burden groups considered. But, as no details regarding stripping practice have been supplied this is purely supposition.

2. (ii) How have changes in ferrotitanium additions affected

- (a) performance and
 (b) mode of failure?

(a) Ferrotitanium versus performance

Data was collated for varying percentages in titanium, signifying the difference between residual titanium content and that arising from deliberate additions by bracketting performance figures for titanium addition moulds, and lives.

Titanium additions were the exception rather than the rule with the moulds that are considered here up to 0.04% titanium. In these moulds the titanium content was derived solely from the charge, especially the pig iron and foundry returns. Additions of ferrotitanium became more prominent in moulds containing more than 0.049% titanium (Table 6).

Histograms showing the frequency of occurrence of moulds in specific life groups, were plotted for each titanium grouping. Variation in steelworks practice and additions, or not, of ferrotitanium to moulds, and mode of failure were also distinguished (Figures 1 to 10). Below is a summary of the predominant life groups for each titanium group.

% Titanium Grouping	Predominant life Group(s)	% of moulds with FeTi Additions	Life Range	Average Life
0.01-0.019	40-50, 60-70		9-100	51.45
0.02-0.029	40-50		15-90	52.07
0.03-0.039	70-80		13-101	60.81
0.04-0.049	60-70		1-104	62.47
0.05-0.059	50-60, 60-70, 90-100	50	2-106	59.04
0.06-0.069	80-90	87	11-118	72.38
0.07-0.079	70-80	100	10-100	64.90
0.08-0.089	70-80	97.62	5-96	60.24
0.09-0.099	50-70, 90-100	100	25-92	60.22
0.10-0.109	80-90	100	43-96	80.80
0.11-0.159	40-50	100	43-100	68.00

The average life for titanium groups taking into account whether deliberate ferrotitanium additions were made, or not, and both steelworks operations were calculated (Table 6). These results were then plotted for average mould life versus titanium content for the BOS moulds (Figure 11), OH moulds (Figure 12) and total average for each titanium group (Figure 13).

It can be seen that where the steelworks operation is basic oxygen (Figure 11), titanium additions produce an increase in performance below 0.06% titanium and in general decrease the performance if added to produce titanium contents in excess of 0.06%. The increase in life experienced below 0.06% titanium is the greatest at 0.03-0.039% where the life is increased by 25. The smallest increase is experienced in the 0.02-0.029 % group where the increase is only 6.5 lives. The decrease in life above 0.06% titanium is 18.5 lives (other figures are not definite enough to allow further specification in decreased lives).

Therefore it would appear for BOS practice moulds below 0.06% titanium additions of ferrotitanium are beneficial producing the largest lives at 0.03-0.039% titanium of 83 lives. Above 0.06% titanium no deliberate additions of titanium appear to be required, the highest performance being recorded at 0.13/0.139% titanium of 100 lives average.

For moulds used with the open hearth steelmaking practice Figure 12 shows the situation is reversed when considering titanium additions. Below 0.058% titanium, deliberate FeTi additions to the ingot mould iron appears to decrease the performance. At 0.02-0.029% titanium the decrease is marginal at 0.21 lives, at 0.03-0.039% it is 33.9 lives, at 0.04-0.049% it is 24.62 lives and at 0.05-0.059% 15.82 lives decrease. Between 0.058 and 0.08% titanium additions appear to improve performance, this being the greatest at 0.06-0.069% titanium level where the lives are increased by 7.5. There is insufficient data in excess of 0.08% titanium to ascertain what effect titanium additions have though one would expect the performance to be better with no additions of FeTi.

Total mould average life for titanium additions, as opposed to each titanium group, were plotted (Figure 13) which showed that for each group, bar that of 0.02-0.029% titanium, the average performance regardless of steelworks operation was better when the titanium content was one of a residual nature and not a deliberate addition.

(b) Ferrotitanium Additions versus the Mode of Failure

In order to assess the changes in ferrotitanium and the effect on the mode of failure, the number of moulds falling into specific failure groups were calculated and split into those which were subjected to deliberate FeTi additions and those whose titanium content was derived solely from the charges (Table 6).

These figures were totalled for each failure group and the percentage in each titanium group found (Table 7).

$$\text{i.e. } \frac{\text{No. of Ti group/failure mode}}{\text{Total no. of moulds in the Ti group}} \times 100\% = \left\{ \begin{array}{l} \% \text{ in Ti} \\ \text{group/} \\ \text{failure} \\ \text{group} \end{array} \right.$$

The discrepancy in the addition, non addition moulds was maintained initially and then disregarded as seen by the < > figures in Table 7. The percentage of figures in particular titanium groups where the total number of moulds with:-

- (1) no addition (designated N in Table 7), and
- (2) Additions of FeTi (designated (N) in Table 7)

were found, then percentages calculated for each failure mode.

$$\text{i.e. } \left[\frac{\text{No. of moulds/failure group/titanium group} - \text{no addition}}{\text{Total no. of moulds in titanium group} - \text{no addition}} \times 100 \right]$$

and

$$\left[\frac{\text{No. of moulds/failure group/titanium group} - \text{titanium additions}}{\text{Total no. of moulds in the titanium group} - \text{titanium additions}} \times 100 \right]$$

Graphs were plotted from the figures. Figure 14 shows the total number of moulds in a particular failure group (expressed as a percentage) versus the titanium group. Attempts were then made to graphically represent the percentage in a failure group versus titanium grouping (Figure 15), distinguishing between those resulting from FeTi additions and those which did not. The percentage in a failure group versus the titanium content, with and without additions, was plotted in Figure 16.

Below is a synopsis of the results ignoring whether titanium additions were made or not.

Crazing:- No crazing occurs in the 0.01-0.019% titanium moulds but it does occur in all other titanium groups, increasing in occurrence to 0.07-0.079% Ti, where-after it decreases. The maximum failure by crazing is 36% and the minimum is 3.45% at 0.02-0.029% Ti.

Vertical Cracking:- has been seen previously to be the largest failure group. Failure by this mode occurs throughout all the titanium groups increasing in the 0.01-0.029% titanium range and thereafter the percentage occurrence decreases to a minimum of 30% at 0.07-0.079% titanium and then increases again.

Horizontal Cracking:- this mode of failure occurs over the 0.02-0.079% titanium groupings. The maximum failure by this mode is 13.34% in the 0.06-0.069% titanium and 13% in the 0.04-0.049% titanium groups, though the increasing and decreasing failure by this mode is erratic.

Torn Seat:-
(due to teeming practice in the Steelworks) occurs in moulds throughout the 0.02-0.159% titanium groups and the percentages in the failure group increase throughout from (1.72-22.23% max.).

Broken lug:- occurs for the 0.01-0.019%, 0.03-0.039% and 0.05-0.159% titanium groups. The minimum percentage for this failure group is 0.9% for 0.03-0.039% titanium and the maximum failure is 17.39% though there is no discernable pattern,

Broken Mould:-
(Mechanical damage) a minority group with the failures by this mode accounting for 1.8-4.35% of failures. The percentage failure increases with increasing titanium content for 0.03-0.039%, 0.05-0.059% and 0.07-0.079% titanium .

Broken Balling:-
(Mechanical damage) occurring in the 0.02-0.059% titanium groups, and the failure mode percentage increases with the increasing titanium content from 1.72-4.35%.

Cold Shut:- occurring in 0.01-0.069% titanium groups but the pattern is erratic. The maximum occurs in the 0.01-0.019% titanium group where the percentage in this failure group is 25%. The minimum occurs in the 0.03-0.039% titanium group of 0.9%.

Torn Seat:-
(due to Foundry Malpractice) this mode of failure occurred at 0.04-0.059% and 0.07-0.079% titanium with the maximum for this failure group occurring at 0.05-0.059% titanium of 6.52%, the minimum, 1%, occurring at 0.07-0.079% titanium group.

The torn seat failures (due to teeming practice), broken mould and broken balling failure groups exhibit increases in percentage failure for increasing titanium contents.

Crazing and torn seats (due to foundry malpractice) show initial increases then decreases in percentage failure with increasing titanium contents, the maximums occurring in 0.07-0.079 and 0.05-0.059% titanium respectively.

Vertical cracking increases in incidence to 0.07-0.079% titanium and then decreases whereas horizontal cracking is very erratic, initially decreasing then increasing, decreasing etc., as are the broken lug and cold shut failure modes.

2. (iii) What implications, if any, does mode of failure have on Steelworks operation?

A chart was drawn up of failure mode versus Steelworks (Table 6). The steelworks operations, BOS and OH, were subdivided into the number of moulds in each failure group and then translated into percentages of the total number of moulds in both steelworks. The calculated percentages for the total number of moulds concerned in each group were then plotted on Figure 16.

Moulds from the BOS steelworks experienced more failures by crazing, vertical cracking, broken balling, and cold shuts than those from the OH steelworks, whilst the incidence of horizontal cracking, broken lugs and broken mould failures was less from the BOS moulds when considering the total number of moulds. There were no torn seat failures (caused by teeming defects) experienced in the OH moulds and no torn seat failures (caused from foundry defects) occurring in the BOS moulds.

Considering the BOS and OH moulds independently, the percentages lend themselves more to a comparison situation. The BOS moulds show a greater incidence in failure by crazing, broken balling and cold shut modes whilst the OH moulds show greater incidence in failure by vertical cracking, horizontal cracking, broken lugs and broken mould modes. The BOS moulds experience torn seat failures due to teeming defects whilst OH moulds experience torn seat failures caused by foundry defects.

2. (iv) How is the mode of failure related to mould metallurgy?

The mode of failure was cross referenced with the steelworks practice and the ultrasonic test results from the data (Table 8). A large proportion of the moulds considered were not subjected to ultrasonic testing as can be seen.

The majority of the ultrasonic values obtained from the moulds considered fell in the 3.4 - 3.8 km/s group. Of the 337 moulds with velocity readings, 42 readings (12.46%) exceeded 3.8 km/s but were within the 3.8-4.3 km/s range i.e. the graphite was coarse whilst the majority, 87.54%, exhibited very coarse graphite.

Experience has shown⁽¹⁻⁵⁾ that the following modes of failure are associated with specific ultrasonic values:-

Ultrasonic Value	Graphite Type	U/S km/s	Mode of Failure
3.1-3.8	V. coarse 'coarser' coarse.	< 3.4	Torn seats
3.8-4.3		< 3.6	Broken lugs
4.3-4.8	compacted & short	> 4.0	Vertical Cracking
4.8-5.2	Quasi flake	3.5-4.0	Optimum life

The data showed the following trends:-

Mode of Failure	Ultrasonic Velocity Range (km/s)	No. of Moulds in		No. of Moulds Reading					
		Group	%	3.4 km/s	%	>3.8 km/s	%	>4 km/s	%
Crazing	3.2-4.03	65	19.29	15	23.08	4	16.15		
Vertical Cracking	3.21-4.14	182	54.01	16	8.79	30	16.48	6	3.30
Horizontal Cracking	3.35-4.0	17	5.04	2	11.76	1	5.88		
Torn Seat (T.D.)	3.21-3.84	38	11.28	7	18.42	3	7.89		
Broken Lug	3.33-3.55	7	2.08	2	28.57				
Broken Mould	3.40-3.58	3	0.89						
Broken Balling	3.47-3.95	4	1.18			1	25		
Cold Shut	3.43-3.86	16	4.75			3	18.75		
Torn Seat (F.D.)	3.25-3.70	5	1.48	3	60				
		<u>337</u>	<u>100%</u>						

The only example of corroboration with previous findings is that of Broken Lugs occurring at less than 3.6 km/s. The remaining information appears not to hold true.

It has been previously stated that ultrasonic testing is a very unreliable method of testing in 'the wrong hands'. With large graphite structures such as those evident from the readings for the majority of the moulds, it is very difficult to judge when the wave begins and thus measurements of cycles might not have been whole - thus leading to discrepancies. This however is a suggestion as to why the present readings do not corroborate the previous findings. It is obvious that no correlation can be made from these figures.

2. (v) Would you recommend Titanium additions under the present operating conditions?

Figures 11 and 12 graphically represent the mould performances versus titanium content of the moulds, differentiating between mould lives of moulds subjected to deliberate additions of ferrotitanium and those deriving their titanium content solely from the charge during ingot mould production, for BOS and OH moulds respectively. Table 9 shows the effect on life, of titanium, for both the BOS and OH moulds along with an economic analysis to ascertain whether or not the life extension makes FeTi treatment a viable proposition.

In assessing the percentage addition of titanium required, for each titanium level, and hence the cost of additions, no compensation has been made for losses of titanium due to 'fade' on addition, and time delay for teeming after the additions have been made. The recovery of titanium up to 0.1% appears, from the research work, to be 80-93% which could be adequately compensated for by the residual titanium in the foundry returns and pig iron in the cupola charges.

For BOS Moulds

Table 9 indicates that ^{for} the moulds in the 0.02-0.059% titanium groups an increase in life is achieved with moulds obtaining their titanium content from deliberate FeTi additions and the increase in life produces a total cost saving.

For the 0.06-0.079% titanium moulds fewer lives are achieved in the FeTi addition moulds and the additions are thus uneconomical.

In the 0.10-0.109% titanium moulds the lives are increased by deliberate FeTi additions but accounting for the cost of additions to the cupola iron this becomes economically non viable.

For OH Moulds

For the 0.03-0.039%, 0.05-0.059% and 0.08-0.089% titanium moulds the performance was better in the residual titanium moulds.

For the 0.06-0.069% titanium moulds the FeTi addition moulds produced better lives and reduced overall costs thus being economically viable, whilst the 0.07-0.079% titanium increased lives but insufficiently to compensate for the increased cost due to FeTi additions.

For the moulds with titanium levels below 0.03% Ti, 0.04-0.049% Ti and above 0.08% Ti there is insufficient data to permit economic analysis of the benefit of ferrotitanium additions to mould iron.

3. SUMMARY OF FINDINGS

(a) B.O.S. Moulds

- (i) FeTi additions to produce $<0.06\%$ titanium moulds increase mould life (a max. is experienced at $0.03-0.039\%$ Ti).
- (ii) FeTi additions to produce moulds with $>0.06\%$ Ti decrease mould life.
- (iii) The FeTi additions increase life significantly making the additions economically viable.
- (iv) Greater percentage failures by crazing, broken balling and cold shuts are achieved.
- (v) In these moulds torn seat failures are due to teeming defects.
- (vi) Moulds containing above 0.09% Ti exhibit greater lives than the OH moulds of the same titanium.

(b) O.H. Moulds

- (i) Moulds with $<0.058\%$ Ti (achieved by FeTi additions) show decreases in life.
- (ii) Moulds with $0.058-0.08\%$ Ti (achieved by FeTi additions) show increased mould life.
- (iii) Insufficient data exists for moulds with $>0.08\%$ Ti to allow comparison between addition and non-addition mould lives.
- (iv) Greater percentage failures occur by vertical and horizontal cracking, broken mould and broken lug modes for these moulds.
- (v) Torn seat failures are due to foundry defects.
- (vi) The average life for the OH $0.01-0.089\%$ Ti moulds is greater than for the BOS moulds.
- (vii) It is uneconomical to make deliberate FeTi additions to the mould iron as only the $0.06-0.069\%$ Ti moulds with additions produce a cost saving (£12.525p).

(c) Titanium

- (i) The largest average life is achieved by $0.06-0.069\%$ titanium, whether one regards or disregards which steelworks practice is involved. (The same is true for the 0.1% Ti group but this is a 'one-off' at 80.8 lives).
- (ii) Increasing titanium content in the moulds increases the failure rates by torn seat, broken mould and broken balling modes.

Regarding Table 7, with increasing titanium content:-

- (iii) Craze and torn seat failure modes parabolically attain a maximum ().
- (iv) The vertical cracking mode parabolically reaches a minimum ().
- (v) Broken lug and cold shut failure modes decrease and increase sinusoidally ().
- (vi) The total average life for residual titanium group moulds are greater than those for added titanium group moulds disregarding steelworks practice (Figure 15).
- (vii) It is uneconomical to add FeTi to produce moulds of >0.06% titanium for use in BOS steelworks and <0.058% titanium for use in OH steelworks, as in both cases residual titanium moulds have superior performance.
- (viii) It is economical to make FeTi additions to produce moulds with <0.06% Ti for use in BOS steelworks and 0.06-0.069% Ti for use in the OH steelworks, these producing superior performance and a cost saving.

Mode of Failure Group	% Failure of total moulds	Average Life	With Increasing Ti (mould life)	% Ti at Which occurs		Steelworks Mould Most Affected
				Max Lives	Min Lives	
1. Craze	15.625	67.54	Reaches a max parabolically ()	0.07/0.079	-	BOS
2. Vertical Cracking	56.45	60.94	Reaches a min parabolically ()	-	0.07/0.079	OH
3. Horizontal Cracking	7.03	82.17	Inc. & dec. sinusoidally ()	-	-	OH
4. Torn Seat (due to teeming defects)	9.18	60.68	The number of failures by this mode incs.	-	-	BOS Only
5. Broken lug (mechanical damage)	4.29	61.57	Incs. & decs. sinusoidally ()	-	-	OH
6. Broken Mould (Mechanical)	2.15	43.29	The % failure increases.	-	-	OH
7. Broken balling	2.946	45.2	"	-	-	BOS
8. Cold Shut	3.914	58.87	Incs. & decs. sinusoidally ()	-	-	BOS
9. Torn Seat (due to foundry malpractice)	0.975	67.83	Reaches a max parabolically ()	0.08/0.89	-	OH Only

Mould Metallurgy - (i) 87.35% of ultrasonic velocities are between 3.2-3.8 km/s.
(ii) 12.65% are > 3.8 km/s

4. CONCLUSIONS

2(i) Changes in burden versus (a) Performance (b) Mode of failure

There must be other significant factors affecting mould life which have not been assessed for example sand technology, stripping practice (controlled or uncontrolled) and steelworks variables.

2(ii) Changes in FeTi addition versus

(a) Performance

1. Regardless of whether deliberate FeTi additions are made, or not, to produce the mould titanium content, the maximum life occurs in the 0.06-0.069% Ti and 0.10-0.109% Ti moulds.
2. In B.O.S. steelworks' moulds, FeTi additions increase the mould performance in moulds of $<0.06\%$ Ti but decrease it $>0.06\%$ Ti. The increase in mould performance is maximised at 0.03-0.039% Ti and minimised at 0.02-0.029% Ti.
3. With the OH steelworks moulds the effect is reversed - the performance decreases with specific FeTi additions below 0.058% Ti and increases above 0.058% Ti. Insufficient figures are available for conclusions to be drawn above 0.08% Ti content of the moulds. With the figures available the greatest improvement is achieved at 0.06-0.069% Ti where mould life is increased by 7.5 casts. The greatest reduction in mould life occurs in moulds of 0.03-0.039% Ti where lives are reduced by 33.9 casts.
4. A greater reduction in mould life is experienced in the OH steelworks' moulds compared to the BOS steelworks moulds with FeTi additions but the greatest increase in life is experienced in the BOS moulds (25:7.5 additional lives).
5. Assessment of the effect of titanium content, arising from deliberate FeTi additions or cupola charge (regardless of the steelworks practice the moulds are subjected to) shows a better overall performance from those moulds with residual titanium content and not those subjected to deliberate FeTi additions.

(b) Mode of Failure

The number of moulds failing by:-

1. Torn seats (due to teeming effects), broken mould and broken balling increases with increasing titanium content.
2. Crazing and torn seats (due to foundry defects) increases to a maximum in a parabolic manner with increasing titanium content ().

3. Vertical cracking decreases to a minimum parabollically with increasing Ti. (U)
4. Horizontal cracking, broken lugs and cold shut modes exhibit sinusoidal increases and decreases with increasing titanium content. (W)

2(iii) What implications, if any, does mode of failure have on steelworks operation?

1. Larger incidences of failure by crazing, broken balling and cold shut modes are evident in B.O.S. steelworks' moulds.
2. Torn seat failures, due to foundry defects, occur only in BOS steelworks' moulds.
3. Longer incidences of vertical and horizontal cracking, broken lugs and broken mould modes are evident in OH steelworks' moulds.
4. Torn seat failures, due to teeming defects, occur only in OH steelworks' moulds.

2(iv) Mode of failure relationship with mould metallurgy

The ultrasonic testing figures do not bear any correlation to previous experience except for moulds failing by broken lugs mode where the ultrasonic velocity is less than 3.6 km/s. No conclusions can be drawn.

2(v) Are FeTi additions recommended under the present operating conditions ?

1. It would appear that, for moulds utilised in the BOS steelworks, it would be beneficial and economically viable to make deliberate FeTi additions to achieve titanium contents in the moulds of up to 0.06-0.069% titanium. This increases the average lives and saves revenue.
2. Above 0.06-0.069% titanium levels it is not viable to make deliberate additions as decreases in average lives are experienced making this practice uneconomical.
3. For moulds utilised in the OH steelworks it is not viable to make deliberate FeTi additions to mould iron to produce moulds of less than 0.058% titanium content.
4. Above 0.058% titanium additions are viable to 0.06-0.069% titanium where increases in average life occur and are economically viable for OH steelworks' moulds.
5. Insufficient data is available to allow assessment of the effect of FeTi additions to produce moulds of more the 0.08% titanium used in the OH steelworks.

REFERENCES

- 1-5. Internal Research reports courtesy of B.S.C.
6. Assessing Ingot Mould Structures by Ultrasonic Techniques.
B.R. Evans and P.J. Emerson Report 1065 BCIRA Journal
March 1972.
7. Nitrogen in Ingot Moulds Produced from the Hot Blast Cupola.
J.K. Kyle and W. Montgomery, Steel Times July 1969.

1. Economics of Ferrotitanium Additions

Cost of FeTi (60/40%) is £600/tonne or 60p/kg.
2.727 kg(6lb) FeTi is added to 2.74 tonnes (2.697 tons) of Fe.

Type 48 moulds are 25 tonnes mass .

Average addition/mould is $2.727 \text{ kg} \times \frac{25,000 \text{ kg}}{2,740 \text{ kg}}$

= 24.88 kg .

Cost of the addition is $\frac{£600}{1,000 \text{ kg}} \times 24.88 \text{ kg}$

= £14.928/mould. Type 48

2. Type 48 Moulds

Mould mass usually 25 tonnes

Production cost is £150/tonne ∴ 1 mould = £3,750/mould

Cost of mould/cast = $\frac{£3,750}{\text{Mould life}}$

N.B.

The analysis of mould lives does not show the cost of losses in terms of steel losses and time costs for removing steel from casting pits. Thus, economics can only be established with respect to the Foundry costs.

3. Cost of Addition for Varying Titanium Levels

With FeTi costs of £600/tonne and FeTi being 60/40% FeTi the following additions would be required:-

Ti % Required	mass (kg)	Cost (£)
0.01	6.25	3.75
0.015	9.375	5.625
0.02	12.50	7.50
0.025	15.625	9.375
0.03	18.75	11.25
0.035	21.875	13.125
0.04	25.00	15.00
0.045	28.125	16.875
0.05	31.25	18.75
0.055	34.375	20.625
0.06	37.50	22.50
0.065	40.625	24.375
0.07	43.75	26.25
0.075	46.875	28.125
0.08	50.00	30.00
0.085	53.125	31.875
0.09	56.25	33.75
0.095	59.375	35.625
0.10	62.50	37.50

TABLE 1
RELATIONSHIP BETWEEN MOULD LIFE AND SOME MANUFACTURING
VARIABLES AS PREVIOUSLY OBSERVED

Cupola Charge	Stripping Practice	Microstructure	Mould Performance	Comments / Average Lives
High pig iron No titanium addition	Uncontrolled	Irresolvable fine pearlitic matrix and fine flake graphite	Failure by cracking	Inherent low resis- tance to thermal shock and cracking but high resistance to crazing. 31.9
High pig iron No titanium addition	Controlled	Fully pearlitic mat- rix with fine flake graphite.	Failure by torn seat	Failure due to insuff- 37.7/ icient strength in the 42.7 iron
High pig iron with titanium addition	Controlled	Coarse graphite in pearlite/ferrite matrix.	Failure by tearing	This is the weakest iron, 52.9/ due to the graphitising 56 effect of titanium coup- pled with controlled stripping, coarse graph- ite is promoted.
High steel scrap FeTi addition (0.1 mass%Ti residual)	Uncontrolled	Fine graphite in an irresolvable pearlitic matrix.	Failure by cracking acceptable	Titanium prevents the 56.7 formation of compacted graphite associated with high nitrogen and off- sets the unfavourable stripping thus producing a normal flake morphology.
"	Controlled	Coarse graphite in a ferritic and pearlitic matrix.	Failure by torn seats. Slower cooling rate plus Ti additions promotes coarse graph- ite	
Pig iron FeTi addition	Uncontrolled	Coarse, random angular graphite in ferrite envelopes and an irresolvable pearlitic matrix.	Failure by cracking.	Rapid cooling rate through the transformation range offsets the graphitising effect of titanium and promotes crazing and tear- ing resistance.
70% Pig Iron No FeTi addition	Uncontrolled	Fine random graphite and some compacted graphite in a pear- litic matrix containing phosphide eutectic.	Failure by cracking prematurely.	Low carbon (3.6 mass %) produces a phosphide eutectic network in the absence of controlled stripping. The iron is craze and tear resistant but fails prematurely due to uncontrolled stripping.
70/80% pig iron FeTi addition (~0.1% resid Ti in iron, max 20% steel scrap & foundry returns)	Controlled	Coarse random graphite, in ferrite envelopes with some pearlite and phosphide eutectic.	Failure by tearing (<10 lives for large no. of moulds)	The proportion of pearlite 87.5 is a function of mould size and hence cooling rate. Coarse graphite is an effect of Ti addition. Crack resistance improved by neutralisation of N_2 by Ti.
High steelscrap No FeTi addition	Controlled	Pearlite with ferrite surrounding coarse random graphite and some compacted graphite	Failure by crazing	Stronger iron than the one above as it lacks the phosphide eutectic. Resists cracking and tearing, hence torn seats are eliminated.
60% pig iron No FeTi addition (20% scrap and 20% returns)	Controlled (700°C)	Flake graphite in a mainly pearlitic matrix.	Premature failure by torn seats eliminated acceptable.	106.97
50% pig, 40% steel, 10% foundry ret- urns (0.075% Ti residual)	Controlled	Coarse graphite in a ferritic and pearli- tic matrix.	Failure by torn seats eliminated.	

KEY TO TABLE 2

AVERAGE LIVES ASSOCIATED WITH SPECIFIC FAILURE MODES
(SUB-DIVIDED ACCORDING TO BOS/OH PRACTICE)

(N) = Figures for mould lives - B.O.S. Steel

N = Figures for mould live - O.H. Steel

[N] = Total average for mould lives regardless of
B.O.S./O.H.

BURDEN	TOTAL AVE. LIVES FOR BURDEN	CRAZING	VERTICAL CRACKING	HORIZONTAL CRACKING	TEEMING DEFECTS		TECHNICAL DAMAGE	FOUNDRY DEFECTS		
					TORN SEAT (43)	BROKEN LUG (51)		COLD SHOT (61)	TORN	
-90/10 5/85/10 60/17/13 60/20/20 63/20/17 70/17/13 70/30/- 71/17/12 78/17/15 85/15/- 90/10/-	87 [(87)] [(9)] 411 [(66)] 34 [(74)] 46 [(25)] [(65)] 54 [(53)] [(53)] [(40)] 45 (44) [(44.5)] 75 (51) [(63)] 79 78 92 [(83)] (50) [(50)] (74) (65) (64) [(67.67)] (70) (71) (72) (70) [(70.75)] (68) (74) (67) (82) (72) (37) 42 [(63.14)] (31) (67) (63) (38) [(49.75)] (59) [(59)] (28) (63) (94) (48) [(58.25)] (2) (6) (18) (40) (86) (77) (41) (74) [(43)] (86) (90) (85) (100) (52) (103) (68) 85 [(84.13)] (73) [(73)] (59) (65) (76) (41) (63) (14) (91) (42) (28) (64) (44) (15) 43 67 28 [(49.33)] (72) 55 75 83 75 76 [(69.33)] (103) (28 104 94 72 84 67 69 85 84) (53 50 35 38 43 40 33) 76 67 58 43 87 64 73 94 67 [(64.32)] (35 50 90 59 42 66 84 39 32) (35 35 40 38 16 13 41 25 69) (41 11 19 45 38 51 53 37 27) 54 60 63 19 68 72 27 44 60 19 74 47 69 58 47 17 32 19 72 43 60 37 64 76 49 43 47 15 69 45 32 22 35 35 24 75 65 68 59 [(46.52)] (58 75 55 74 118 93 41 62 65) (44 53 60 29 60) 45 87 81 82 87 57 87 42 80 77 40 96 77 80 70 [(66.73)] (51 79 91 78 98 46 70 73 78) (48 79 49 91 66 53 96 37 120) (81 67 100 61 85 71 91 54 82) (95 97 66 63 47 84 73 96 92) (95 80 72 73 97 100 93 41 63) 56 42 30 49 12 25 34 39 61) 53 82 94 29 87 87 37 90 69 49 94 85 101 80 69 58 68 56 49 50 24 71 84 76 39 30 43 57 49 90 80 71 64 69 61 63 78 90 64 51 [(68.26)]	(9) (66) 34 (74) 46 (25) (65) 54 [(53)] [(53)] 45 (44) [(44.5)] 75 (51) [(63)] 79 78 92 [(83)] (50) [(50)] (74) (65) (64) [(67.67)] (70) (71) (72) (70) [(70.75)] (68) (74) (67) (82) (72) (37) 42 [(63.14)] (31) (67) (63) (38) [(49.75)] (59) [(59)] (28) (63) (94) (48) [(58.25)] (2) (6) (18) (40) (86) (77) (41) (74) [(43)] (86) (90) (85) (100) (52) (103) (68) 85 [(84.13)] (73) [(73)] (59) (65) (76) (41) (63) (14) (91) (42) (28) (64) (44) (15) 43 67 28 [(49.33)] (72) 55 75 83 75 76 [(69.33)] (103) (28 104 94 72 84 67 69 85 84) (53 50 35 38 43 40 33) 76 67 58 43 87 64 73 94 67 [(64.32)] (35 50 90 59 42 66 84 39 32) (35 35 40 38 16 13 41 25 69) (41 11 19 45 38 51 53 37 27) 54 60 63 19 68 72 27 44 60 19 74 47 69 58 47 17 32 19 72 43 60 37 64 76 49 43 47 15 69 45 32 22 35 35 24 75 65 68 59 [(46.52)] (58 75 55 74 118 93 41 62 65) (44 53 60 29 60) 45 87 81 82 87 57 87 42 80 77 40 96 77 80 70 [(66.73)] (51 79 91 78 98 46 70 73 78) (48 79 49 91 66 53 96 37 120) (81 67 100 61 85 71 91 54 82) (95 97 66 63 47 84 73 96 92) (95 80 72 73 97 100 93 41 63) 56 42 30 49 12 25 34 39 61) 53 82 94 29 87 87 37 90 69 49 94 85 101 80 69 58 68 56 49 50 24 71 84 76 39 30 43 57 49 90 80 71 64 69 61 63 78 90 64 51 [(68.26)]								
66/17/17 69/17/14 75/17/10 74/17/9 50/50/- 64/17/19 65/17/18 83/17/- 67/17/16 68/17/15 65/20/15 80/20/- -/80/20 10/80/10 60/20/12 63/17/20 80/10/10 70/10/20 53/17/30 50/40/10 70/20/10	[(50.5)] [(40)] (44) 45 [(44.5)] [(63)] [(83)] (35.5) 2 [(24.33)] [(67.67)] [(70.75)] (66.67) [(63.14)] 42 (59.80) [(43.5)] 2.5 (62.13) 98 [(66.62)] [(69.70)] [(47.75)] (75.56) 71.60 [(74.14)] (50.35) 44 [(50.10)] (50.0) 53.8 [(50.95)] (68.70) 77.11 [(71.62)] (63.12) 72.88 [(67.07)] (47.65) 47.92 [(47.80)] (60.53) 72.5 [(65.42)] (67.97) 67.17 [(67.64)]	(9) (66) 34 (74) 46 (25) (65) 54 [(53)] [(53)] 45 (44) [(44.5)] 75 (51) [(63)] 79 78 92 [(83)] (50) [(50)] (74) (65) (64) [(67.67)] (70) (71) (72) (70) [(70.75)] (68) (74) (67) (82) (72) (37) 42 [(63.14)] (31) (67) (63) (38) [(49.75)] (59) [(59)] (28) (63) (94) (48) [(58.25)] (2) (6) (18) (40) (86) (77) (41) (74) [(43)] (86) (90) (85) (100) (52) (103) (68) 85 [(84.13)] (73) [(73)] (59) (65) (76) (41) (63) (14) (91) (42) (28) (64) (44) (15) 43 67 28 [(49.33)] (72) 55 75 83 75 76 [(69.33)] (103) (28 104 94 72 84 67 69 85 84) (53 50 35 38 43 40 33) 76 67 58 43 87 64 73 94 67 [(64.32)] (35 50 90 59 42 66 84 39 32) (35 35 40 38 16 13 41 25 69) (41 11 19 45 38 51 53 37 27) 54 60 63 19 68 72 27 44 60 19 74 47 69 58 47 17 32 19 72 43 60 37 64 76 49 43 47 15 69 45 32 22 35 35 24 75 65 68 59 [(46.52)] (58 75 55 74 118 93 41 62 65) (44 53 60 29 60) 45 87 81 82 87 57 87 42 80 77 40 96 77 80 70 [(66.73)] (51 79 91 78 98 46 70 73 78) (48 79 49 91 66 53 96 37 120) (81 67 100 61 85 71 91 54 82) (95 97 66 63 47 84 73 96 92) (95 80 72 73 97 100 93 41 63) 56 42 30 49 12 25 34 39 61) 53 82 94 29 87 87 37 90 69 49 94 85 101 80 69 58 68 56 49 50 24 71 84 76 39 30 43 57 49 90 80 71 64 69 61 63 78 90 64 51 [(68.26)]								
TOTAL AVE. LIVES FOR	(51.21) 67.94 [(54.09)]	(70.60) 60.96 [(66.64)]	(66.86) 81.04 78.28	[(65.62)]	[(43.0) 58.92 [(52.35)]	[(49.5) 87 [(58.59)]	(66.31) 46.03 [(58.81)]	(17.3)		

TABLE 3

PERCENTAGE DISTRIBUTION OF MOULD FAILURES WITHIN THE BURDEN GROUPS

BURDEN PIG/STEEL/RETURNS	No. IN GROUP	AVE. GROUP LIFE TOTAL	DISTRIBUTION OF MOULDS WITH THE MODE OF FAILURE GROUPS										AVE. GROUP LIFE					
			CRAZING		CRACKING		TEEMING DEFECTS		MECHANICAL DAMAGE		FOUNDRY DEFECTS		COLD SHUT	TORN SEAT	B. O. S.	O. H.		
			VERTICAL	HORIZONTAL	I.	TORN SEAT	B. LUG	%	%	%	%	%						
66/17/17	2	50.5	[1]	50%	1	50%											50.5	
69/17/14	2	40	[1]	50%													40	
73/17/10	2	44.5	[2](1)	100%													44	45
74/17/9	2	63	[2] 2	100%													63	
50/50/-	3	83	[3]	100%													83	
64/17/19	3	24.33	[(1)]	33%													35.5	2
65/17/18	3	67.67	[(3)]	100%													67.7	
83/17/-	4	70.75	[(4)]	100%													70.75	
67/17/6	7	63.14	[7] (6) 1	100%													66.67	42
68/17/15	7	43.5	[(4)]	57.15%													59.8	2.
65/20/15	8	66.62	[(5)]	62.5%													62.13	98
80/20/-	10	64.70	[(3)]	40%													64.7	
-/80/20	12	47.75	[(1)]	66%													47.75	
10/80/10	14	74.14	[(1)]	7.1%													75.56	71.
68/20/12	18	50.11	[(10)]	55.56%													50.35	46.
63/17/20	20	50.95	[1]	5%													50.00	53.
80/10/10	26	71.62	[(7)]	26.93%													68.70	77.
70/10/20	36	67.07	[1]	2.77%													63.12	72.
53/17/30	85	47.8	[(6)] 4(27)	80%													47.65	47.
50/40/10	83	65.42	[(16)]	19.27%													60.53	72.
70/20/10	165	67.64	[(35)] (22) 13	21.2%													67.97	67.
NO. IN FAILURE GROUP			[80] 16(64)	15.50%														

[X] TOTAL NO. IN FAILURE GROUP

[(X)] TOTAL NO. ALL B.O.S. IN FAILURE GROUP

(X) PROPORTION B.O.S. IN FAILURE GROUP

X PROPORTION O.H. IN FAILURE GROUP

% FIGURE IS PERCENTAGE OF MOULDS WITHIN BURDEN GROUP UNIQUE TO SPECIFIC MODE OF FAILURE DISREGARDING B.O.S./O.H. VARIATION

TABLE 4
BURDENS ORDERED IN DECREASING INGOT LIVES

Table 4a - Disregarding Whether Titanium Additions Have Been Made

Order	Burden Pig/Steel/Returns	Average Life	No. of Moulds In Burden Mould	Titanium Additions	
				Yes	No
1	60/50/-	83.00	3		*
2	10/80/10	74.14	14	*	*
3	74/17/9	73.00	2		*
4	80/10/10	71.62	26	*	*
5	83/17/-	70.75	4		*
6	80/20/-	69.70	10	*	*
7	70/10/20	68.72	36		*
8	65/17/18	67.67	3	*	*
9	65/20/15	65.67	8	*	*
10	50/40/10	65.40	83	*	*
11	67/17/16	63.14	7	*	*
12	70/20/10	62.29	164	*	*
13	63/17/20	52.16	20		*
14	66/17/17	50.50	2		*
15	68/20/12	48.44	18	*	*
16	53/17/30	47.24	85	*	*
17	-/80/20	46.83	12	*	*
18	73/17/10	44.50	2	*	*
19	68/17/15	43.43	7	*	*
20	69/17/14	40.00	2		*
21	64/17/19	24.30	3	*	*

(1-21) Burdens arranged in order of descending average lives regardless of FeTi/no FeTi additions

Table 4b - Moulds With No Titanium Additions

Order (as above)	Expected Order From Burden Composition	Burden	Average Life	No. of Moulds In Burden Group
		Pig/Steel/Returns		
1	(xvi)	50/50/-	83.00	3
3	(ii)	74/17/9	73.00	2
9	(xi)	65/20/15	73.00	1
11	(viii)	67/17/16	72.00	3
5	(i)	83/17/-	70.75	4
8	(x)	65/17/18	70.00	2
7	(iv)	70/10/20	68.72	36
2	(xvii)	10/80/10	64.25	4
19	(vii)	68/17/15	59.28	5
10	(xv)	50/40/10	59.00	11
12	(v)	70/20/10	56.95	123
13	(xiii)	63/17/20	52.16	20
14	(ix)	66/17/17	50.50	2
16	(xiv)	53/17/30	47.24	83
18	(iii)	73/17/10	44.00	1
20	(vi)	69/17/14	40.00	2
21	(xii)	64/17/19	35.50	2
17	(xviii)	-/80/20	27.65	8

1-21 is position of burden in decreasing order of average life disregarding whether FeTi had been added
(i)-(xviii) Expected order of life from burden composition

Table 4c - Moulds With Titanium Additions

Order (as in 4a)	Expected Order From Burden Composition	Burden	Average Life	No. of Mould In Burden Group	
		Pig/Steel/Returns			
12	}	70/20/10	78.85	41	
4		(i)-(iii)	80/10/10	71.62	26
6			80/20/-	69.70	10
2	(v)	10/80/10	68.10	10	
10	(vi)	50/40/10	65.40	72	
8	(x)	65/17/18	64.00	1	
17	(iv)	-/80/20	60.25	4	
11	(xi)	67/17/16	57.00	4	
9	(ix)	65/20/15	56.50	4	
16	(vii)	53/17/30	56.00	2	
15	(xiii)	68/20/12	48.44	18	
18	(xiv)	73/17/10	45.00	1	
19	(xii)	68/17/15	2.50	2	
21	(viii)	64/17/19	2.00	1	

1-21 Burden position not accounting for FeTi/no FeTi additions
(i)-(xiii) Expected ordering of descending average life from burden composition

TABLE 5

BURDENS ORDERED IN DECREASING PERCENTAGE VERTICAL CRACKING

Burden Pig/Steel>Returns	No. of Moulds In Group	Average Mould Life	Vertical Cracking	Crazing	Teeming		Horizontal Cracking	Mech. Damage		Foundry Damage		Mechanical Damage	Foundry Torn Seat		Teen Defect
					Torn Seat	Seat		Broken Lug	Lug	Cold Shut	Shut		Torn Seat	Seat	
73/17/10	2	44.5	100%	-	-	-	-	-	-	-	-	-	-	-	-
74/17/9	2	63	100%	-	-	-	-	-	-	-	-	-	-	-	-
50/50/-	3	83	100%	-	-	-	-	-	-	-	-	-	-	-	-
65/17/18	3	67.67	100%	-	-	-	-	-	-	-	-	-	-	-	-
83/17/-	4	70.75	100%	-	-	-	-	-	-	-	-	-	-	-	-
67/17/16	7	63.14	100%	-	-	-	-	-	-	-	-	-	-	-	-
53/17/30	85	47.8	80%	-	-	-	-	-	-	-	-	-	-	-	-
63/17/20	20	50.95	75%	5%	-	-	-	-	-	-	-	1.175%	-	-	-
70/10/20	36	67.07	69.45%	2.77%	18.33%	19.45%	-	-	-	-	-	10%	-	-	-
-/80/20	12	47.75	66.33%	8.33%	8.33%	8.33%	8.33%	8.33%	-	-	-	-	-	-	-
70/20/10	165	67.64	58.18%	21.26%	6.66%	9.08%	9.08%	1.2%	1.21%	-	-	-	-	-	0.61
68/17/15	7	43.5	57.15%	-	-	-	-	14.28%	-	-	-	-	-	-	-
10/80/10	14	74.14	57.12%	7.14%	7.14%	-	-	28.60%	-	-	-	-	-	-	-
66/17/17	2	50.5	50%	-	-	50%	50%	-	-	-	-	-	-	-	-
69/17/14	2	40.0	50%	-	-	-	-	-	-	-	-	50%	-	-	-
80/20/-	10	64.70	40%	30%	30%	-	-	-	-	-	-	-	-	-	-
50/40/10	83	65.42	34.94%	19.27%	20.48%	12.05%	12.05%	10.84%	-	-	-	1.21%	1.21%	-	-
80/10/10	26	71.62	23.49%	26.93%	23.09%	3.84%	3.84%	15.37%	-	-	-	7.68%	-	-	-
65/20/15	8	66.62	12.5%	62.5%	12.5%	12.5%	12.5%	-	-	-	-	-	-	-	-
68/20/12	18	50.11	5.56%	55.56%	22.2%	-	-	5.56%	-	-	-	5.56%	-	-	5.56%

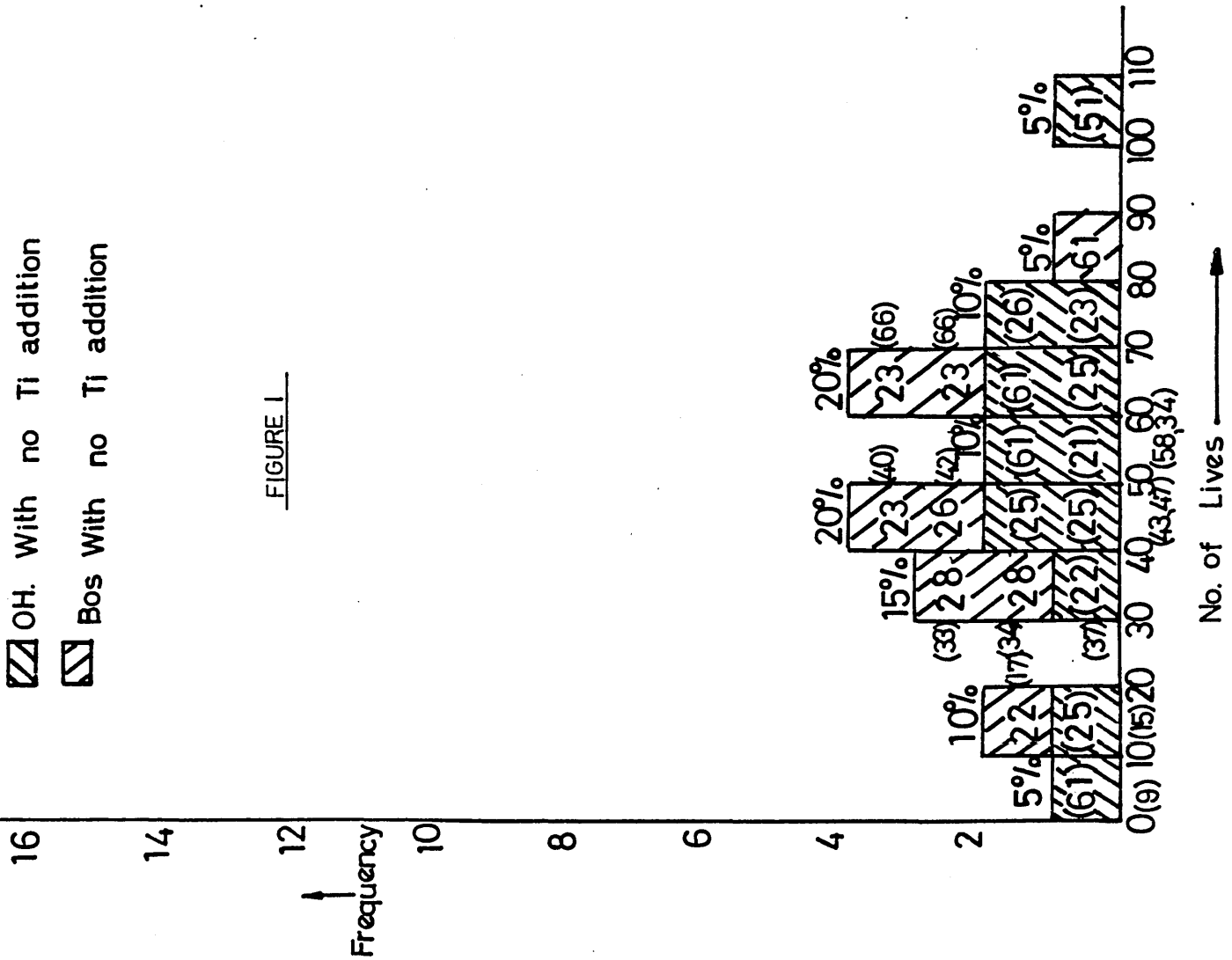
TABLE 6
THE EFFECT OF TITANIUM CONTENT ON MOULD LIFE AND MODE OF FAILURE

Steelworks BOS	Titanium Group %	No. of Lives Grouping										Average Life	Av. Life Disregarding Ti. Add. in OH, BOS	Failure Modes & No. of Failures/Failure Mode					Foundry Torn Seat	No. of Mould					
		0-9	10-19	20-29	30-39	40-49	50-59	60-69	70-79	80-89	90-99			100+	Cracking Crasing	Vert.	Horiz.	Torn Seat (Teeming)			Mechanical Damage Lug Mould Balling	Gold Shot			
*	.01/.019	-	17	-	33,34	40,42	-	66,66	-	88	-	-	48.25	-	7	-	-	-	1	-	8				
*	.02/.029	-	15	15,16	28,28	39,37	43,43	51,51	62,69	74	84,82	-	46.64 (53)	46.82	(51.98)	1	25(1)	2	1	-	1	2	-	32(1)	
*		-	-	27,27	33,37	49,45	56,50	65,69	75,76	80,82	90	-	59.21 (59)	59.2	[52.07]	1	18(1)	3	-	-	-	2	-	24(1)	
**	.03/.039	-	13,15	21,25	30,32	40,41	50,53	63,63	71,71	83,83	91,91	100	57.98 (83)	58.42	(56.50)	4	40(1)	2	2	1	-	3	1	-	53(1)
**		-	19	22,24	32,34	40,43	51,51	60,60	70,73	80,82	90,90	101	-	-	69.69	-	-	-	-	-	-	-	-	-	-
**		-	19	22,24	32,34	40,43	51,51	60,60	70,73	80,82	90,90	101	63.91 (30)	63.29	[60.81]	7	41	5(2)	-	-	2	-	-	-	55(2)
**	.04/.049	-	11,13	25	31,32	42,44	51,53	60,60	70,70	89,89	90,91	-	59.90 (6)	59.90	(42)	4(1)	40(1)	1(1)	2	-	-	1	5	-	53(3)
**		1	19	24,28	37,39	40(42)	50,50	63,63	71,72	80,82	93,93	103,103	66.62 (42)	65.97	[62.47]	6	23(1)	11	-	-	-	-	-	-	40(1)
**	.05/.059	-	(16)	22(26)	30,38	44,49	53(53)	66,67	(72)	-	96(93)	(103)	51.33 (62.07)	57.87	(58.92)	2(3)	7(5)	-	1(3)	-	-	1	1	-	12(8)
**		(2,2)	29	30(35)	49,49	54(52)	69	75	87(84)	91,92	97(94)	(106)	65.64 (64.90)	60.27	[59.04]	1(1)	8(3)	1(1)	-	(4)	-	-	-	(3)	10(12)
**	.06/.069	-	11(13)	(29)	(33)	(41)	(56)	(60)	(71)	(80,82)	-	(108,108)	77.75 (67.37)	68.71	(71.74)	(11)	2(9)	-	1(6)	(1)	-	-	-	-	3(27)
**		-	-	-	(45)	(56)	61	(71,76)	(80)	(81,87)	(93)	(101,102)	74.00 (61.58)	80.50	72.38	-	2(4)	(6)	-	(1)	(1)	-	-	-	2(12)
**	.07/.079	-	(10)	(27)	(35)	(41,45)	(50,52)	(63,63)	(72,72)	(80,81)	(91,92)	-	80.00 (61.51)	62.03	(64.67)	(17)	(7)	-	1(9)	(2)	-	-	-	-	1(35)
**		-	-	-	(45,47)	(63)	(74,75)	(83,87)	(91,99)	(100)	(100)	(100)	72.57	72.57	64.90	(1)	(8)	(2)	-	(2)	-	-	-	(1)	(14)
**	.08/.089	(5)	(11)	(21,28)	(35,38)	(44,44)	(52,53)	(60,62)	(75,75)	(84,86)	(95,96)	-	(58.19)	58.19	(60.02)	(8)	(7)	-	(9)	(5)	(2)	-	-	-	(31)
**		-	-	-	(42)	(53,57)	(64,68)	(70,71)	(82)	(92)	-	69.00 (66.56)	66.80	[60.33]	-	(12)	-	-	1(2)	-	-	-	-	-	1(14)
**	.09/.099	-	-	(25)	(31)	-	(55,56)	(60,62)	(71)	-	(90,92)	-	(60.22)	-	[60.22]	(2)	1(9)	-	(4)	-	-	-	-	-	1(15)
**		-	-	-	-	-	-	-	-	-	-	-	-	-	-	(1)	-	-	(1)	-	-	-	-	-	(2)
**	.10/.109	-	-	-	-	-	-	-	(85)	(94)	-	86.00 (89.50)	88.33	(79.50)	-	-	-	-	-	-	-	-	-	-	-
**		-	-	-	(43)	-	-	-	-	(96)	-	(69.50)	69.50	86.00 80.50	-	-	-	-	-	-	-	-	-	-	-
**	.11/.159	-	-	-	(47)	-	(65)	-	(85)	-	100	100.0 (65.67)	74.25	100.0 (60.00)	-	-	-	-	-	-	-	-	-	-	-
**		-	-	-	(43)	-	-	-	-	-	-	(43.00)	43.00	[68.0]	-	-	-	-	-	-	-	-	-	-	-

0.01 - 0.019% Ti

-  OH. With no Ti addition
-  Bos With no Ti addition

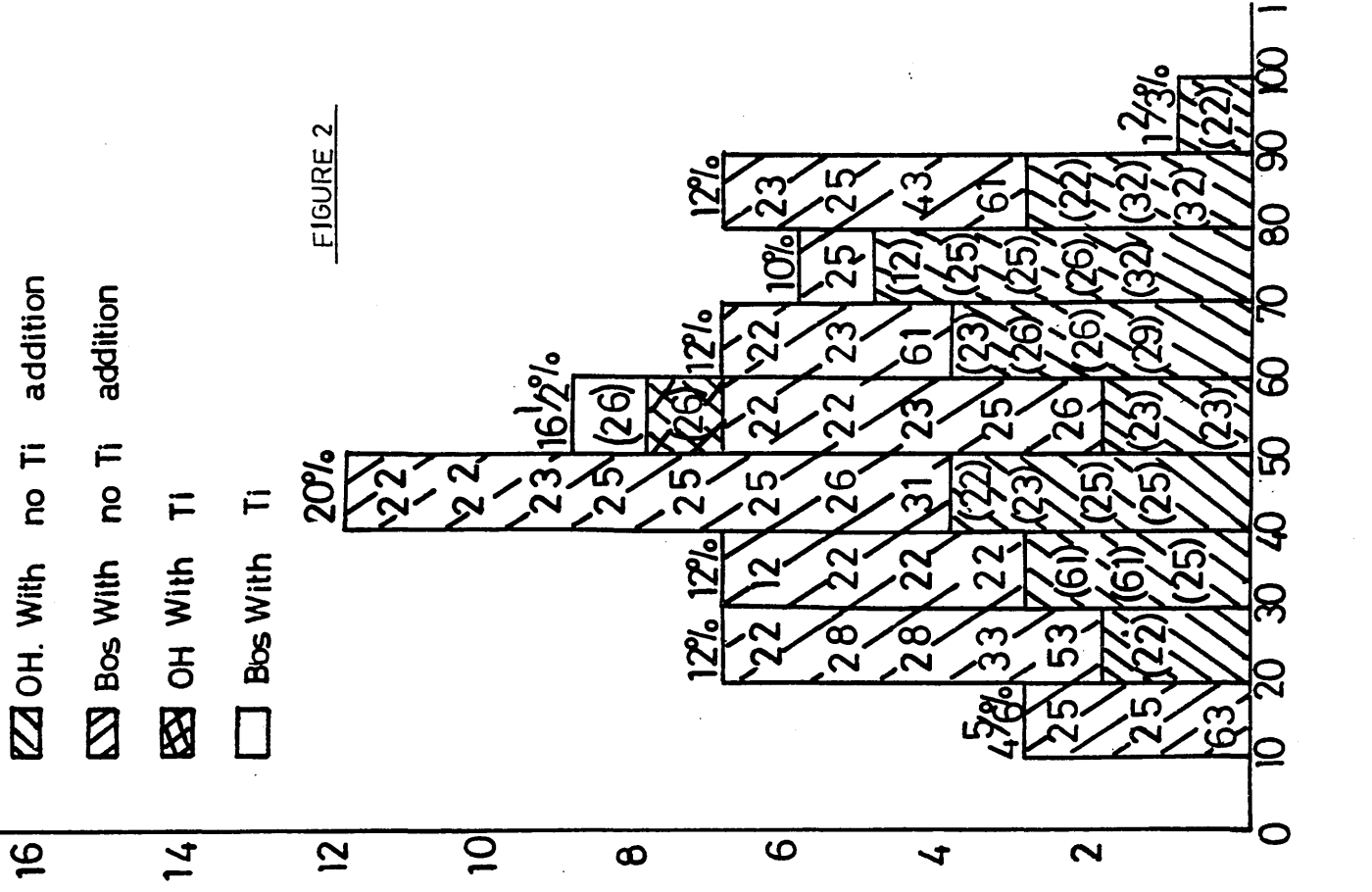
FIGURE 1



0.02 - 0.029% Ti

-  OH. With no Ti addition
-  Bos With no Ti addition
-  OH With Ti
-  Bos With Ti

FIGURE 2



0.03-0.039% Ti

-  OH With no Ti addition
-  Bos With no Ti addition
-  OH With Ti
-  Bos With Ti

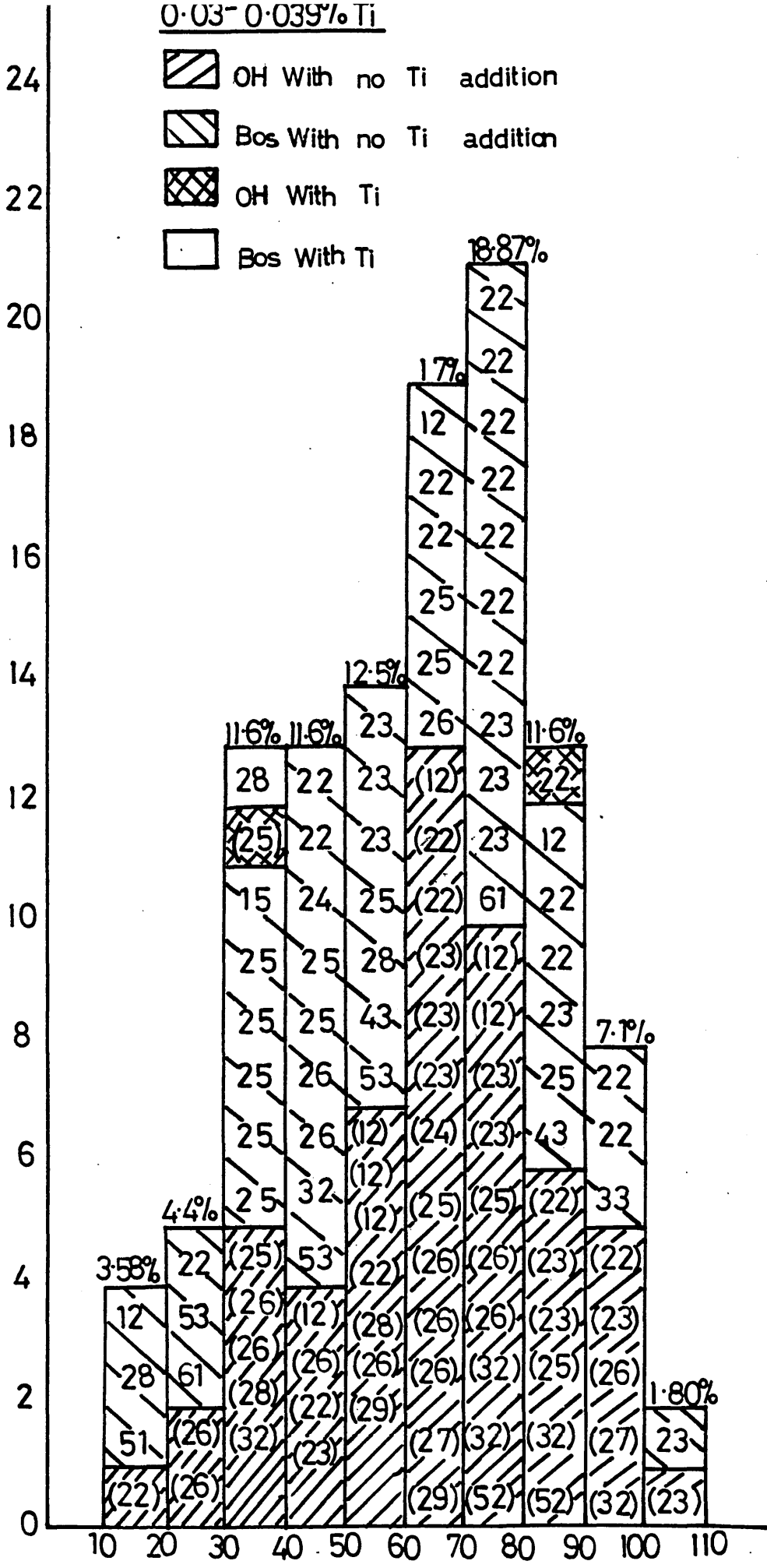


FIGURE 3

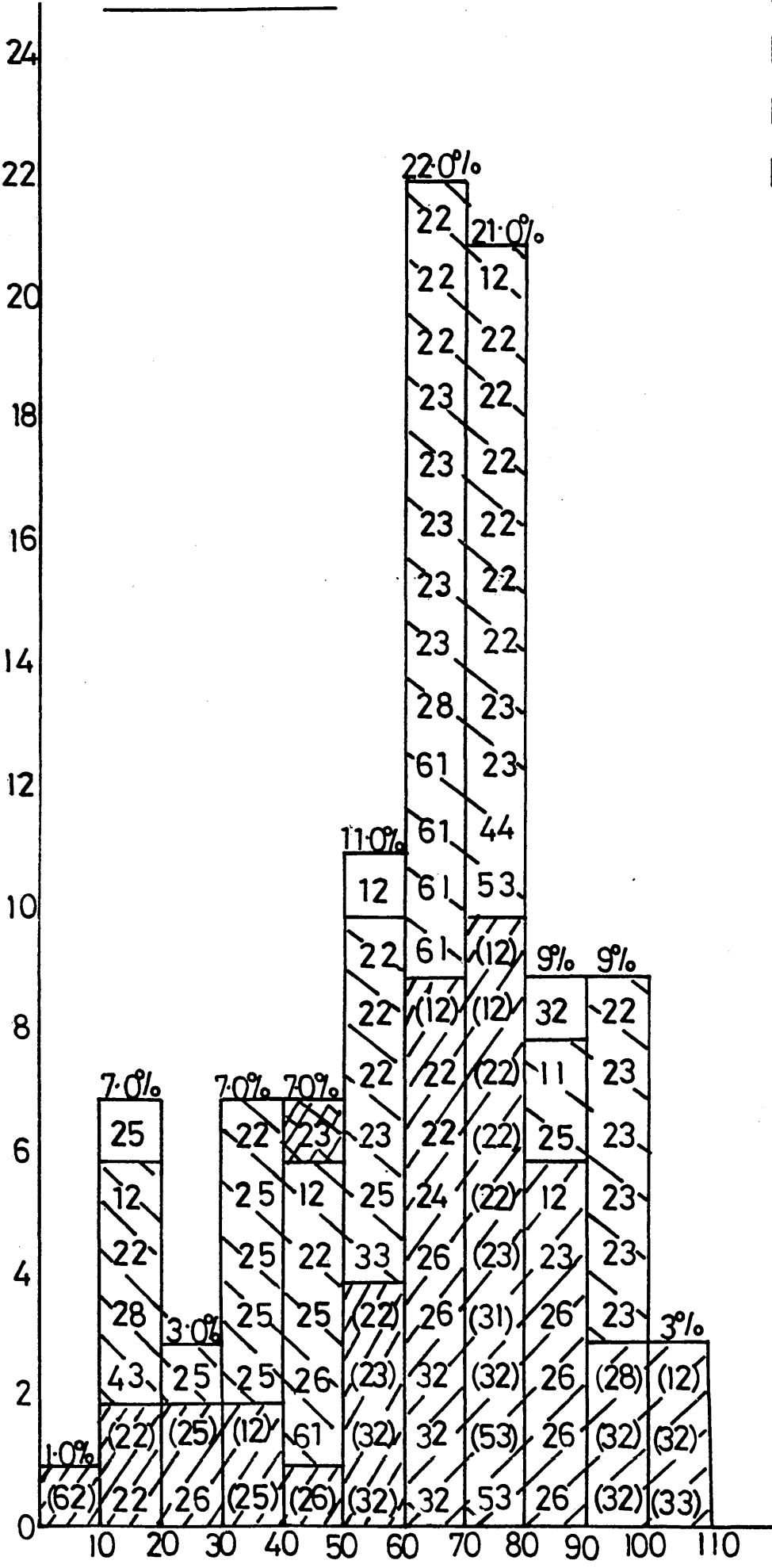
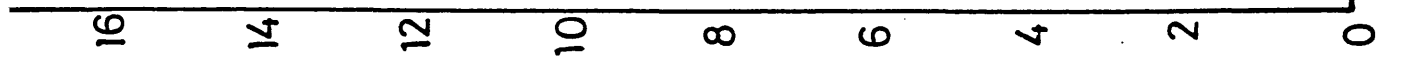


FIGURE 4

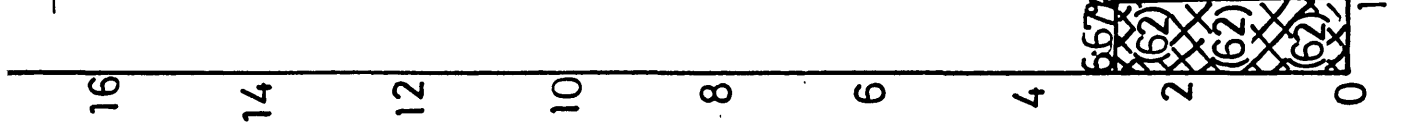
0.06 - 0.069% Ti

FIGURE 6



0.05 - 0.059% Ti

FIGURE 5



0.09 - 0.159

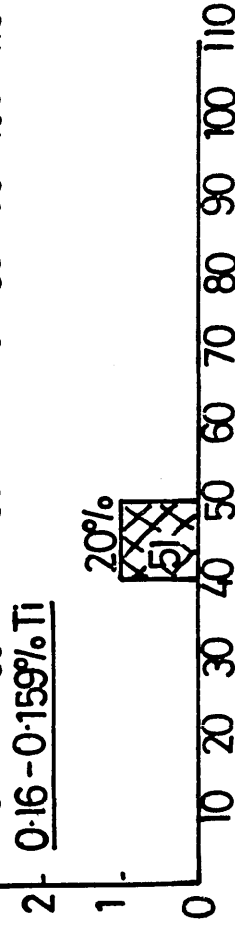
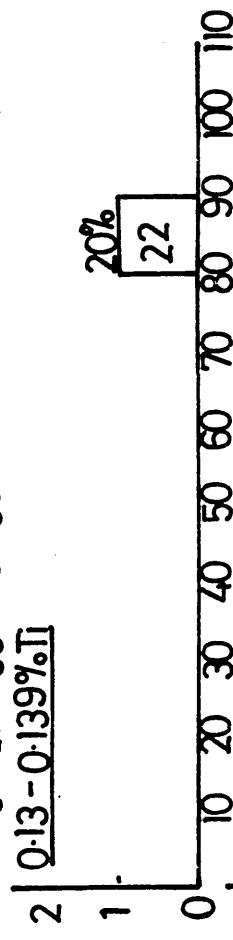
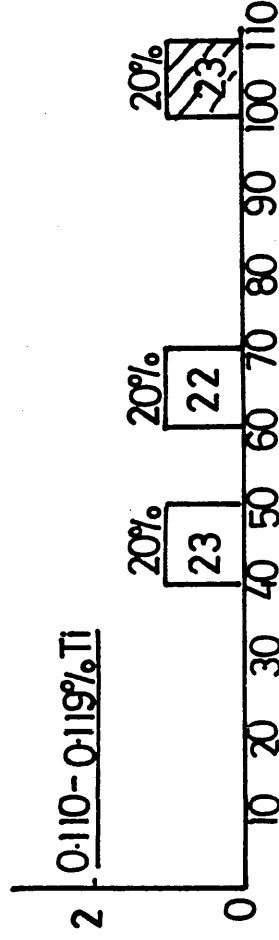
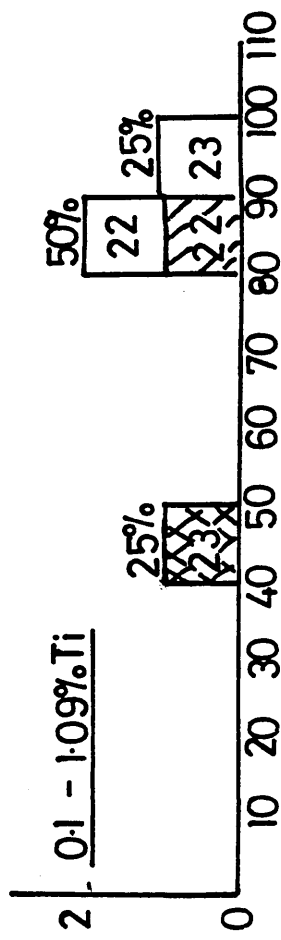
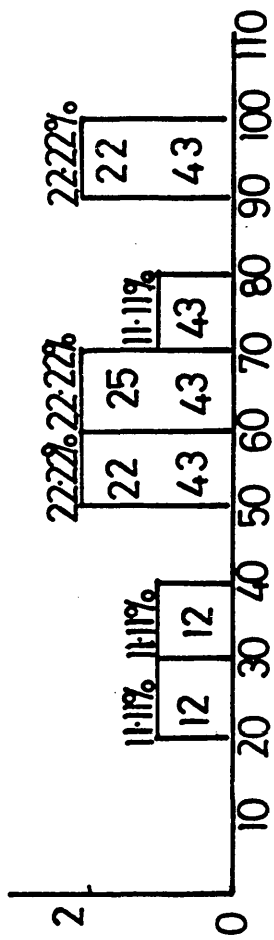


FIGURE 9

0.09 - 0.159

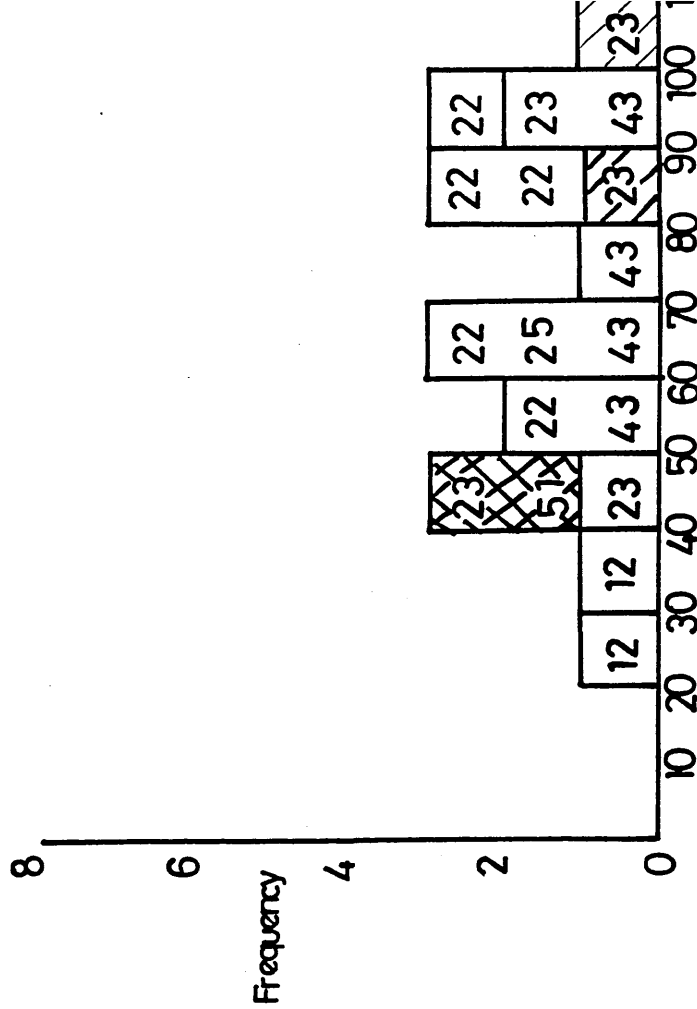
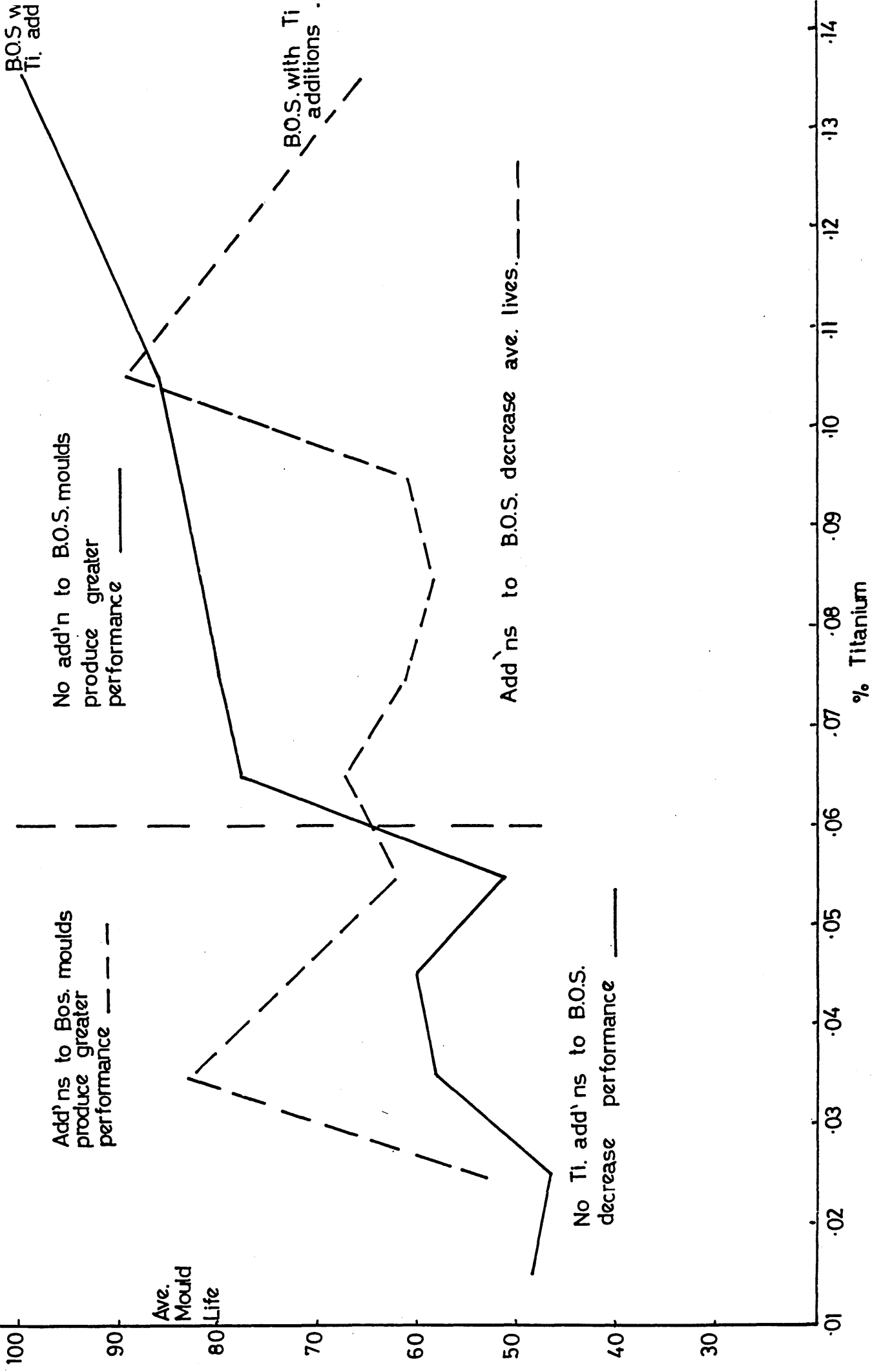


FIGURE 10

RESIDUAL TITANIUM AND AVE. MOULD LIFE.



Add'ns to Bos. moulds produce greater performance - - -

No add'n to B.O.S. moulds produce greater performance - - -

No Ti. add'ns to B.O.S. decrease performance - - -

Add'ns to B.O.S. decrease ave. lives. - - -

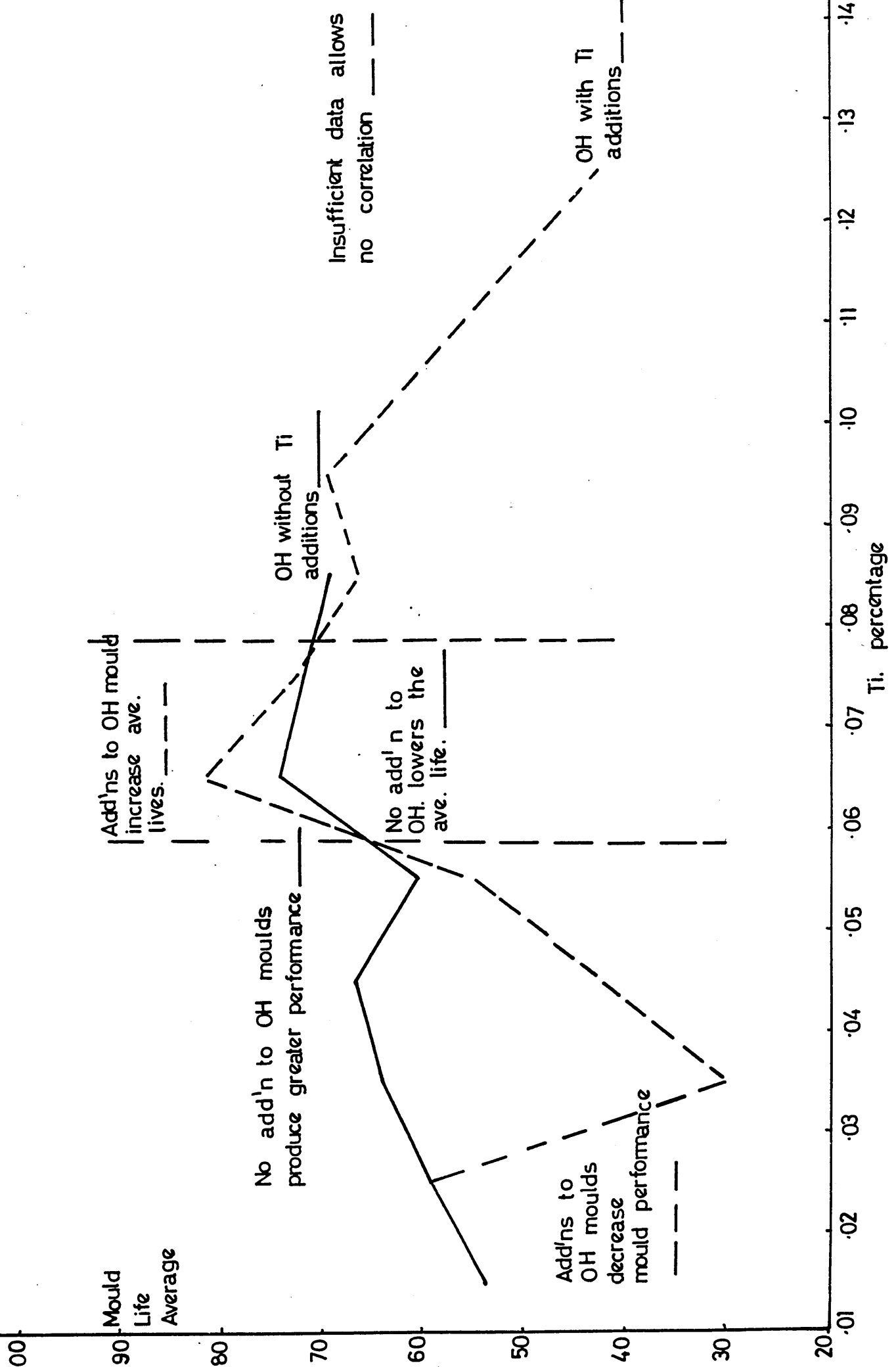
B.O.S. with Ti additions

B.O.S. w Ti. add

Ave. Mould Life

% Titanium

FUNCTION OF MOULD LIFE - AVERAGE



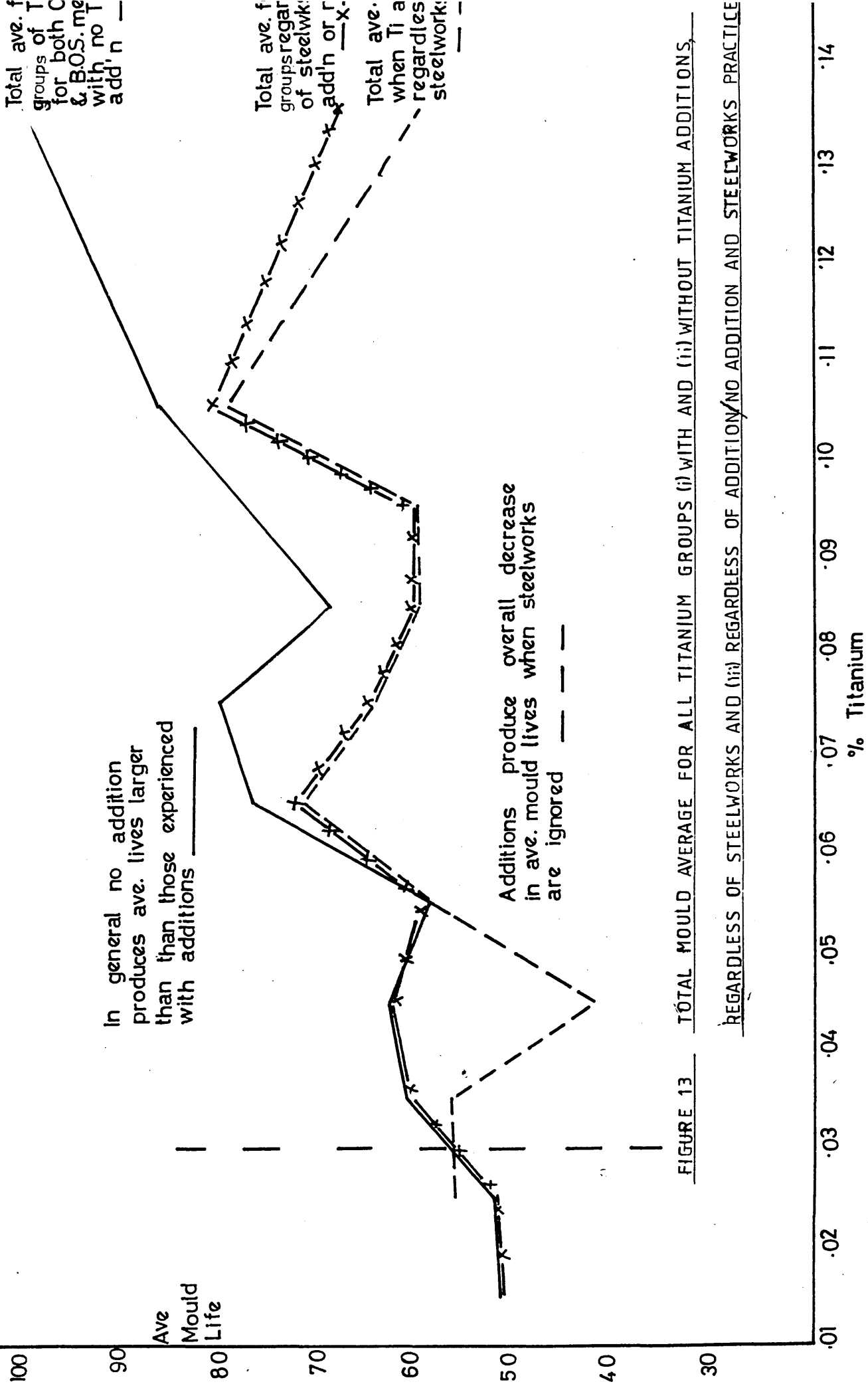


FIGURE 13 TOTAL MOULD AVERAGE FOR ALL TITANIUM GROUPS (i) WITH AND (ii) WITHOUT TITANIUM ADDITIONS, REGARDLESS OF STEELWORKS AND (iii) REGARDLESS OF ADDITION/NO ADDITION AND STEELWORKS PRACTICE

KEY TO TABLE 7

< >

Represents $\frac{\text{No. of moulds in Ti group/failure mode} \times 100\%}{\text{Total no. of moulds in Ti group}}$

= % in Ti group/failure mode

X and (X)

Represents the percentage of figures in particular titanium groups with no deliberate Fe Ti additions and deliberate Fe Ti additions respectively.

[]

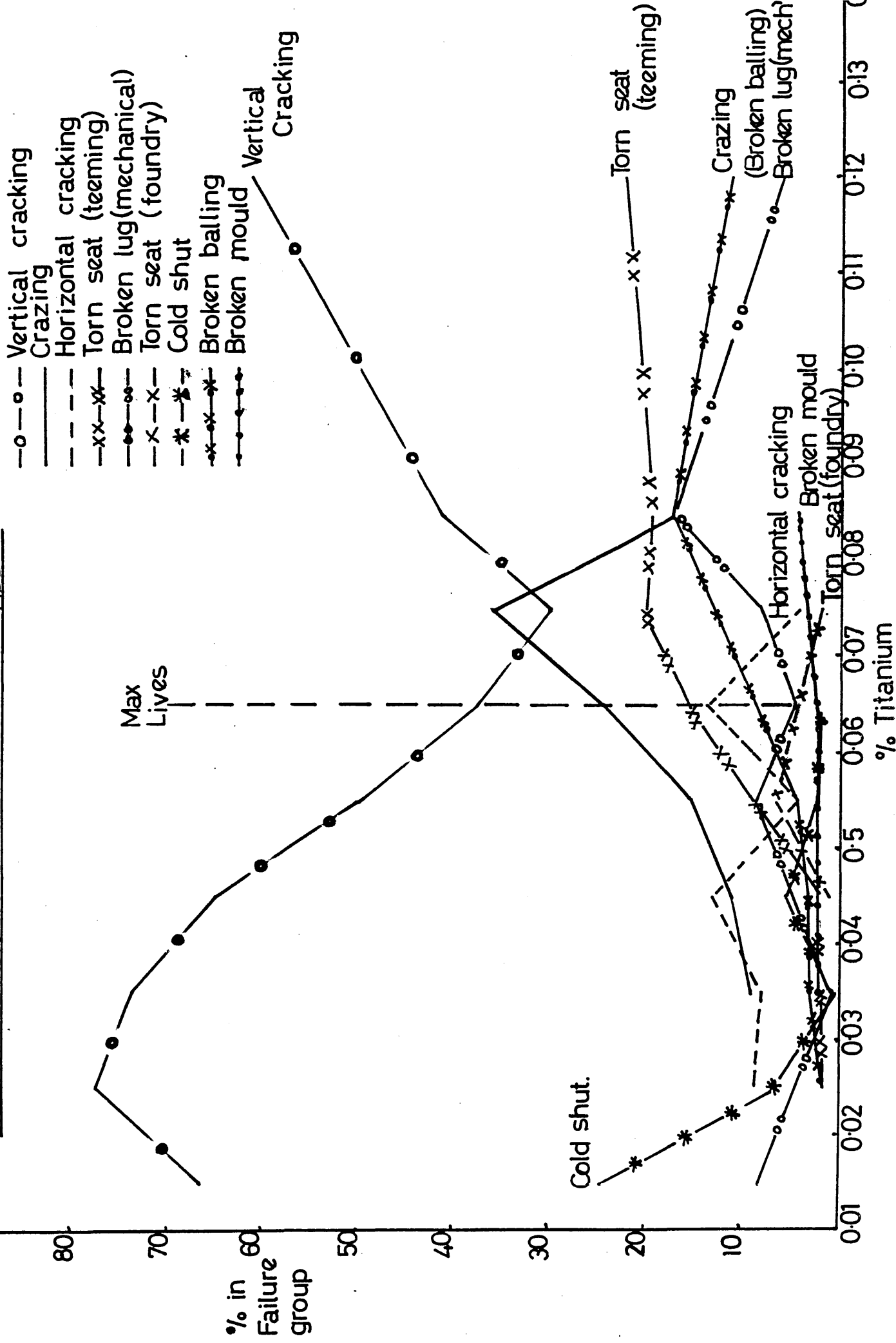
% for each failure mode = $100 \times \frac{\text{No. of moulds/failure group/Titanium group - no Fe Ti addition}}{\text{Total no. of moulds/Titanium group - no Fe Ti addition}}$

[()]

As above with Fe Ti additions

[] + [()] = < >

90 FIGURE 14. PERCENTAGE IN FAILURE GROUP VERSUS TITANIUM PERCENT
IGNORING WHETHER OR NOT Ti. ADDED

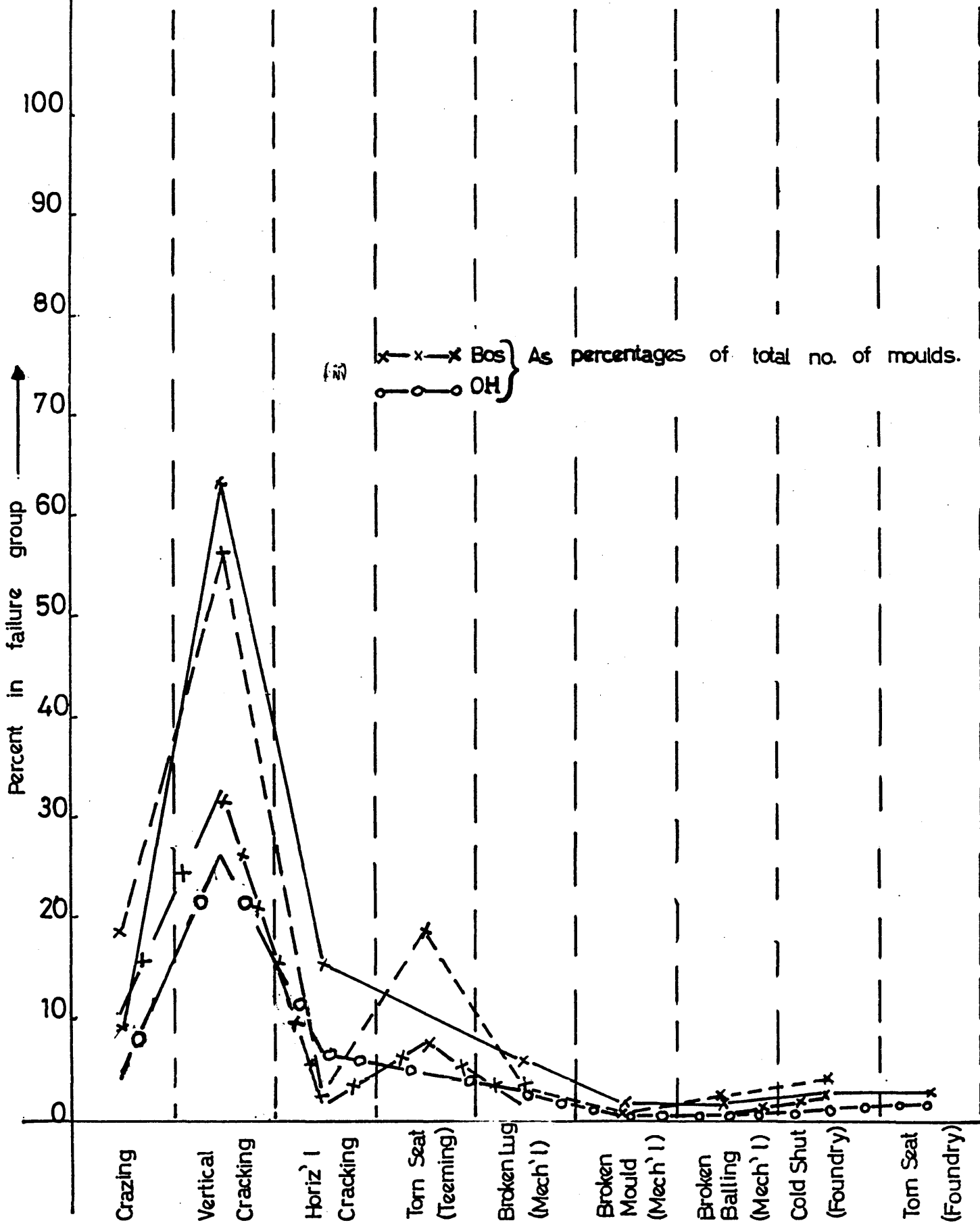


STEELWORKS OPERATIONS (i) AS A PERCENTAGE REGARDING THE SPECIFIC

STEELWORKS FAILURES AND (ii) AS A PERCENTAGE OF THE TOTAL NO. OF

MOULDS CONSIDERED

(i) OH Steelworks x—x
 Bos Steelworks x—x



THE ECONOMICS OF TITANIUM ADDITIONS TO BOS AND OH MOULDS

Steelworks Practice	Titanium Range (%)	Increase in Life With Ti Addition	Cost per cast (£)		Saving/Cast (£)	Saving for Improved Lives (£)	Cost of Ti Addition (£)	Total Saving Ti Group (£)	Savin
			With No Ti Addition	With Ti Addition					
BOS	0.02-.029	6.5	$\frac{3750}{46.5}$ = 80.65	$\frac{3750}{53}$ = 70.75	9.90	64.35	-9.375	54.975	✓
	0.03-.039	25.0	$\frac{3750}{58}$ = 64.66	$\frac{3750}{83}$ = 45.18	19.48	487.0	-13.125	473.875	✓
	0.04-.049	12.0	$\frac{3750}{61}$ = 61.475	$\frac{3750}{73}$ = 51.37	10.105	121.26	-16.875	104.385	✓
	0.05-.059	10.75	$\frac{3750}{51.25}$ = 73.17	$\frac{3750}{62}$ = 60.48	12.69	136.42	-20.625	115.795	✓
	0.06-.069	-10.00	$\frac{3750}{78}$ = 48.08	$\frac{3750}{68}$ = 55.15	-7.07	-70.07	-24.375	-94.445	
	0.07-.079	-18.50	$\frac{3750}{80.0}$ = 46.88	$\frac{3750}{61.5}$ = 60.98	-14.10	-260.85	-28.125	-288.975	
	0.10-.109	4.0	$\frac{3750}{88}$ = 42.615	$\frac{3750}{92}$ = 40.76	1.855	7.42	-39.375	-31.955	
	OH	0.03-.039	-3.4	$\frac{3750}{64}$ = 58.59	$\frac{3750}{30}$ = 125	-66.41	-2257.94	-13.125	-2271.065
0.05-.059		-6	$\frac{3750}{60}$ = 62.5	$\frac{3750}{54}$ = 69.44	-6.94	-41.64	-20.625	-62.265	
0.06-.069		+7.5	$\frac{3750}{74}$ = 50.68	$\frac{3750}{81.5}$ = 46.01	4.67	35.025	-22.5	12.525	✓
0.07-.079		1	$\frac{3750}{71.5}$ = 52.450	$\frac{3750}{72.5}$ = 51.725	0.725	0.725	-28.125	-27.400	
	0.08-.089	-3	$\frac{3750}{69}$ = 54.35	$\frac{3750}{66}$ = 56.82	-2.47	-7.41	-31.875	-39.285	